2018

Development of Hydraulic Models, Mass Transfer Models, and Dynamic Models of Solvent-Based Carbon Capture Processes with Uncertainty Quantification and Validation with Pilot Plant Data

Anderson Soares Chinen

Development of Hydraulic Models, Mass Transfer Models, and Dynamic Models of Solvent-Based Carbon Capture Processes with Uncertainty Quantification and Validation with Pilot Plant Data

Anderson Soares Chinen

Dissertation submitted to the Statler College of Engineering and Mineral Resources at West Virginia University in partial fulfillment of the requirements for the degree of Doctor of Philosophy in Chemical Engineering

Debangsu Bhattacharyya, Ph.D., Chair

Brian Anderson, Ph.D.

David Mebane, Ph.D.

David C. Miller, Ph.D.

Richard Turton, Ph.D.

Stephen Zitney, Ph.D.

Department of Chemical and Biomedical Engineering Morgantown, West Virginia

2018

Keywords: Carbon capture, monoethanolamine, mass transfer, uncertainty quantification, design of dynamic experiments

ABSTRACT

Development of Hydraulic Models, Mass Transfer Models, and Dynamic Models of Solvent-Based Carbon Capture Processes with Uncertainty Quantification and Validation with Pilot Plant Data

Anderson Soares Chinen

To accelerate the development and commercial deployment of CO_2 capture technologies, computational tools and models are being developed under the auspices of the U.S. Department of Energy's Carbon Capture Simulation Initiative (CCSI). The CCSI process modeling team was tasked with developing a "gold-standard" model that will serve as a definitive reference for benchmarking the performance of solvent-based CO_2 capture systems under steady-state and dynamic conditions over a large operating-range. The main three areas that this work focused on are: development of the hydrodynamic and mass transfer submodels for a monoethanolamine (MEA) solvent system, uncertainty quantification of these submodels, development of a dynamic model for this system, and development of a dynamic design of experiment methodology for model validation and parameter estimation of this system.

For the gold-standard model, it was desired that the pressure drop and holdup models must be applicable over a wide range of operating conditions. In this work, a large range of liquid and gas flowrates, and wide range of viscosity and density for the liquid phase are considered and an optimal model is developed. The pressure drop and holdup models are also evaluated with data from numerous process scales.

Typically the mass transfer models and their parameters such as the liquid and gas-side mass transfer coefficients, diffusivity, and interfacial area are regressed using the data obtained from different experimental set-ups and scales, often in a sequential and sub-optimal way. In this work, a novel methodology is developed where parameters of the mass transfer models are simultaneously regressed by using the data from the wetted wall column, and packed towers, simultaneously. It is observed that the technique helps to improve the predictive capability of the process model.

Uncertainty in process models and their parameters are unavoidable. A Bayesian uncertainty quantification technique is applied for the first time to quantify the parametric uncertainty of the hydraulic and mass transfer models.

Dynamic models of CO_2 capture solvent systems are very few in the existing literature. Model validation with the dynamic data from pilot plant has been scarcely reported. In this project, dynamic models are developed in Aspen Plus Dynamics®. Approximate pseudo random binary sequences are designed for the input signals and applied to the National Carbon Capture Center (NCCC) pilot plant during the 2014 MEA campaign. The pilot plant data were found to be noisy, did not satisfy mass and energy balances. In addition, some key variables were not measured. Preprocessing of the data followed by solution of a dynamic data reconciliation problem showed that the model could predict the transient response reasonably well.

For the first time, a dynamic design of experiments (DDoE) is developed for solvent-based CO_2 capture processes using pseudo-random binary sequence and Schroeder-phased input techniques. The design ensured plant friendliness and could be successfully implemented in NCC during the 2017 campaign. The transient data are used to solve a dynamic data reconciliation and parameter estimation problem. Due to the computational expense and large dimensionality of the underlying problem, only the parameters corresponding to the holdup model could be estimated. It is observed that the holdup parameters could be optimally estimated by using the dynamic data collected over only a day. The parameters are slightly superior to those that have been regressed by using a large amount of the steady-state data collected over weeks. The techniques shows promise for the model development and parameter estimation by using the

dynamic data that can be collected very quickly as opposed to the traditionally used steady-state data that take months thereby saving considerable resources.

Dedication

To my wife, son and family

Whose smiles keep me going forward

Acknowledgements

Seeking to accomplish a Ph.D. in chemical engineering at West Virginia University has showed me much more than the scientific contributions in this document. I had an unexpected growth in perspective and perception through all the experiences I had since I joined the program in 2013, and God's grace has been generously put in my life in the form of the many I am thankful for.

I would like to thank my advisor, Dr. Debangsu Bhattacharyya, for being an example of a great mentor, showing how an engineering researcher should look at (and question) the world. He pushed me to be able to achieve goals that I misjudged as unfeasible, and I am grateful for all the confidence deposited in me. I also would like to thank my Advisory and Examining Committee members (Dr. Brian Anderson, Dr. David Mebane, Dr. David Miller, Dr. Richard Turton, and Dr. Stephen Zitney) for the guidance on this work, especially during my dissertation research proposal. Likewise, I would like to thank Ben Omell, who gave valuable guidance on how to approach many of the challenges of developing the process models.

I had the honor of working with an awesome group (Joshua, Qiao, Yuan, Pratik, Prokash, Dustin, Qiang, Jacob, Sarah, Samson, Chirag, Anca, Yifan, Paul, Ryan, Goutham, Pushpitha, Christian, Katie, Elijah, Parikshit) during these years in Prof. Bhattacharyya's Advanced Process and Energy Systems Engineering Group. It was a fun ride to discuss and share ideas about our works, seminar presentations and life, as well as to travel to different places, even if we were simultaneously trying to fulfill deadlines. Particularly, it has been a great honor to work directly with Joshua Morgan on the development of the MEA process model and the extra project with the high-viscosity solvent, without his insights and contributions this dissertation would not be possible.

I also had the opportunity to work with many other competent professionals who assisted me in the fulfillment of this dissertation. I would like to thank John Eslick from NETL for providing much assistance and advice for the integrated mass transfer methodology, particularly with respect to implementing large optimization problems into the FOQUS software. I would like to thank the National Carbon Capture Center (NCCC) and the involved staff for providing high quality data for the 2014 and 2017 test campaigns for the MEA solvent system, including the assistance in designing a proper set of dynamic experiment, while providing insights to what was necessary to achieve plant-friendliness in their facility. I would like to thank Prof. Gary Rochelle from the University of Texas at Austin for providing the "Phoenix Model", which was used as a starting point to all the contributions in this work, and Brent Sherman, for all the assistance in building subroutines for Aspen plus. I also would like to thank everyone in the high-viscosity solvent model

side project for the great opportunity to work directly with industry. I am grateful for the other opportunities that working in CCSI and CCSI^2 research programs brought, but especially for David Miller's and Michael Matuszewski's inspiring leaderships.

In my Ph.D. pursuit I have been fortunate to be able to complement my research with outstanding courses from the Department of Chemical and Biomedical Engineering (CBE) and others in West Virginia University. I would like to acknowledge the professors who have assisted me, and contributed to my research and professional development in these years: Prof. Charter Stinespring (who made thermodynamics fun), Prof. Ray Yang (who not only improved my knowledge of transport phenomena and reaction engineering, but also gave me critical advices for the graduate student life), Prof. John Zondlo (who gave such enthusiasm and humor to heat transfer and hydrodynamics), Prof. David Klinke (mathematical methods in chemical engineering), and Prof. Rakesh Gupta (mass transfer). I would also like to acknowledge the courses offered by Prof. Gary Ganser (mathematical modeling), and Prof. Erdogan Gunel (statistical theory) from outside the CBE department for an excellent approach to their respective fields. I wasn't fortunate to attend a class lectured by Prof. Fernando Lima, but I hold an enormous gratitude for all his encouragement and support in my application for a PhD position at WVU.

I am grateful for all the support I receive from my family, as none of this would have been possible without your countless hours of care, love and encouragement. I am thankful for my wife, Rani, who never doubted this was going to be possible and was brave enough to sail with me in this journey. I also thank my son, Eliot, who received me with such happiness every single day after long hours of research.

Finally, I would like to acknowledge the financial support to this research. This research was conducted through the Carbon Capture Simulation Initiative (CCSI), funded through the U.S. DOE Office of Fossil Energy. A portion of this work was also funded by Lawrence Berkeley Laboratory through contract# 7210843.

Disclaimer

This project was funded by the Department of Energy, National Energy Technology Laboratory, an agency of the United States Government, through a support contract with URS Energy & Construction, Inc. Neither the United States Government nor any agency thereof, nor any of their employees, nor URS Energy & Construction, Inc., nor any of their employees, makes any warranty, expressed or implied, or assumes any legal liability or responsibility for the accuracy, completeness, or usefulness of any information, apparatus, product, or process disclosed, or represents that its use would not infringe privately owned rights. Reference herein to any specific commercial product, process, or service by trade name, trademark, manufacturer, or otherwise, does not necessarily constitute or imply its endorsement, recommendation, or favoring by the United States Government or any agency thereof. The views and opinions of authors expressed herein do not necessarily state or reflect those of the United States Government or any agency thereof.

Contents

List of Figures

List of tables

Chapter 1. Introduction

Fossil fuels are currently being utilized to provide most of the world's energy needs. However, their utilization releases large amount of CO_2. Due to the anticipated strong reliance on fossil fuels in the foreseeable future and increased concern over global warming, there is strong interest in the development of CO_2 capture and sequestration (CCS) technologies as effective means for reducing greenhouse gas emissions from fossil fuel burning power plants (Gibbins, 2008; Folger, 2010). These power plants release over 30 billion metric tons of CO_2 a year. To accelerate the development and commercial deployment of CO_2 capture technologies, computational tools and models are being developed under the auspices of the U.S. Department of Energy's Carbon Capture Simulation Initiative (CCSI). As part of CCSI, it was desired to develop a comprehensive model of a solvent-based CO_2 capture system, that can serve as a definitive reference for benchmarking the performance of solvent-based CO_2 capture systems under both steady-state and dynamic conditions. It was desired that the model should be validated with the experimental data over wide operating regime and should be well-documented.

The MEA-based CO_2 capture technology is evaluated in this work since this technology is matured, there is large amount of physical properties data in the open literature for the MEA-H_2O-CO_2 system, and the solvent is not proprietary in nature. Therefore, it was decided that a model of the MEA-H_2O-CO_2 system be developed first as the desired benchmark model. A typical MEA-based post-combustion CO_2 capture process of a coal-fired power plant is shown in Figure 1.1 (Folger, 2010). The flue gas from the power plant enters at the bottom of the column with a high CO_2 concentration. The lean MEA solvent enters at the top of the column. The CO_2-rich solvent from the bottom of the absorber is sent to the stripper where the solvent is heated to release the CO_2. The regenerated MEA is then recycled back to the absorber.

Development of the properties models for the benchmark model, uncertainty quantification of the properties models and validation of the steady-state model with the data from National Carbon Capture Center (NCCC), Wilsonville, AL have been described in details in the PhD dissertation of Morgan (2017).

This thesis mainly focuses on four tasks:

- Development of the mass transfer model and hydraulic model for the benchmark model
- Uncertainty Quantification of the mass transfer model and hydraulic model
- Development of the dynamic model for the MEA-H_2O-CO_2 system and its validation using dynamic data from NCCC
- Design of dynamic design of experiments (DoE) for NCCC and development of dynamic data reconciliation and parameter estimation framework using the NCCC data

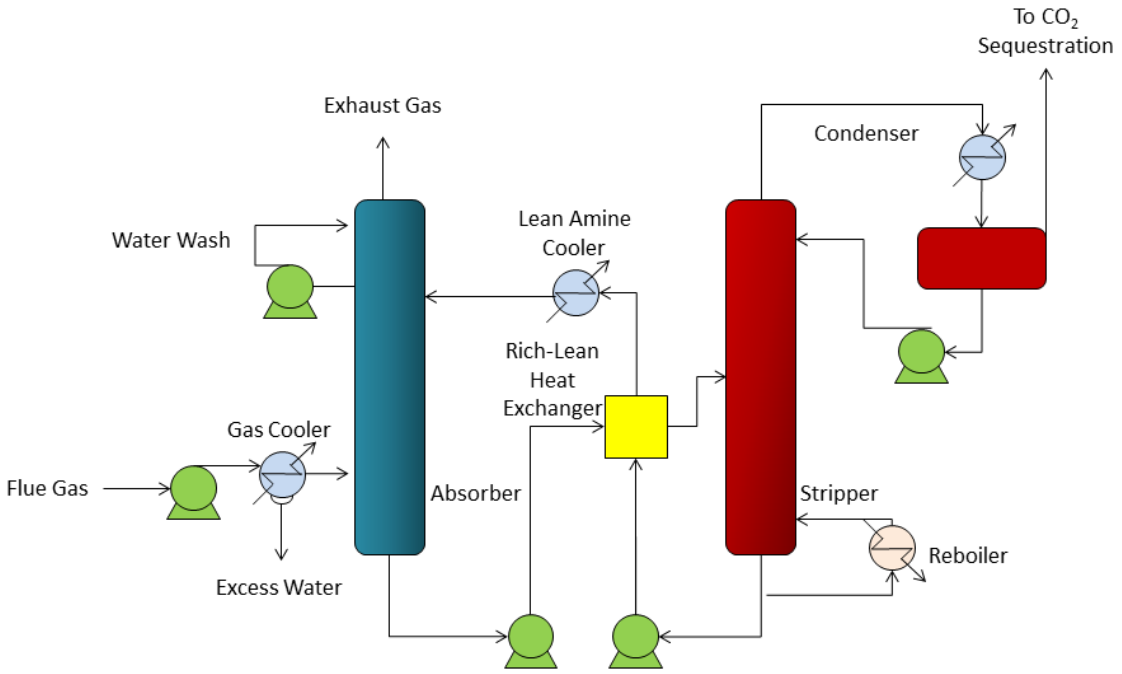

Figure 1.1- Post-combustion, chemical absorption CO_2 capture process of a coal-fired power plant

1.1. Mass transfer and hydraulic models and their uncertainty quantification and model validation

Mass Transfer Models

Mass transfer models for the towers mainly comprise of four models-mass transfer coefficient model for the liquid-side, mass transfer coefficient model for the gas-side, diffusivity model, and the interfacial area model. Mass transfer coefficients and interfacial area depend on the packing-type and the operating system (Razi et al. 2012). Sensitivity studies performed by evaluating different combinations of the literature models for the interfacial area, mass transfer coefficients and holdup show that the model selection has strong impact especially when the operating range is 50-85% CO_2 capture. (Cormos and Gaspar, 2012; Kvamsdal and Hillestad, 2012; Razi et al., 2014). However, most of the correlations available in the open literature for mass transfer coefficients and interfacial area were neither developed for nor tested on the packing-types that have been recently developed. Furthermore, they were not developed specifically for the MEA-H_2O-CO_2 system. Although it is common practice to apply the literature models for the mass transfer directly to the MEA system without any adjustments (Tobiesen et al., 2007; Zhang et al., 2009; Dugas, 2009; Faramarzi et al., 2010; Tonnies et al., 2011; Khan et al., 2011; Cormos and Gaspar, 2012; Simon et al., 2011; Kvamsdal and Hillestad, 2012; Saimport et al., 2013; Jayarathna et al., 2013; Afkhamipour and

Mofarahi, 2013; Kale et al., 2013, Razi et al., 2014; Zhang and Chen 2013; Afkhamipour and Mofarahi, 2014; von Harbou et al., 2014), the model and the parameters are likely to be sub-optimal. A pioneering work on mass transfer phenomena for recently developed packing-types has been presented by Tsai (2010) by studying various flow regimes and operating conditions, but for a H_2O-NaOH-CO_2 system.

For solvent-based CO_2 capture systems, it is difficult to separate the effects of mass transfer and chemical reactions since they take place simultaneously. Therefore, the reaction model needs to be considered as well while developing the mass transfer model and estimating its parameters. In the open literature, these models are obtained and their parameters are estimated one by one, i.e. by following a sequential approach. In this approach, typically, the diffusivity model is developed assuming no reaction and by using correlations such as the Stokes-Einstein relation. This diffusivity model is then applied while developing the models for mass transfer coefficients and reaction kinetics by using the experimental data from the wetted wall column (WWC) (Simon et al. 2011; Dugas 2009; Plaza 2011). Finally, an interfacial area model is developed for a given packing based on the experimental data from the absorbers/regenerators. Another approach is to obtain the mass transfer coefficient model by using the experimental data from a nonreactive system in the packed tower. Then data are collected for the actual, reactive system and are used to develop the interfacial area model assuming that the mass transfer coefficient models are still accurate. There are two issues with this traditional approach. First of all, it is implicitly assumed that the diffusivity and mass transfer coefficient models obtained from a different equipment type such as the WWC column experiments or from the non-reactive system would still be valid for the experiments with the reactive system in a given packing. However, the hydrodynamics, liquid and gas velocities, loading of the solvent and operating temperatures can be very different between the WWC and the packing operation. Considerable differences can exist between the reactive and non-reactive flows in terms of density, viscosity, surface tension, etc. that can affect the wettability and flow characteristics of the fluids. Furthermore, mass transfer for electrolyte systems are affected by the ionic species present in the solution, ion-molecule interactions, ion mobility, etc. Therefore, the errors and uncertainties in the models and their parameters obtained at one step gets propagated to the next step. The second issue is that instead of using the full-blown rate-based model, most researchers have used a simple model for the WWC using the enhancement factor approach so that the parameters for the kinetic and mass transfer coefficient models can be easily estimated (Dang and Rochelle 2003, Puxty et al. 2010, Darde et al. 2011). Recently, a few researchers have considered the rigorous rate-based model while analyzing the WWC experiments (Frailie 2014, Li 2015, Sherman 2016), albeit, following a sequential approach. Another alternative is to develop a model of the volumetric mass transfer coefficient, where the mass transfer coefficients are multiplied by the interfacial area. While the model of the volumetric mass transfer coefficients can be obtained directly using the data from the packing

experiments (Piche et al. 2001 and 2002), the main difficulty with this approach is that the mass transfer coefficients and interfacial area become indistinguishable.

In this paper an approach to the development of an integrated mass transfer model is proposed where the model selection and parameter estimation for diffusivity, interfacial area, liquid- and gas-side mass transfer coefficients, and the kinetic model are done simultaneously using the data from the WWCs along with the data from the packed towers for the MEA-H_2O-CO_2 system. Existing commercial process simulation software such as Aspen Plus is inadequate for parameter estimation of such an integrated model due to the segregation of these models in such software. Diffusivity belongs to the transports model package; reactions belong to a separate callable class while the hydraulics and mass transfer models belong to the tower model. Furthermore, large number of WWC experiments and tower experiments should be considered simultaneously for parameter estimation of the integrated model. This large-scale optimization problem is computationally expensive and can be difficult to solve in many commercial software. An external optimization framework, named FOQUS (Miller et al. 2015), that can read from and write to Aspen Plus models has been developed as part of CCSI and has been utilized in this work for developing the integrated model.

Hydraulic Models

Hydraulic models mainly comprise of the pressure drop model and hold up model in addition to models developed for predicting flooding and weeping. An accurate model for the pressure drop is important for calculating the fluid flowrates particularly that of the gas phase, especially during dynamic simulations, because of the pressure-driven flow across the columns. Hold up in the packing affects the extent of reaction. In addition, due to close coupling between holdup and pressure drop, as will be explained in more details later, it is important to have accurate models for both, especially for transient simulation when both of these variables can significantly change leading to undesired tower operation such as flooding. Hold up also directly affects the rate of change in the transport variables such as the temperature and concentration.

Similar to the mass transfer model, most of the correlations available in the open literature for column hydraulics were neither developed for nor tested on the packing-types that have been recently developed. It should be noted that significant advances have been made in recent commercial packings for improving their hydraulic performance by reducing the pressure drop and increasing the operational regime without flooding or weeping. Similar to the mass transfer model, while it is common practice to apply the literature models for column hydraulics directly to the MEA system without any adjustments (Tobiesen et al., 2007; Kvamsdal and Hillestad, 2012; Afkhamipour and Mofarahi, 2014; von Harbou et al., 2014), the hydraulic

model and its parameters are likely to be sub-optimal. Tsai (2010) has presented their work on hydraulic models for recently developed packing-types by studying various flow regimes and operating conditions, but for a H_2O-NaOH-CO_2 system.

Correlations developed for air-water systems are typically applied to the hydraulic modeling of the MEA-H_2O-CO_2 systems (Kvamsdal et al., 2008; Kvamsdal and Hillestad, 2012; Cormos and Gaspar, 2012; Jayarathna et al., 2013). Stichlmair et al. (1989) and Billet and Schultes (1993) proposed pressure drop and holdup models that can be applied to both random and structured packings from the loading region up to the flooding point. Billet and Schultes (1999) later improved and expanded their models by considering a larger database. Rocha et al. (1993) proposed a correlation for pressure drop and holdup in the loading region of a structured packing. Other notable works in this area are due to Bravo et al. (1985), Bravo et al. (1986) and Fair and Bravo (1990). It is important to note that these models utilize packing-specific parameters to address the effect of geometry on the pressure drop and holdup and, therefore, the existence of experimental data for a given packing-type is critical for development of these hydraulic models. Appropriate parameters for a number of recently developed packings with improved mass transfer rate and hydraulics performance are not available in the open literature. In this work, updated parameters for the hydraulics of one of the newer packing types have been estimated.

Uncertainty Quantification

Uncertainty in models and their parameters is unavoidable and therefore must be quantified for predictive models. To the best of our knowledge, there is no work in the existing literature on uncertainty quantification (UQ) of the mass transfer and hydraulic models for the solvent-based CO_2 capture system. In the existing literature, a systematic approach to UQ of not only the mass transfer and hydraulic models, but of process models, in general, is rare. Uncertainty in model parameters has been evaluated by a few authors through perturbation method (Mathias and Gilmartin, 2014; Mathias, 2014) or Monte Carlo analysis (Whiting, 1996; Gel et al., 2014; Lane et al., 2014). A rigorous approach to UQ of the thermodynamic models by using the fully Bayesian approach has been reported by some authors (Mebane et al., 2013; Weber et al., 2006; Sarkar et al., 2012).

Uncertainty quantification of density, surface tension and viscosity models using a Bayesian approach has been reported by Morgan et al. (2015). More recently, Morgan et al. have presented a Bayesian inference procedure for UQ of the thermodynamic model of a MEA-H_2O-CO_2 system where the VLE, enthalpy and chemistry models were considered together (Morgan et al., 2017). One significant difference in the UQ of the mass transfer and hydraulic models in comparison to the UQ of the thermodynamic and transport models

is the consideration of the tower model. Therefore, the input space spanned by the prior belief of the parametric uncertainties and the space of operating conditions must be propagated through the complicated and computationally demanding rate-based tower model for Bayesian UQ of the parameter space. This leads to challenging computational issues that are undertaken in this research.

Model Validation

In the existing literature, typically, the range of validation is usually narrow, around 90-100% CO2 capture, (Faramarzi et al. 2010, Tonnies et al. 2011, Khan et al. 2011, Simon et al. 2011, Afkhamipour and Mofarahi 2013, Kale et al. 2013, Razi et al. 2013, Zhang and Chen 2013, Afkhamipour and Mofarahi 2014). Validation for lower capture rates, such as 50-85%, is rather limited in literature and are typically limited to only a few data points. Higher errors in model predictions have been reported for lower capture in comparison to the cases when CO_2 capture is more than 90% (Tobiesen et al. 2007, Zhang et al. 2009, Dugas et al. 2009, Kvamsdal and Hillestad 2012, Saimport et al. 2013, Jayarathna et al. 2013, von Harbou et al. 2014).

Currently, most of the models available in the open literature for solvent-based CO2 capture systems are steady-state and validated with a narrow set of operating conditions. Plaza (2011), Dugas et al. (2008) and Tobiesen et al. (2007) developed steady-state models for the solvent-based CO_2 capture systems, however, the experimental data considered in these studies for model validation were limited and did not include comparison of all key variables.

Tobiesen et al. (2007) compared results from the commercially available tools and models with the pilot plant data. Very little variation in the CO_2 captured was observed in the pilot plant data of Dugas et al. (2008). The CO_2 content of the flue gas was not varied in the work of Plaza (2011). Furthermore, most of the authors have collected data using synthetic flue gas, rather than the flue gas from actual power plant that contains species other than CO_2 and N_2. In addition, sizes of most of the pilot plants from which data have been presented in the literature are rather small in comparison to what would be expected at the commercial scale.

1.2. Dynamic model development

Dynamic models for the MEA-based CO_2 capture process are not as common in the literature as steady-state models. A thorough review of the dynamic models in this area has been presented by Bui et al. (2014)

Biliyok et al. (2012) validated a gPROMS model using the data from the SRP pilot plant in Austin, TX. The dynamic CO2SIM model has been validated by using the data from the Brindisi pilot-plant (Flø et al., 2014) and the Gløshaugen pilot-plant (Flø et al., 2015).

(Kvamsdal, Chikukwa, Hillestad, Zakeri, & Einbu, 2011) is an example of a collection of previous works from the authors, with the full PCCC model being an update to a singular absorber model previously discussed (Kvamsdal, Jakobsen, & Hoff, 2009). This gPROMS/Matlab model was validated with dynamic data from the VOCC pilot-plant operated by NTNU and SINTEF. This same data set has been used to validate the CO2SIM model (Tobiesen et al., 2012).

Harun et al. (2012) developed a dynamic model of the Pickle pilot-plant at UT, Austin in gPROMS®. The model was used to simulate a MEA-Campaign described by Dugas (2006). The model was used to predict the steady-state lean loading and capture efficiency and to study the transient response due to single-step changes and due to the sinusoidal change in the flue gas flowrate. But the transient model was not validated with any experimental data.

The same authors later presented a plant-wide model of a CO_2 capture process and evaluated three control structures (Nittaya et al., 2014a). Disturbance rejection characteristics of these controllers due to the flue gas flowrates were studied. The model was then scaled-up to a 750 MW capacity power plant (Nittaya et al. 2014b). Here authors studied the effect of the CO_2 concentration in the flue gas. The authors also presented a study on CO_2 capture scheduling.

An Aspen Plus Dynamics® model of a MEA-based CO_2 capture process has been presented by Lin et al. (2011) by developing an equilibrium-stage model for the towers. The authors observed, similar to others, that there is strong impact of the water make-up, solvent flowrate and lean loading on CO_2 capture. Their control scheme could successfully reject disturbances due to change in the flue gas flowrate while avoiding column flooding. The authors later developed a model of a 580 MW power plant (Lin et al. 2012) integrated with CO_2 capture. The extent of CO_2 capture range was varied between 50- 90%. The manipulated variable was either the lean solvent flowrate at constant lean loading, or the lean loading at a constant solvent flowrate. While both works rely heavily on an accurate model of the column hydraulics for flooding prediction, no discussion on the hydraulics model could be found.

Walters et al. have developed a dynamic model in MATLAB® for CO_2 capture (Walters et al., 2016). The steady-state model was validated with the data from Frailie (2014). The dynamic model was validated using the data from the Separation Research Program (SRP) pilot-plant at the University of Texas at Austin for a single step change. The input signals were filtered prior to their implementation in the model and relatively

satisfactory fit to the data was obtained. However, dynamic data reconciliation (DDR) was not performed to account for errors in mass and energy balances in the collected data. The model was later scaled up to a CO_2 capture unit as part of a 550 MW power-plant (Walters et al., 2016b) and used for plant-wide control studies. The authors evaluated open loop responses to single step changes in the flue gas CO_2 concentration, the steam flowrate to the reboiler and flue gas flowrate. Control system performance was evaluated by considering disturbances in the flue gas flowrates among others (Walters et al., 2016a) , but the open loop and closed-loop studies were limited to only single step changes in one variable at a time.

Zhang et al. have developed a dynamic model in Aspen plus® dynamic model using a steady-state Aspen plus® model as a starting point (Zhang et al., 2016). As rate-based equations are not supported in Aspen plus dynamics, their approach relied on a methodology based on the Murphree efficiencies to obtain an accurate 550 MW PCCC equilibrium steady-state model, that can be exported to the dynamic platform. The model was used for several control studies of PID and LMPC strategies, including an extensive set of scenarios that mimic the typical disturbances observed in the process. The same authors later (Zhang et a., 2018) modified the dynamic model by incorporating additional variables in the efficiency model. The improved dynamic model was then utilized to design Nonlinear Model Predictive Control (NMPC) and H_∞ control strategies, while evaluating the effects of uncertainty due to measurement noise and model discrepancy.

Following observations are made from the review of the existing literature on dynamic models:

- Validation of the dynamic models with the data from experimental systems, especially from pilot plants, is seriously lacking. In few cases, where the models have been validated, they have been done using data from a single step change. Data from single step changes cannot maintain persistence of excitation for such a high order system. More discussion on this aspect is provided later.
- Typically, step changes in only one variable is provided at a time. Such studies do not necessarily capture the confounding effects when multiple variables change simultaneously, which is realistic.
- Data from experimental systems especially from larger scale systems such as pilot plants would invariably have noisy data, data that do not satisfy mass and energy balances and possibly missing measurements of some crucial variables. How to treat the data from such real-life systems for model validation is not addressed in the open literature.

It was desired to address the issues mentioned above. The dynamic test runs are conducted at the NCCC. Transient responses of the following variables are investigated:

- Lean solvent flowrate
- Flue gas flowrate
- Reboiler steam flowrate

Data collected during the experiments include the expansive measurements available from the highly-instrumented NCCC. The lean and rich solvent compositions (both CO_2 loading and MEA concentration) were measured both online and manually through titration and gas chromatography.

From these measurements, it was observed that the data have significant mass balance errors. Considerable discrepancy was observed between CO_2 capture estimated from the liquid side with that estimated from the gas side. Furthermore, estimates of CO_2 capture from the absorber side did not agree well with that from the stripper side even when due consideration of the holdup and transport lag was made. Under these circumstances, solving a DDR problem becomes necessary (Montañés et al., 2017). This step becomes critical for validation of dynamic models and estimation of model parameters (Mobed et al., 2014). Therefore, a DDR methodology is developed applied tin the Aspen Plus Dynamics framework.

The dynamic model is used to perform two case studies. In the first study, transient response due to the change in the solvent flow rate, gas flowrate, and steam flowrates are studied. The study provides valuable information about the gain and time constant of the process and can provide valuable insight into operational strategies.

The second study in this work evaluates the effect of variable CO_2 capture rate, that is desired from an upper-level scheduler. The scheduler maximizes the power plant profit by considering short term and long term impacts due to load demand, price of electricity, and CO_2 release penalty/award over a base period (Bankole et al., 2018). The objective of this study is to evaluate the thermal efficiency of a large pilot-plant under variable capture scenario.

1.3. Dynamic Design of Experiments (DoE)

Current literature lacks work on systematic design of experiments (DoE) for CO_2 capture plants even though considerable amount of data do exist in the literature for MEA-based CO_2 capture systems (Llano-Restrepo & Araujo-Lopez, 2015).

While steady-state DoE for non-CO_2 capture systems has been widely available in the Literature (Fedorov, 1972; Jiju, 2003; Mead, 1988), there is not much work on the dynamic DoE (Georgakis, 2013) especially

for pilot plants. However, one can draw from the rich literature in the area of system identification to develop dynamic DoE. The typical approach for identifying non-linear processes is to determine the minimum number of experimental runs for estimating model parameters with reduced uncertainty, under a cost or time constraint (Körkel, et al., 2004).

One of the methods applied for system identification is the utilization of a series of step changes signal to keep each variable being studied constantly excited, with the goal of capturing the process non-linear effects. This signal is called Pseudo-random binary, and is often employed in control studies. Alternatively, a sinusoid signal can also be used to keep the process excited, but without relying on rapid changes of the experimental variables being studied. Both of these methods have been applied in the past to linear systems as a demonstration (Gaikwad & Rivera, 1996) and to other system identification applications.

One of the methods applied for system identification is to design a series of step changes so that the underlying process remains persistently excited. A pseudo-random binary sequence (PRBS) is often employed due to its practicality in obtaining a sufficient spectral content (Gaikwad & Rivera, 1996). Due to the long sequence size, the PRBS signal can be time-consuming and prohibitive for large-order systems. A multisine signal can be designed that has similar characteristics as the PRBS yet can be implemented within realistic time for higher-order systems. A Schroeder-phased input signal is such a multisine signal with the desired characteristics (Rivera, et al., 1993). Both PRBS and Schroeder-phased input signals have been applied to the linear (Rivera, et al., 1994) and nonlinear systems (Rivera, et al., 1997). These input signals have been designed also for case studies including distillation towers (Gaikwad & Rivera, 1996; Mart, et al., 2015), but with no implementation in an actual chemical plant has been reported.

A nonlinear pH neutralization process was identified by a PRBS signal (Lara & Milani, 2003), where the data for system identification was obtained from a Simulink® process model.

For real-life implementation of the inputs signals, the designed signal should be plant-friendly. Plant-friendliness of the input signals ensures that the designed signals do not lead to unacceptable change in the products quality and controller set-points that cause “wear and tear” on the process equipment (Rivera, et al., 2009). Furthermore, input signals should not lead to unsafe operation of the plant. For designing plant-friendly input signals, one needs to also consider crest factor in addition to the persistence of excitation. If these properties are not considered, it can lead to signals that are practically unacceptable due to the signal variability, frequency content (harsh changes), amplitude (designed values cannot be achieved at implementation) and waveform (some forms of signals may not be integrated in a given control system of a plant) (Hjalmarsson, 2014). One can ensure plant-friendliness to minimize the experimental cost by developing a suitable cost model (Narasimhan & Bombois, 2012). This design philosophy has been applied

to both PRBS and a multisine signals for the identification of a process represented by a finite impulse response model (Kumar & Narasimhan, 2013).

In this work, experiments for the National Carbon Capture Center are designed using both the Schroeder phased input and PRBS methodologies. The generated signals are focused on key input variables of the process:

- Flue gas flowrate
- Flue gas CO_2 concentration
- Lean solvent flowrate
- Steam flowrate

The generated signals are designed for plant-friendliness and persistence of excitation by leveraging the dynamic model developed in this work.

1.4. Scope of the research

The main contributions of this work are summarized below:

- A novel approach to the integrated model development and parameter estimation is proposed. The approach is used for simultaneous parameter estimation of interfacial area models, mass transfer coefficient models, and kinetic models by considering the experimental data from wetted wall column and packed column simultaneously.
- Hydraulic models are developed for MellapakPlus™ 252Y, a new promising packing-type with very little investigation on its hydraulic properties in the literature.
- Rigorous uncertainty quantification of the mass transfer models as well as the hydraulic models is performed by considering a fully Bayesian approach.
- A dynamic model of a large-scale pilot plant is developed in Aspen Plus® Dynamics, where a modified Murphree efficiency approach and a rigorous hydraulic model, developed for the specific packing-type used in NCCC, are implemented
- A quasi-PRBS signal was developed and implemented in the NCCC pilot plant. The raw data were filtered and processed through a DDR framework for dynamic model validation.

- A dynamic DoE was designed and implemented for the first time in a pilot plant by designing both Schroeder-phased input and PRBS signals. These signals not only ensured persistence of excitation, but also plant-friendliness.

- A dynamic data reconciliation and parameter estimation framework was developed where the dynamic data collected from the dynamic DoE were utilized. The framework also considers implementation error in the input signals.

- A number of open-loop and closed-loop transient studies are conducted by using the dynamic model developed in this work. These studies provide valuable information on the operation of CO_2 capture units integrated with load-following power plants and when they are operated under variable capture rates.

In addition, the integrated model development and parameter estimation methodology was successfully applied to a novel solvent system being developed by an industrial collaborator by using the data from the laboratory scale and bench-scale system. The process model was validated against data from both pilot-plant scale (NCCC) and bench-scale systems. Several economic studies were performed for scaling the process to a 550 MW power plant scale. Due to the proprietary nature of the project detailed information is not included in this dissertation, but limited information approved by the industrial partner is provided in appendix B.

Chapter 2. Hydraulic and Mass Transfer Models

The methodologies developed in this work are generic and can be readily applied to any solvent system operating on any packing type. However, the hydraulic and mass transfer performances strongly depend on the packing type as well as the solvent system. Therefore, optimal models and their parameters can be different depending on the packing type and the solvent. In this work, it was desired that the models be tested using pilot plant data collected from the National Carbon Capture Center (NCCC) in Wilsonville, AL. This pilot plant uses MellapakPlus™ 252Y, one of the newer packings from Sulzer (Sulzer Chemtech 2015), in both the absorber and regenerator. It can be noted that there are very few studies in the open literature on this packing. This packing offers low pressure drop, can operate in a wide range of operating conditions without flooding or channeling, and offers a high interfacial area resulting in high mass transfer efficiency (Sulzer Chemtech 2015). Therefore, the experimental data used in this work are from MellapakPlus™ 252Y or packings that are structurally similar to it. The final FORTRAN code of each one of the sub-models presented in this chapter, and implemented in Aspen plus®, are presented in Appendix A.

2. 1. Models for Column Hydraulics

Table 2.1 presents three leading hydraulic models that have been widely used for calculating pressure drop and holdup. Equations 2.1-5 represent the hydraulic models due to Rocha et al. (1993). This model was developed as an update of the previous hydraulic models (Bravo et al. (1985), Bravo et al. (1986), Fair and Bravo (1990)). Equations 2.6-14 represent the models developed by Billet and Schultes (1999) while Equations 2.15-17 are due to Stichlmair (1989). These models typically consider holdup and pressure drop to be dependent on each other. On the other hand, Equation 2.18 represents a model of the holdup which is independent of the pressure drop. It is observed in the work of Tsai (2010) that the accuracy of Equation 2.18 is higher than the models for holdup that are coupled with the pressure drop model. This model showed an average error of 12% for the entire database considered by Tsai (2010), but the results for the MellapakPlus™ 252Y had an error of above 20% for most of the cases.

The pressure drop, ΔP , can be calculated using Equations 2.1 and 2.2, as a function of the gas density ρ_G, he packing channel size *S*, the packing void fraction ε, the packing corrugation angle α, the gas velocity u_G and the gas viscosity μ_G.

The holdup calculation is presented in Equations 2.3-5, in which ρ_L is the liquid density, μ_L is the liquid viscosity, u_L is the liquid velocity. It is important to note that the holdup model is tied to the pressure drop

calculation by the effective gravity g_{eff} and the correction factor F_T, which is calculated as a function of the dimensionless numbers of the liquid phase: Re_L, We_L and Fr_L.

In the hydraulics correlation given by the Equations 2.6-13 (Billet and Schultes, 1999), the pressure drop, $\Delta P/z$, is a function of the parameter C_P , the gas phase Reynolds number, $Re_{G,}$ the void fraction of the packing, ε, the column holdup, h_L , the holdup bellow the loading point, $h_{L,S}$, the Froude number, Fr_L , the specific packing area, a, and the gas capacity factor, F_0 . The parameter *K* is a lumped term that is a function of the packing void fraction, ε, the packing specific diameter, d_P, and the column diameter, d_S. The holdup, h_L, is a function of liquid viscosity, μ_L, the packing specific area, a, the gravity acceleration, g, the liquid velocity, u_L, the liquid density, ρ_L. Above the loading point, the holdup becomes also a function of the gas velocity, u_G, the gas velocity in the flooding point, $u_{G,FL}$, the water viscosity, μ_{water}, the water density, ρ_{water}, and the parameter C_H.

Pressure drop and holdup of a packing depend on the flooding point of a given packing and therefore can restrict applicability of a given model. In the work of Tsai (2010), a value of 1025 Pa/m for the pressure drop has been suggested at the flooding point. The model developed by Billet and Schultes (1999) explicitly takes care of this aspect. In this model, under the loading point, which is defined as the flow regime in which the liquid flow does not significantly decrease the packing void fraction available for the gas flow, the holdup model is given by Equation (2.8). As the liquid flowrate is increased, the towers goes through a transition region ($u_{G,S}<u_G<u_{G,FL}$) before it eventually floods ($u_G>u_{G,FL}$). The model provides two correlations, one for the pre-loading region ($u_G < u_{GS}$) and another for the loading region ($u_{GS} < u_G$).

Table 2.1 - Summary of hydraulic models

Authors	Correlation	Eq. No.
Rocha (1993)	$\frac{\Delta P_{dry}}{Z} = \frac{0.177\,\rho_G}{S\varepsilon^2(\sin\alpha)^2}u_G^2 + \frac{88.774\,\mu_G}{S^2\varepsilon\sin\alpha}u_G$	(2.1)
	$\frac{\Delta P}{Z} = \frac{\Delta P_{dry}}{Z}\left(\frac{1}{1-C_1 h_L}\right)^5$	(2.2)
	$h_L = \left(4\,\frac{F_t}{S}\right)^{2/3}\left(\frac{3\mu_L u_L}{\rho_L(\sin\alpha)\varepsilon g_{eff}}\right)^{1/3}$	(2.3)

$$g_{eff} = g\left[\left(\frac{\rho_L - \rho_G}{\rho_L}\right)\left(1 - \frac{\Delta P/Z}{\Delta P/Z_{flood}}\right)\right] \tag{2.4}$$

$$F_t = 29.12(We\ Fr)_L^{0.15}\frac{S^{0.359}}{Re_L^{0.2}\varepsilon^{0.6}(1 - 0.93\cos\gamma)(\sin\alpha)^{0.3}} \tag{2.5}$$

Billet and Schultes (1999)

$$\frac{\Delta P}{Z} = C_P\left(\frac{64}{Re_G} + \frac{1.8}{Re_G^{0.08}}\right)\left(\frac{\varepsilon - h_L}{\varepsilon}\right)^{1.5}\left(\frac{h_L}{h_{L,S}}\right)exp\left(13300\frac{Fr_L}{a^{1.5}}\right)\frac{a}{(\varepsilon - h_L)^3}\frac{F_G^2}{2}\frac{1}{K} \tag{2.6}$$

$$\frac{1}{K} = 1 + \frac{2d_P}{3(1-\varepsilon)d_S} \tag{2.7}$$

ug < ugs (bellow loading point)

$$h_L = h_{L,S} = \left(\frac{12\mu_L u_L a^2}{g\rho_L}\right)^{1/3} \tag{2.8}$$

ug > ugs (above loading point)

$$h_L = h_{L,S} + (h_{L,FL} - h_{L,S})\left(\frac{u_g}{u_{g,FL}}\right)^{13} \tag{2.9}$$

$$h_{L,FL} = 2.2h_{L,S}\left(\frac{\mu_L\rho_{water}^2}{\mu_{water}\rho_L^2}\right)^{0.05} \tag{2.10}$$

$$h_{L,S} = \left(\frac{12\mu_L u_L a^2}{g\rho_L}\right)^{1/3}\left(\frac{a_h}{a}\right)^{2/3} \tag{2.11}$$

$$Re_L < 5: \quad \frac{a_h}{a} = C_h\left(\frac{u_L\rho_L}{\mu_L a}\right)^{0.15}\left(\frac{u_L^2 a}{g}\right)^{0.1} \tag{2.12}$$

$$Re_L \geq 5: \quad \frac{a_h}{a} = C_h 0.85\left(\frac{u_L\rho_L}{\mu_L a}\right)^{0.25}\left(\frac{u_L^2 a}{g}\right)^{0.1} \tag{2.13}$$

$$\frac{\Delta P_{dry}}{Z} = C_P\left(\frac{64}{Re_G} + \frac{1.8}{Re_G^{0.08}}\right)\frac{a}{\varepsilon^3}\frac{F_G^2}{2}\frac{1}{K} \tag{2.14}$$

Stichlmair (1989)

$$\frac{\Delta P}{Z} = 0.75\frac{1-\varepsilon}{\varepsilon^{4.65}}f_0\rho_G\frac{u_G^2}{d_P}\left[\frac{1 - \varepsilon\left(1 - \frac{h_L}{\varepsilon}\right)}{1-\varepsilon}\right]^{\frac{2+C}{3}}\left(1 - \frac{h_L}{\varepsilon}\right)^{-4.65} \tag{2.15}$$

$$C = \frac{-\frac{C_1}{Re_G} - \frac{C_2}{2Re_G^{0.5}}}{\frac{C_1}{Re_G} + \frac{C_2}{Re_G^{0.5}} + C_3} \tag{2.16}$$

$$h_L = 0.555 u_G^2 \frac{a_p}{g \varepsilon^{4.65}} \left[1 + 20 \left(\frac{\Delta P}{Z \rho_L g}\right)^2\right] \quad (2.17)$$

Tsai (2010)

$$h_L = H_{L1} \left[\frac{1}{S^2 g^{2/3}} \left(\frac{\mu_L}{\rho_L}\right)^{1/3} \frac{A\, u_L}{L_P}\right]^{H_{L2}} \quad (2.18)$$

Holdup model selection

For parameter regression and model evaluation, the holdup data reported by Tsai (2010) for Mellapakplus™ 252Y were used. Experimental conditions in the work of Tsai (2010) span gas and liquid flowrates from under the loading region up to the flooding point for low viscosity (1 mPa.s) and high viscosity systems (10 mPa.s). A nonlinear least squares method was used for regression of the packing-specific parameters in Matlab. The optimization problem was solved considering an objective function weighted/normalized by the experimental data variance. In this work, parameters for both holdup and pressure drop models were simultaneously regressed for the Stichlmair model (Stichlmair, 1989) and Rocha model, (Rocha, 1993) due to their interdependence while for the Billet and Schultes model (Billet and Schultes, 1999), the parameters for the holdup model were regressed first followed by regression of the parameters of the pressure drop model. Comparisons of the regressed models are presented in Figure 2.1 and Figure 2.2 for low and high viscosity systems, respectively. The root mean squared error for each model for the entire data is presented in Table 2.2. It should be noted that even though Tsai (2010) did consider the same data that are considered here while regressing the same parameters, the model error could be reduced further as observed in Figure 2.3 and Figure 2.4 and in Table 2.2.

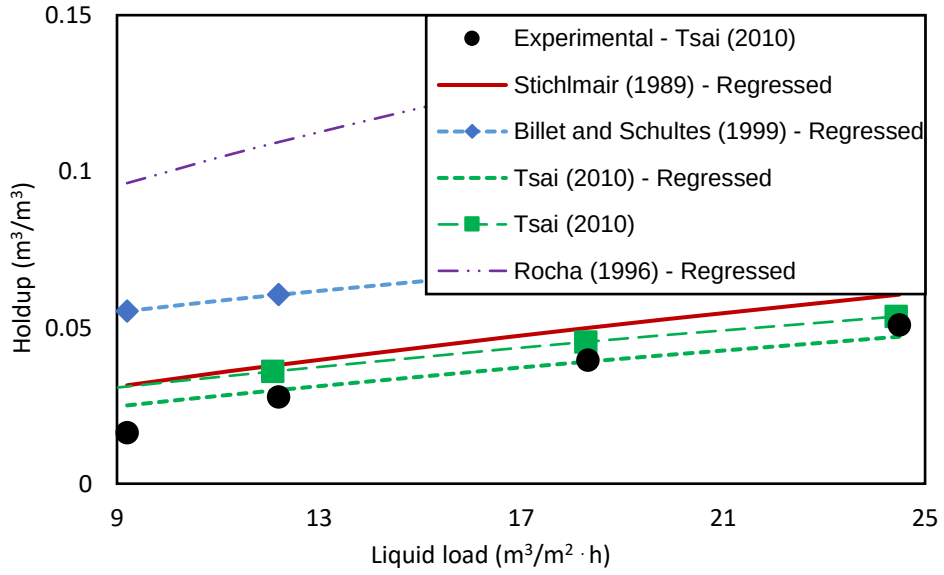

Figure 2.1 - Comparison of various holdup models for MellapakPlusTM 252Y operating with a low viscosity liquid (1 mPa. s) at FV=1.02 $Pa^{0.5}$

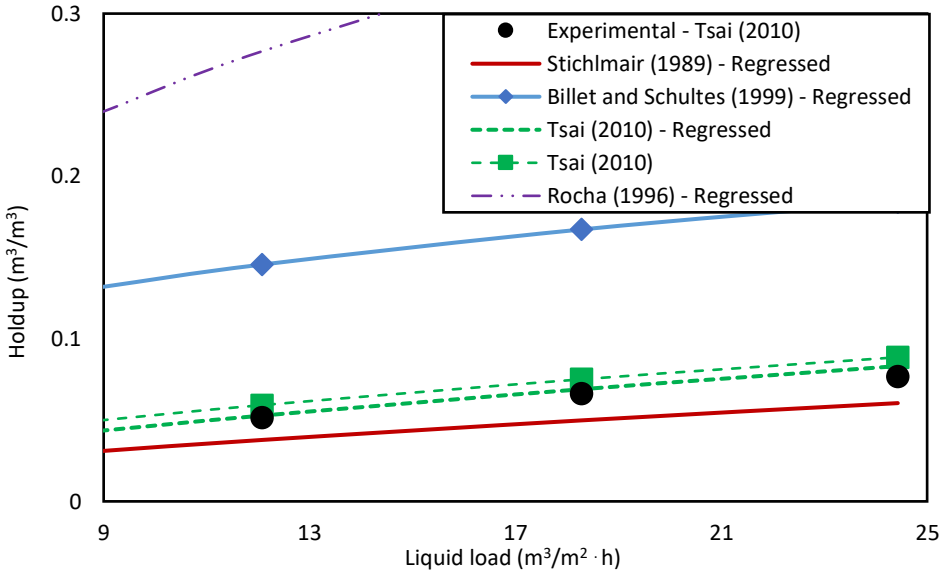

Figure 2.2 - Comparison of various holdup models for MellapakPlusTM 252Y operating with a high viscosity liquid (10 mPa. s) at FV=1.02 $Pa^{0.5}$

Table 2.2 shows that the RMSE for the Billet and Schultes (1999), Stichlmair (1989) and Rocha (1996) models has negligible change due to regression when compared to the corresponding unregressed models with parameters for Mellapak™ 250Y, which has a strong structural similarity to MellapakPlus™ 252Y. For both the high viscosity and low viscosity systems, the Rocha (1996) model has large error followed by the Billet and Schultes (1999) model. Both the Stichlmair (1989) and Tsai (2010) models have low errors while the regressed Tsai (2010) model has the least error for both the low viscosity and high viscosity systems and therefore it is selected as the final model.

Table 2.2 - Root Mean Squared Error values for the holdup models

Model	RMSE ($\%v$)
Stichlmair (1989)	0.0138
Stichlmair (1989) - Regressed	0.0135
Billet and Schultes (1999)	0.0665
Billet and Schultes (1999) - Regressed	0.0665
Tsai (2010)	0.0095
Tsai (2010) - Regressed	0.0074
Rocha (1993)	0.1748
Rocha (1993) - Regressed	0.1745

Pressure drop model selection and optimization

Other than the simultaneous regression of the pressure drop and holdup model parameters for the Stichlmair model (Stichlmair, 1989) and the Rocha model, (Rocha, 1993), and sequential regression for the Billet and Schultes model (Billet and Schultes, 1999), it was desired to evaluate error of the Stichlmair, Rocha and Billet and Schultes pressure drop models while using the regressed Tsai model (2010) for holdup. Figure 2.5 compares experimental data with the model results for pressure drop as a function of the F-factor F_G,

which is the square root of the product between the gas superficial velocity and its density, for the low and high viscosity systems, respectively. The RMSE values of the investigated models are presented in Table 2.3. It can be observed from Figure 2.5 and Table 2.3 that when the regressed Tsai model is used for holdup, errors of all three pressure drop models get significantly reduced. Furthermore, Table 2.3 shows that while the unregressed Rocha (1993) model has the highest and very large error, its error gets significantly reduced upon regression, finally yielding much lower error than the regressed Stichlmair model when the regressed Tsai model is used as the holdup model for both cases. The final models selected for the MellapakPlus™ 252Y are the regressed Billet and Schultes (1999) model for pressure drop and the regressed Tsai (2010) model for holdup. It is worth mentioning that although this hydraulic model can satisfactorily predict the pressure drop, the quality of the prediction deteriorates at higher pressure drop values, or under higher liquid and gas flowrates approaching the flooding point. This behavior can be observed in the parity plot of the entire data from Tsai (2010), presented in Figure 2.7.

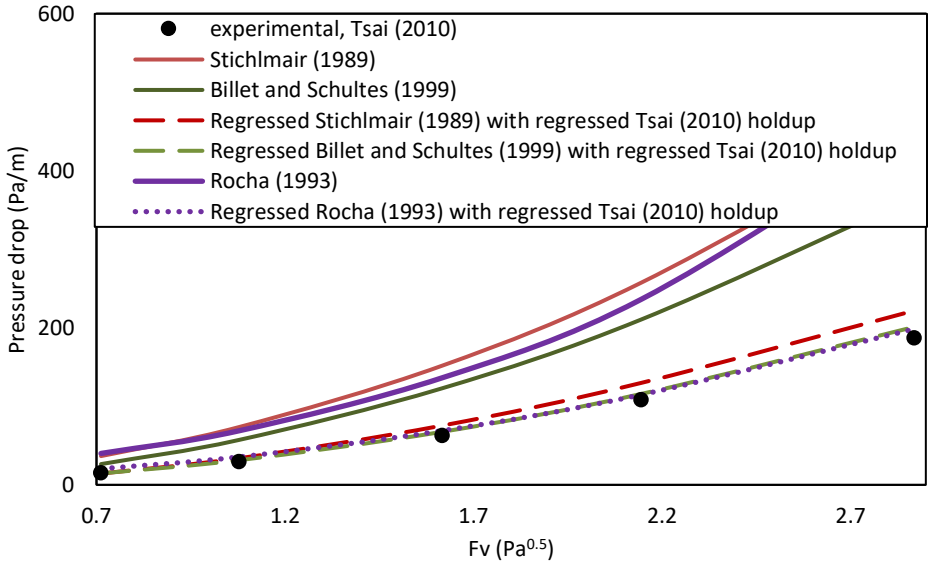

Figure 2.3 - Comparison of pressure drop models for the low-viscosity case

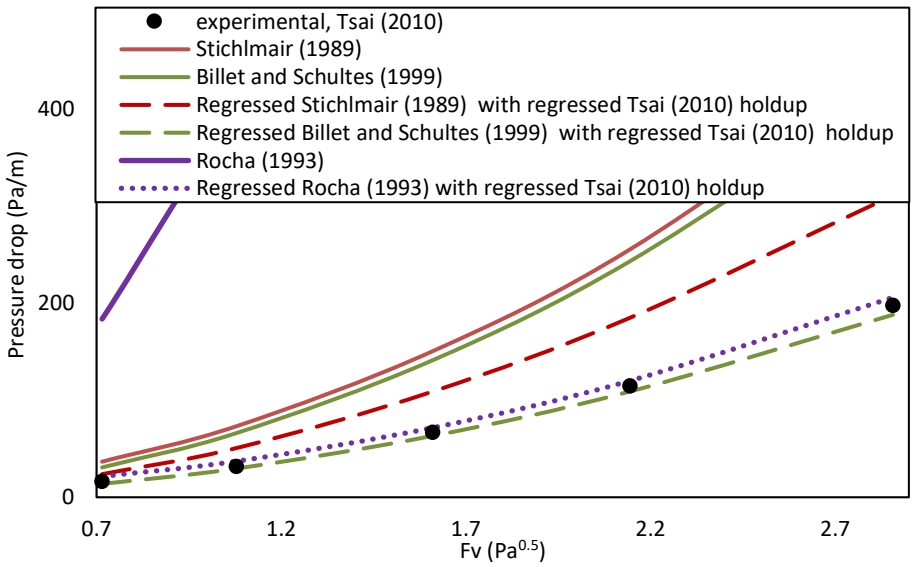

Figure 2.4 - Pressure drop candidate models validation in a high-viscosity case

Table 2.3 - Total root mean squared error values for the pressure drop models

Correlation	RMSE values (Pa)
Stichlmair (1989)	162.97
Billet and Schultes (1999)	95.97
Rocha (1993)	325.58
Stichlmair (1989) regressed	57.36
Billet and Schultes (1999) regressed	40.25
Rocha (1993) regressed	48.48
Regressed Stichlmair (1989) with modified holdup model	46.26
Billet and Schultes (1999) regressed with modified holdup model	10.49
Rocha (1993) regressed with modified holdup model	25.88

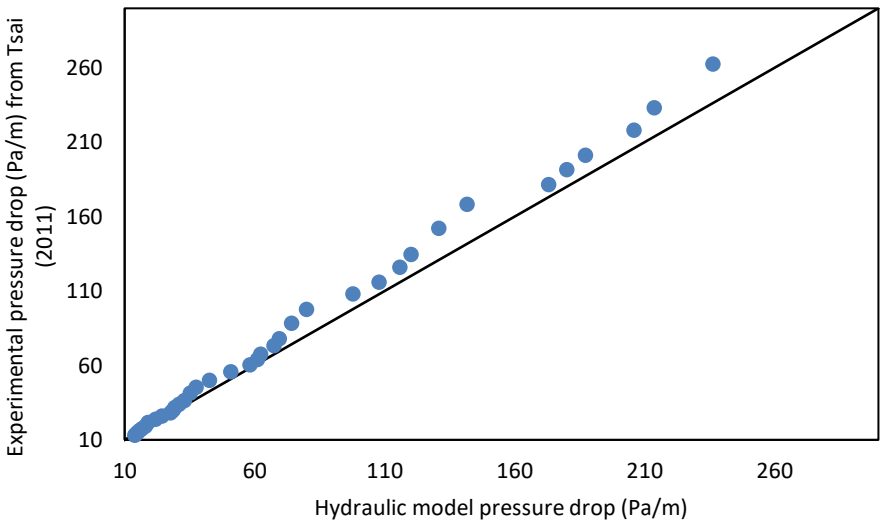

Figure 2.5 - Parity plot of the regressed Billet and Schultes (1999) with regressed Tsai (2010) holdup

2. 2. Mass transfer and kinetic models

As mentioned earlier, an integrated mass transfer model is developed here where the model selection and parameter estimation for diffusivity, interfacial area, liquid- and gas-side mass transfer coefficients, and reaction kinetics are carried out simultaneously using the data from the WWCs and packed towers. Mathematically, the key differences of this simultaneous approach to the traditional sequential approach are due to the solution to the optimization problem that are solved. In the traditional approach, assume, that two steps of sequential optimization problems are solved as shown below.

Sequential Optimization Approach (assuming a two stage approach is used):

First Stage Optimization (Typically applied to a smaller scale apparatus or equipment type such as WWC)

$$\min_{\theta_1} \left(y_1 - y_{1,meas}\right)' \Sigma^{-1} \left(y_1 - y_{1,meas}\right) \tag{2.19}$$

$s.t.$

$$f_1(\eta_1\ ,\ u,\ \theta_1) = 0$$

$$g_1(\eta_1,\ u, \theta_1) \leq 0$$

$$y_1 = h_1(\eta_1,\, u)$$

$$u_{L_1} \le u \le u_{U_1}$$

$$y_{L_1} \le y_1 \le y_1$$

Second Stage Optimization (Typically applied to a larger scale apparatus or equipment type such as a packed tower)

$$\min_{\theta_2} \left(y_2 - y_{2,meas}\right)' \Sigma^{-1} \left(y_2 - y_{2,meas}\right) \tag{2.20}$$

$s.t.$

$$f_2(\eta_2,\, u,\, \theta_1, \theta_2) = 0$$

$$g_2(\eta_2,\, u, \theta_1, \theta_2) \le 0$$

$$y_2 = h_2(\eta_2,\, u)$$

$$u_{L_2} \le u \le u_{U_2}$$

$$y_{L_2} \le y_2 \le y_{U_2}$$

Simultaneous Optimization Approach (apparatus/equipment of all types spanning different scales):

$$\min_{\theta_1, \theta_2} \left(y_1 - y_{1,meas}\right)' \Sigma^{-1} \left(y_1 - y_{1,meas}\right) + \left(y_2 - y_{2,meas}\right)' \Sigma^{-1} \left(y_2 - y_{2,meas}\right) \tag{2.21}$$

$s.t.$

$$f_1(\eta_1\, ,\, u,\, \theta_1) = 0$$

$$f_2(\eta_2,\, u,\, \theta_1, \theta_2) = 0$$

$$g_1(\eta_1,\, u, \theta_1) \le 0$$

$$g_2(\eta_2,\, u, \theta_1, \theta_2) \le 0$$

$$y_1 = h_1(\eta_1, u)$$

$$y_2 = h_2(\eta_2, u)$$

$$min(u_{L1}, u_{L2}) \leq u \leq max(u_{U1}, u_{U2})$$

$$y_{L_1} \leq y_1 \leq y_{U_1}$$

$$y_{L_2} \leq y_2 \leq y_{U_2}$$

In Equations (19-21), y represents an arbitrary measured variable bounded between y_L and y_U , η represent process variables, and θ represents model parameters. Input variables, u, are bounded between u_L and u_U.

Remarks:

- If the solutions to the 1st step and 2nd step optimizations of the sequential optimization techniques are unique, then the solutions obtained from the simultaneous and sequential optimizations would be the same.
- Total estimation errors can be the same between two approaches, i.e. estimation error from the 1st step plus 2nd step of the sequential approach can be the same as the error from the simultaneous approach if the same data are used in both the approaches, but parameters can be different. Therefore, the models/ parameters from both approaches should be evaluated for their prediction capability for new sets of data that have not been 'seen' by both approaches.
- The solutions from the simultaneous approach can be superior to the sequential approach, but should not be inferior as information content and the search space in each step of the sequential optimization is a subset of those in the simultaneous optimization approach.

First the individual models are described followed by a description of the methodology developed in this work. Finally, the results from the integrated mass transfer model are presented.

2.2.1. Mass transfer coefficient model

Several correlations for calculating mass transfer coefficients exist (Razi et al., 2012). The correlations that are evaluated in this work are listed in Table 2.4. Equations 2.22 and 2.23 represent the mass transfer coefficients proposed by Bravo et. al (1985) as part of the Separation Research Program in UT-Austin. These were later updated in the work of Rocha et al. (1996), represented by Equations 2.24 and 2.25. Equations 2.26 and 2.27 represent the model proposed by Billet and Schultes (1999), in which a large data base was utilized to regress parameters C_G and C_L.

Table 2.4 - Mass transfer coefficients models

References	Correlation	
Bravo et al. (1985)	$k_G = 0.0338 \frac{D_G}{d_{eq}} \left(\frac{\rho_G d_{eq} (u_{Le} + u_{Ge})}{\mu_G} \right)^{0.8} Sc_G^{0.33}$	(2.22)
	$k_L = 2 \sqrt{\frac{D_L}{\pi S} u_{Le}}$	(2.23)
	$u_{Le} = \frac{9\,\Gamma^2 g}{8\,\rho_L \mu_L \sin\alpha}\ ;\ u_{Ge} = \frac{u_G}{\varepsilon \sin\alpha}$	
Rocha et al. (1996)	$k_G = 0.054 \frac{D_G}{S} \left(\frac{\rho_G S (u_{Le} + u_{Ge})}{\mu_G} \right)^{0.8} Sc_G^{0.33}$	(2.24)
	$k_L = 2 \sqrt{\frac{0.9 D_L}{\pi S} u_{Le}}$	(2.25)
	$u_{Le} = \frac{u_L}{\varepsilon\, h_L \sin\alpha}\ ;\ u_{Ge} = \frac{u_G}{\varepsilon(1 - h_L)\sin\alpha}$	
Billet and Schultes (1999)	$k_G = D_G C_G \left(\frac{a}{d_H} \right)^{0.5} Sc_G^{0.333} \left(\frac{u_G \rho_G}{a \mu_G} \right)^{0.75} \sqrt{\frac{1}{\varepsilon - h_L}}$	(2.26)
	$k_L = C_L \left(\frac{g \rho_L}{\mu_L} \right)^{0.167} \left(\frac{D_L}{d_H} \right)^{0.5} \left(\frac{u_L}{a} \right)^{0.333}$	(2.27)

2.2.2. Interfacial area model

The effective interfacial area depends on a number of factors including packing geometry and its surface properties, physical properties of the system such as the surface tension, and density of the liquid as well as the operating conditions such as the liquid velocity. Table 2.5 shows the leading correlations for interfacial area that are evaluated in this work. The interfacial area model proposed by Bravo et. al (1985), presented in Equation 2.28, is based on the assumption that the packing is entirely wetted during operation. Billet and Schultes (1999) proposed a model that is presented in Equation 2.29. Equation 2.30 is due to Tsai (2010) and uses dimensionless numbers for the prediction of the wetted area.

Table 2.5 - Interfacial area models

Authors	Correlation	
Bravo (1985)	$a_e = a_p$	(2.28)
Billet and Schultes (1999)	$a_h = 1.5\left(\frac{a_p}{d_h}\right)^{-0.5}\left(\frac{\rho_L u_L d_h}{\mu_L}\right)^{-0.2}\left(\frac{\rho_L u_L^2 d_h}{\sigma_L}\right)^{0.75}\left(\frac{u_L^2}{g\, d_h}\right)^{-0.45}$	(2.29)
Tsai (2010)	$a_h = A_1\left[\frac{\rho_L}{\sigma} g^{1/3}\left(\frac{u_L A}{L_P}\right)^{4/3}\right]^{A_2}$	(2.30)

2.2.3. Diffusivity model

It is practically impossible to measure diffusivity of CO_2 in the MEA-H_2O system due to the fast chemical reactions. Typical approach to circumvent this issue is to consider a non-reactive system such as the diffusion of CO_2 into H_2O (Glasscock, 1990; Versteeg et al., 1987; Versteeg et al., 1988) or the diffusion of N_2O into a MEA-H_2O system (Ying and Eimer, 2012). However, as discussed before, diffusivity of CO_2 measured from such non-reactive systems may not be necessarily the same as in the reactive system. Since the mass transfer data from the WWCs and packing captures the effect of diffusivity as well, it is desired to regress the parameters of the diffusivity model as well in the integrated approach. Equations 2.31 and 2.32 represent the diffusivity models, where D_{CO2o} and D_{MEAo} refers to CO_2 and MEA diffusivity in water, respectively, under reference condition (Plaza, 2011). In this work, only the parameter n is regressed.

$$D_{CO2-sln} = \frac{D_{CO2o}}{D_{MEAo}}\left(\frac{\mu_{water}}{\mu_{sin}}\right)^{0.8}\left(\frac{T}{313.15}\right)^{n} \quad (2.31)$$

$$D_{MEA-sln} = D_{MEAo}\left(\frac{\mu_{water}}{\mu_{sin}}\right)^{0.8}\left(\frac{T}{313.15}\right)^{n} \quad (2.32)$$

2.2.4. Reaction Kinetics

Reaction kinetics of the MEA-H_2O-CO_2 system has been studied by several authors (Austgen et al. 1989; Versteeg et al. 1996; Hilliard, 2008; Plaza, 2011). In this work a reduced set of reactions represented by Equations 2.33 and 2.34 is considered (Plaza ,2011; Morgan et. al., 2017). Corresponding rate expressions are given by Equations 2.35 and 2.36. As discussed in the work of Morgan et. al. (2017), this particular form of reaction rate that includes activity coefficients of species given by a_i, ensures that the electrolyte system correctly approaches equilibrium consistent with the chemistry model (Mathias and Gilmartin, 2014). Expressions for the equilibrium constants and more details about the reactions models are available in our previous publication (Morgan et. al., 2017).

$$2MEA + CO_2 \underset{K_{EQ1}}{\longleftrightarrow} MEA^+ + MEACOO^- \quad (2.33)$$

$$MEA + CO_2 + H_2O \underset{K_{EQ2}}{\longleftrightarrow} MEA^+ + HCO_3{}^- \quad (2.34)$$

$$r_1 = k_{F1}e^{-\frac{EA1}{R}\left(\frac{1}{T}-\frac{1}{298.15}\right)}\left(a_{MEA}^2 a_{CO_2} - \frac{a_{MEACOO}a_{MEAH}}{K_{EQ1}}\right) \quad (2.35)$$

$$r_2 = k_{F2}e^{-\frac{EA2}{R}\left(\frac{1}{T}-\frac{1}{298.15}\right)}\left(a_{MEA}a_{CO_2} - \frac{a_{MEAH}a_{HCO_3}}{K_{EQ2}a_{H_2O}}\right) \quad (2.36)$$

2.2.5. Integrated model selection and methodology

Models of the tower and WWC are developed in Aspen Plus® V8.4 by using the Aspen plus® RateFrac™ block. As it was desired to obtain the packing specific parameters for the interfacial area model for MelapakPlus 252Y, it was desired to use mass transfer data from a tower with MellapakPlus 252Y or with

a packing that is structurally similar to it. Therefore, mass transfer data from Tobiesen et al. (2007) for MEA-H_2O-CO_2 system in a relatively wide range of operating conditions are used. Even though the data from Tobiesen et al. (2007) is from Mellapak 250Y, it is structurally similar to MellapakPlus 252Y (Tsai, 2010). The tower model is set up as per the dimensions and packing information from Tobiesen et al. (2007). The WWC data are obtained from the work of Dugas (2009). The WWC model is developed using the same rate-based model as the tower, but a fixed interfacial area is used instead.

As noted earlier, parameter estimation of such an integrated model is not currently feasible in Aspen Plus mainly because of the segregation of the diffusivity model, reactions model, and the selected mass transfer coefficients and interfacial area models. To circumvent this issue, the FOQUS framework developed as part of U.S. DOE's CCSI (Miller et al., 2015) is used. The FOQUS framework facilitates optimization, quantification of uncertainty and development of surrogate models (Miller et al., 2015). The objective function is presented in Equation 2.37. The problem is solved by the derivative free optimizer "BOBYQA" (Powell, 2009) as the derivative calculation is not feasible due to the external call to Aspen Plus.

$$objective = \left(\frac{Cap_{CO_2,exp} - Cap_{CO_2,pred}}{Cap_{CO_2,exp}}\right)' \Sigma^{-1} \left(\frac{Cap_{CO_2,exp} - Cap_{CO_2,pred}}{Cap_{CO_2,exp}}\right) + \left(\frac{Flux_{CO_2,exp} - Flux_{CO_2,pred}}{Flux_{CO_2,exp}}\right)' \Sigma^{-1} \left(\frac{Flux_{CO_2,exp} - Flux_{CO_2,pred}}{Flux_{CO_2,exp}}\right) \quad (2.37)$$

2.2.6. Integrated mass transfer model regression results

Mass transfer sub-models presented in Table 2.4 and Table 2.5 are implemented using FORTRAN subroutines, if not available in the Aspen plus® model library. Minimum value of the objective function of each combination is presented in Table 2.6, which shows that the Billet and Schultes (1999) model for the mass transfer coefficients, combined with the Tsai (2010) model for the interfacial area provide the best combination out of the candidate models considered here.

Table 2.6 - Minimum value of the objective function for various combinations of mass transfer coefficient and interfacial area models

Combination	Mass transfer coefficient	Interfacial area	Objective Function
1	Billet and Schultes (1999)	Billet and Schultes (1999)	1.32
2	Billet and Schultes (1999)	Bravo (1985)	2.58
3	Billet and Schultes (1999)	Tsai (2011)	1.15
4	Bravo (1985)	Billet and Schultes (1999)	3.53
5	Bravo (1985)	Bravo (1985)	2.43
6	Bravo (1985)	Tsai (2011)	1.75
7	Rocha et al. (1996)	Billet and Schultes (1999)	5.40
8	Rocha et al. (1996)	Bravo (1985)	5.18
9	Rocha et al. (1996)	Tsai (2011)	5.04

Table 2.7 compares the typical values of the parameters from the literature versus the optimal values of the parameters for all models considered in the simultaneous optimization approach. Typical values of the parameters are extracted from literature models that have regressed one or more parameters by using at least a portion of the experimental data considered here. For example, Plaza (Plaza, 2011) has used the same WWC data considered here (Dugas, 2009) for obtaining their kinetic parameters. The final integrated mass transfer model comprises of the regressed Billet and Schultes (1999) model for mass transfer coefficient (Equations 2.26-27), the regressed Tsai (2010) model for interfacial area (Equation 2.30), the regressed diffusivity model given by Equations 2.31-32 and the regressed kinetic model given by Equations 2.33-36 with the regressed parameters presented in Table 2.7.

Figure 2.6 - 2.8 present parity plots for the packed tower and WWC comparing the final integrated mass transfer model using the regressed parameters with the same models as the integrated mass transfer model but using the literature parameters listed in Table 2.7. Both figures show that the accuracy of the selected models especially in the 60-80% CO_2 capture rate was improved due to regression. In Figure 2.7Figure 2.6, the gain in the WWC model is not apparent looking at the figure, as most of the improvements on the model

occurred at lower fluxes. Figure 2.8 zooms into the lower flux region showing the improvements due to simultaneous regression. The objective function value corresponding to only the WWC data is 177.02 and 163.22 for literature parameters and the integrated model parameters, respectively. Likewise, the objective function value corresponding to only the packed tower data is 1.06 and 0.41 for literature parameters and the integrated model parameters, respectively.

Table 2.7 - Literature values vs the optimal values obtained through simultaneous regression approach for all models considered in the integrated mass transfer model

Parameter	Typical value from the literature	Reference	Regressed value
C_L	0.50	Billet and Schultes (1999)	0.203
C_G	0.37	Billet and Schultes (1999)	0.35
A_1	1.34	Tsai (2010)	1.42
A_2	0.12	Tsai (2010)	0.12
n	22.19	Plaza (2011)	21.81
k_{F1}	3963.90	Morgan et al. (2017)	3763.9
EA1	2.51×10^9	Morgan et al. (2017)	2.51×10^9
k_{F2}	22991.13	Morgan et al. (2017)	22959.57
EA2	49000.00	Morgan et al. (2017)	49745.08
RMSE	0.1040	-	0.0674

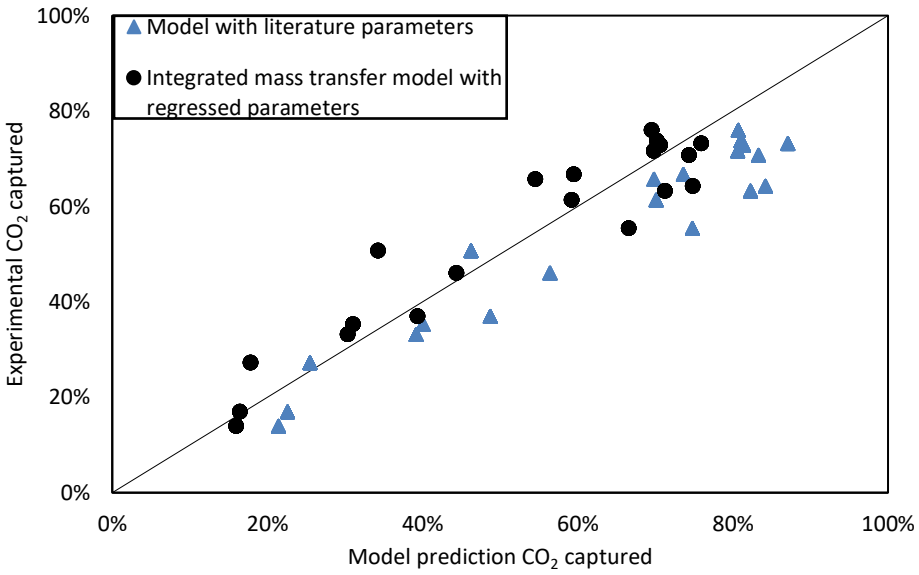

Figure 2.6 - Parity plot of the CO2 (%) capture in the absorber (Experimental data from Tobiesen et al., 2007)

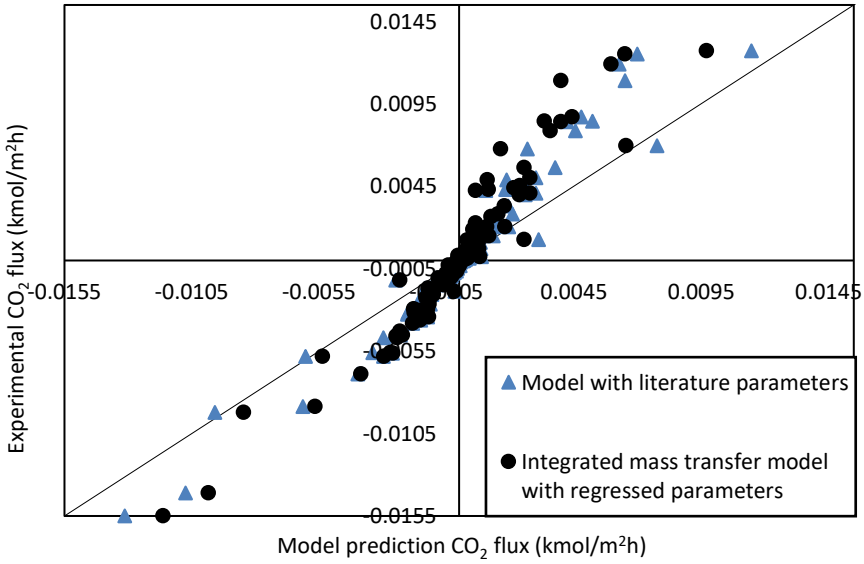

Figure 2.7 - Parity plot of the CO_2 flux in the WWC (Experimental data from Dugas, 2009)

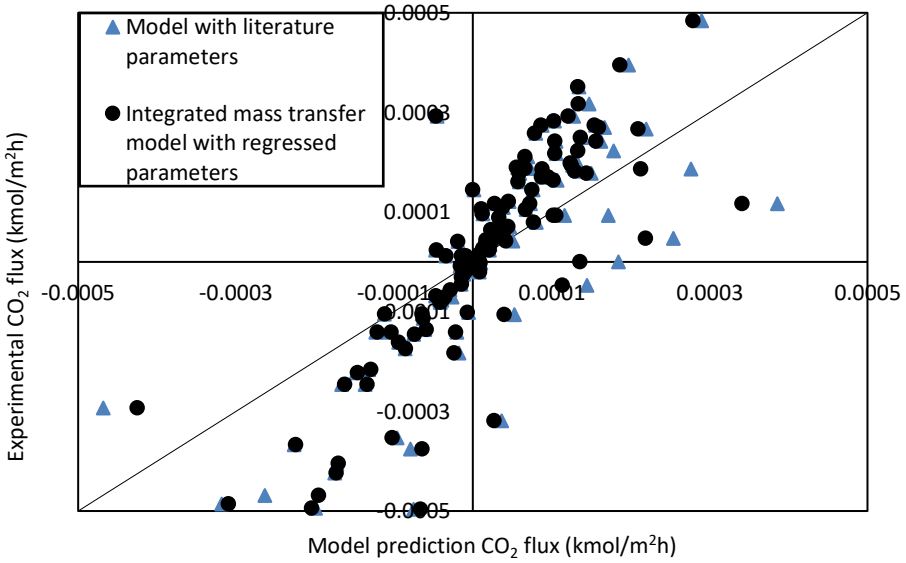

Figure 2.8 - Zoomed parity plot of the CO_2 flux in the WWC (Experimental data from Dugas, 2009)

Since the same data used in the simultaneous regression approach have been used in the sequential approach (for which the literature parameters have been presented in Table 2.7), regression results between the simultaneous approach vs the sequential approach may not differ much as seen in Figure 2.8, but the value

of the parameters may differ as seen in Table 2.7, since the parameters are not necessarily unique. To evaluate the improvement, if any, due to the simultaneous regression approach in comparison to the literature parameters that were obtained through sequential approach, predictive capabilities of the models/ parameters from both approaches should be evaluated using data that have not been 'seen' by both. The pilot plant data from the open literature for a similar packing (Notz et al., 2012) are used for this purpose. The data set span a wide range of operating conditions, with CO_2 capture rates varying from 40% to 90% and therefore serves as an excellent test set. The column has a diameter of 0.125 m, a height of 4.20 m packed with Mellapak™ 250Y similar to Tobiesen et al. (2007)), but was operated under a much wider range of liquid and gas flowrates. Figure 2.9 shows comparison between the integrated mass transfer model and literature parameter values for the absorber. The integrated mass transfer model has the lower error (RMSE of 5%) showing good prediction capability of the model when compared to parameter values from the literature (RMSE of 9%).

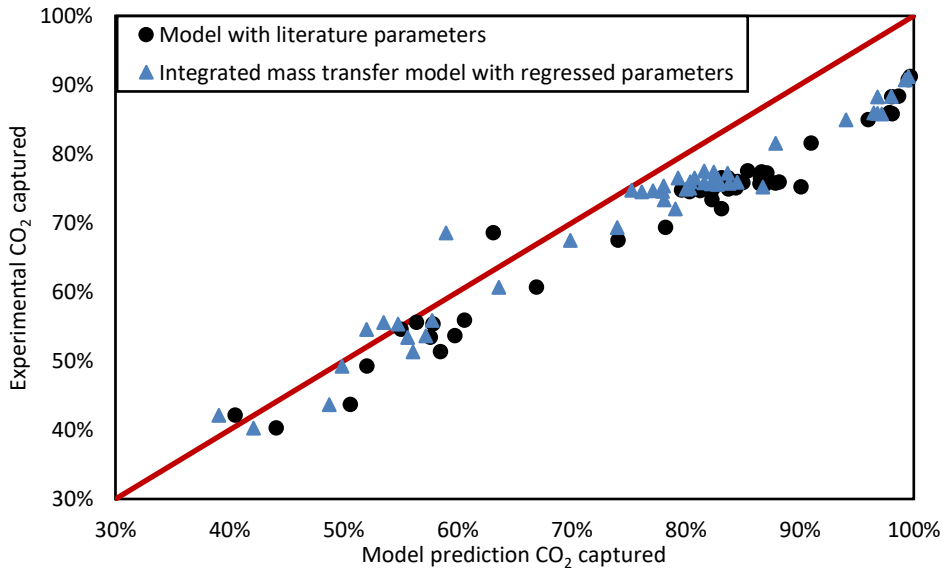

Figure 2.9 - Comparison of the literature model and integrated mass transfer model with data from Notz et al. (2012)

2. 3. Uncertainty Quantification (UQ)

The methodology for Bayesian UQ used in this work is similar to Morgan et al. (2015, 2017). However, Morgan et al. (2015, 2017) focused on thermodynamic and properties models where tower model was not required. Since the rate-based tower model with embedded thermodynamic and transport models needs to be considered for UQ of hydraulic and mass transfer models and the rate-based tower model is

computationally very expensive, complex, and highly nonlinear, UQ of hydraulic and mass transfer models becomes challenging. A brief summary of the UQ methodology is presented here.

2.3.1. Uncertainty quantification methodology

As per Bayes theorem:

$$\pi\left(\tilde{\theta}\middle|Z\right) \propto P\left(\tilde{\theta}\right)L\left(Z\middle|\tilde{\theta}\right) \tag{2.35}$$

, where $\pi\left(\tilde{\theta}\middle|Z\right)$ denotes the posterior distribution, $P\left(\tilde{\theta}\right)$ denotes the prior distribution of the parameters based on the initial belief, and $L\left(Z\middle|\tilde{\theta}\right)$ denotes the likelihood function.

Since the Bayesian inference requires thousands of simulations and the rate-based tower model is computationally expensive, a response surface model is developed by using the data generated by simulating the rigorous model the over the entire range of the prior distribution of the parameters as well as over the range of the operating conditions that spans the experimental input space. Multivariate Adaptive Regression Splines (MARS) models are found to be satisfactory as response surface models as evidenced by cross validation. It can be noted that for higher-order nonlinear systems, the MARS models have been reported to yield mean values estimates with lower errors and relatively higher robustness in comparison to other typical response surface models such as radial basis functions, polynomial regression, and kriging (Chen et al. (2001)).

To generate a response surface model, a normal distribution of the parameters is considered as priors with the standard deviations being estimated from the regression results. From this distribution, *N* samples are drawn by using Monte Carlo sampling method by adequately sampling from the priors. The rigorous model is then simulated for *M* process variables over the parameter samples resulting in (*M* x *N*) observations. The Markov Chain Monte Carlo (MCMC) algorithm with Gibbs sampling is used for approximating the multi-dimensional integral in the Bayesian inference finally yielding the posterior distributions of the parameters. More details about this approach can be found in our earlier publications (Morgan et al., 2015, 2017).

2.3.2. Hydraulics model UQ

Parametric UQ of the final pressure drop and hold models, i.e. regressed Billet and Schultes model (1999), given by Equation 2.6, and regressed Tsai (2010) model given by Equation 2.18, respectively, is carried out by using the experimental data from by Tsai (2010) for Mellapakplus™ 252Y. Means of the priors for the

parameters $C_{P,}$ H_{L1} and H_{L2} are taken to be the value obtained in the deterministic regression and their standard deviations are obtained using the covariance matrix and the matrix of correlation coefficients. By drawing 100 samples from three prior distributions using Monte Carlo sampling technique and by considering 68 experimental conditions (Tsai, 2010), a total of 20,400 (=68 x 300) data points are generated by simulating the rigorous model. These data are then used to generate the response surface model. Single-parameter marginal probability density functions for prior and posterior distributions are shown in Figure 2.10 while Figure 2.11 shows the two-parameter prior and posterior marginal distributions.

The probability density functions presented in Figure 2.10 and Figure 2.11 imply that no significant information about the holdup parameters H_{L1} and H_{L2} uncertainty could be obtained using the Bayesian Inference, as the prior and posterior probability density functions are almost overlapping. However, the pressure drop model parameter, C_P , has a narrower posterior distribution than the priors pointing to the improvement obtained using the Bayesian inference approach.

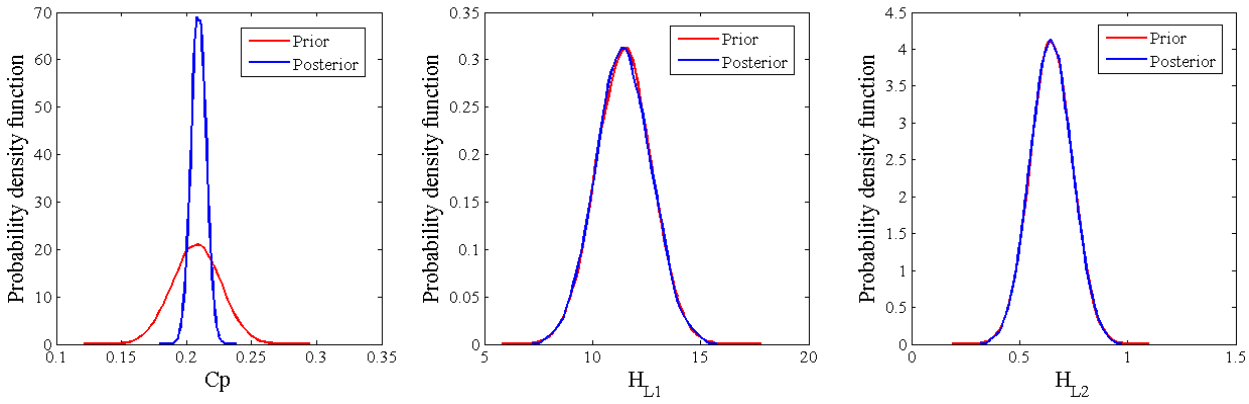

Figure 2.10 - Single-parameter prior and posterior marginal probability density functions of the parameters in the hydraulics model

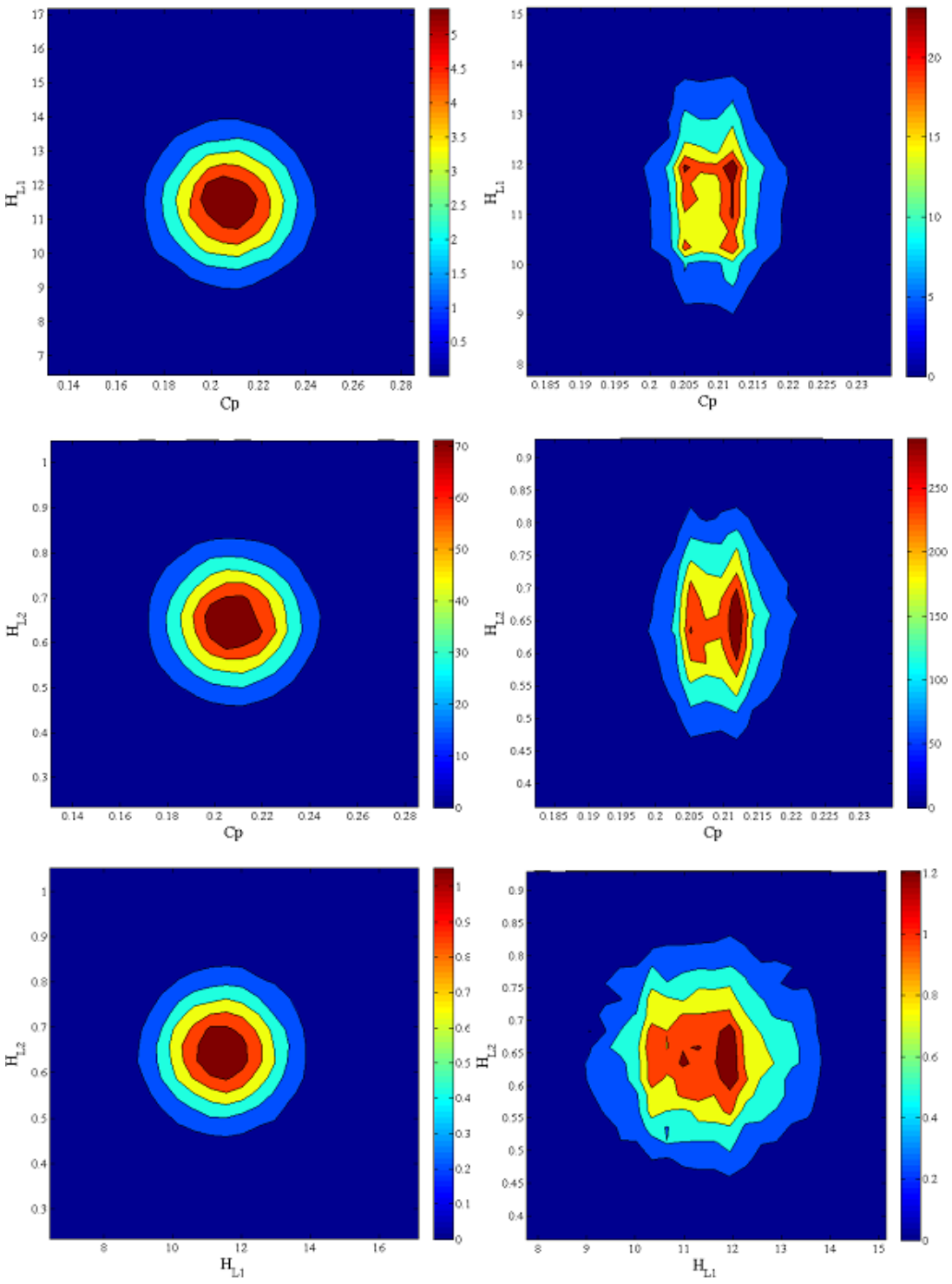

Figure 2.11 - Two-parameter prior and posterior marginal posterior distributions of the parameters in the hydraulics model.

Posteriors are propagated through the process models and uncertainties in pressure drop and holdup calculations are observed. Figure 2.12 shows uncertainty in pressure drop calculations with respect to F-factor, for a given liquid load, or velocity. Figures 2.12a/12b and Figures 2.12c/12d are generated for a liquid load of 6 $m^3/m^2 \cdot h$ and 18 $m^3/m^2 \cdot h$, respectively. Figures 2.12a/12c and Figures 12b/12d correspond to a system of viscosity 1 cP and 12 cP, respectively. Figure 2.13 shows uncertainty in holdup calculations with respect to the liquid load for a given F-factor. Figures 2.13a/13b and Figures 2.12c/13d are generated for an F-factor of 0.71 $Pa^{0.5}$ and 1.6 $Pa^{0.5}$, respectively. Figures 2.13a/13c and Figures 2.13b/13d correspond to a system of viscosity 1 cP and 12 cP, respectively. In both Figure 2.12 and Figure 2.13, relatively high uncertainty is observed. It should be noted that overall uncertainty could be further reduced if more experimental data were available.

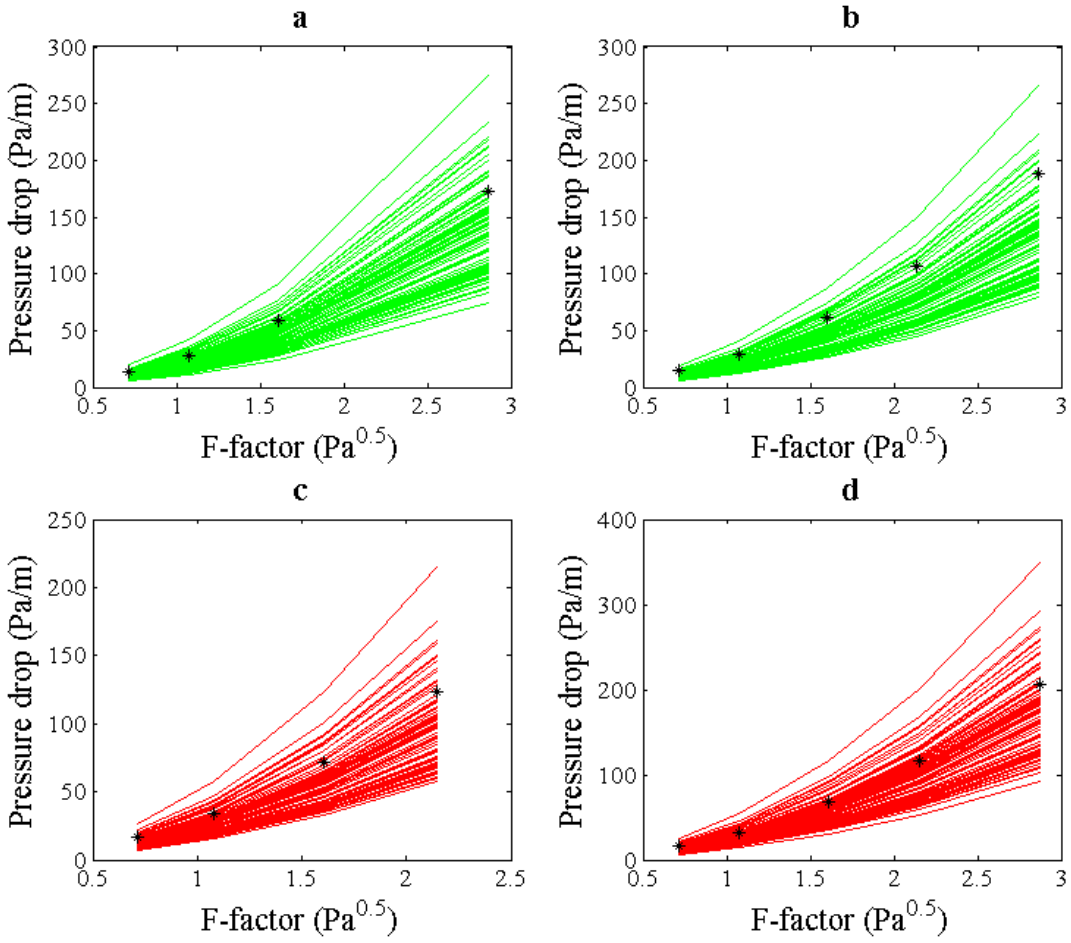

Figure 2.12 - Stochastic pressure drop model for a water-air system in a tower packed with MellapakPlusTM 252Y. The green lines represent a liquid load of 6 m3/m2·h and the red lines a liquid load of 18 m/h. Cases 'a' and 'c' corresponds to the liquid viscosity of approximately 12 cP '*' represent corresponding experimental data

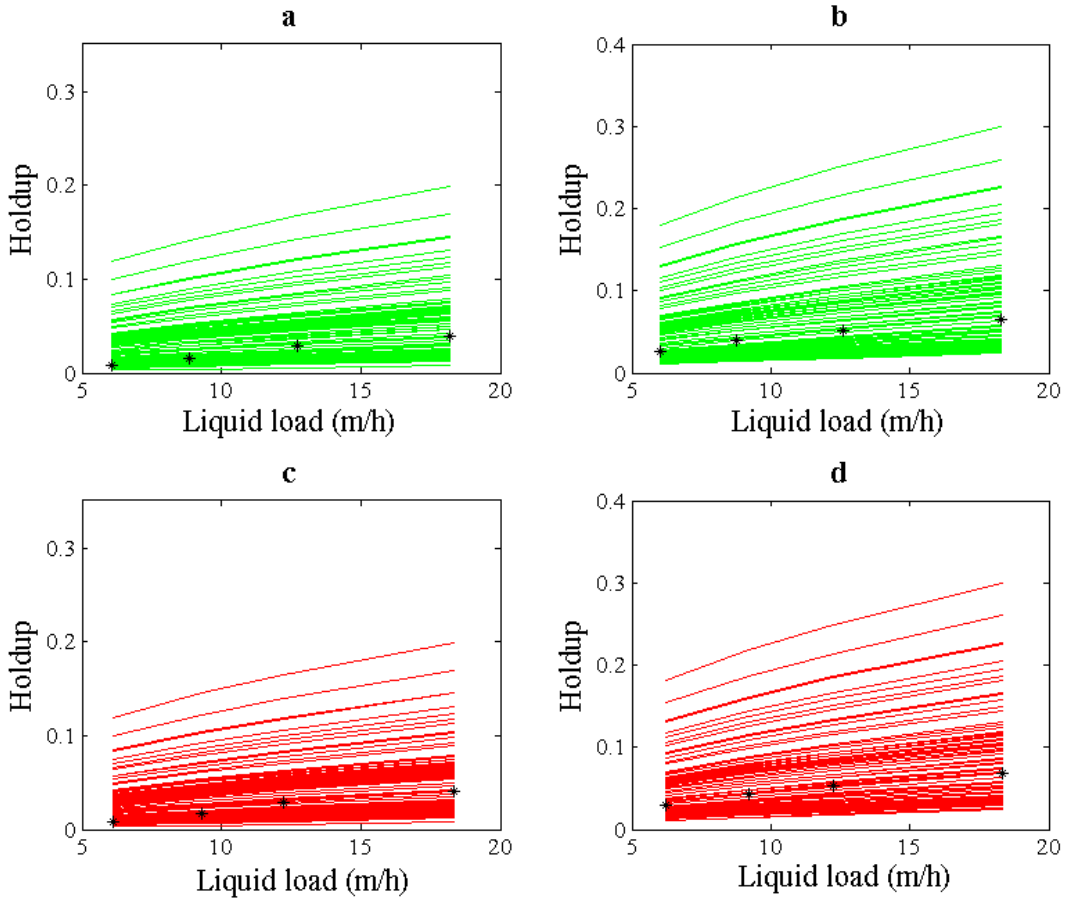

Figure 2.13 - Stochastic holdup model for a water-air system in a tower packed with MellapakPlusTM 252Y. The green lines represent an F-factor of 0.71 Pa0.5 and the red lines an F-factor of 1.6 Pa0.5. Cases 'a' and 'c' regards a viscosity of approximately 1 cP and 'd' a viscosity of approximately 12 cP

2.3.3. UQ of the integrated mass transfer model

Parametric UQ of the final integrated mass transfer model where the mass transfer coefficient model is given by Equation 2.23 and 2.14, the interfacial area model is given by Equation 2.27, the diffusivity model is given by Equations 2.28-29 and the kinetic model is given by Equations 2.30-33, respectively, is obtained by using the experimental data from Tobiesen et al. (2007). Unlike only three uncertain parameters in the hydraulic model, the integrated mass transfer model has 9 parameters, namely C_L, C_G, A_1, A_2, n, k_{F1}, $EA1, k_{F2}$, $EA2$. Generation of the response surface model and Bayesian inference can be very time consuming for large number of parameters. In addition, Bayesian inference is not expected to provide any useful insight on uncertainty of a given parameter if sensitivity to that particular parameter in the space of the experimental space is low. To reduce the parameter space that is investigated during UQ, a global sensitivity analysis using the Sobol index is performed so that parameters with relatively low sensitivity (low Sobol index) can be eliminated without compromising the result of the Bayesian inference. It can be noted that the Sobol sensitivity analysis is a popular variance-based method for identifying important parameters (Sobol, 1993). Figure 2.14 presents the results of the Sobol analysis for the input parameters. Considering a threshold of 0.08 for the Sobol index, the parameters C_G, A_2, n, k_{F1}, $EA1, k_{F2}$, $EA2$ are disregarded for the UQ.

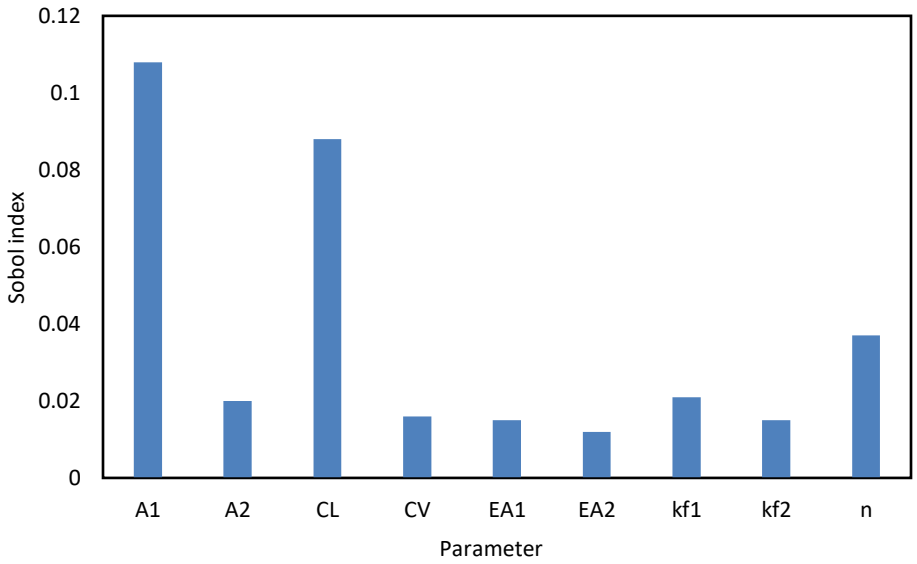

Figure 2.14 - Sobol analysis of the integrated mass transfer model

Therefore the only remaining parameters that are used to develop the response surface and subsequent Bayesian inference are A_1, corresponding to the interfacial area model, and C_L, corresponding to the liquid side mass transfer coefficient.

Methodology for developing the response surface model and Bayesian inference are similar to before. The posterior distributions are presented in Figure 2.15.

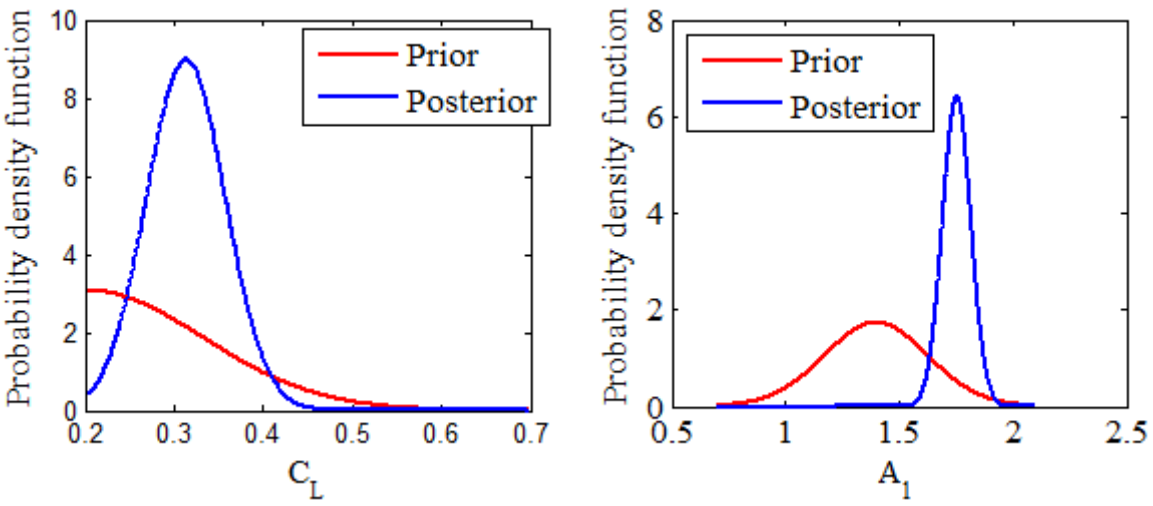

Figure 2.15 - Parameters distributions

Samples are drawn from posterior distribution of parameters and then propagated through the process model. Figure 2.16 represents one such realization showing the uncertainty in CO_2 capture for changes in the flowrate of incoming CO_2. Additional realizations were not included in the plot because they have distinct operating conditions.

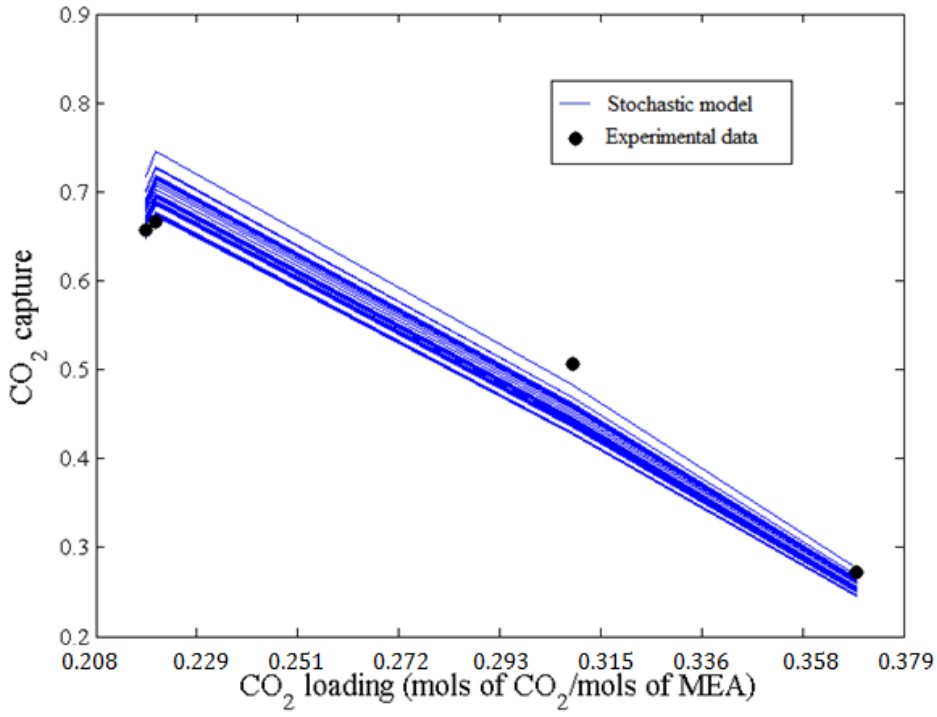

Figure 2.16 - Stochastic response obtained from the uncertainty propagation compared with data from Tobiesen et al. (2007)

It was desired to study the effect of the Bayesian UQ procedure on the overall uncertainty in CO_2 capture prediction. Figure 2.17 shows the probability density function for CO_2 capture corresponding to prior and posterior distributions of the mass transfer parameters for a specific set of conditions when the flow gas flowrate at the inlet is 165.5 kg/h with 2.6 wt% CO_2 and the solvent flowrate is 254.4 kg/h with a CO_2 loading of 0.22 mol CO_2/mol MEA. It is observed that the Bayesian UQ resulted in reduced uncertainty in predicting CO_2 capture as reflected by a narrower distribution obtained using the posteriors.

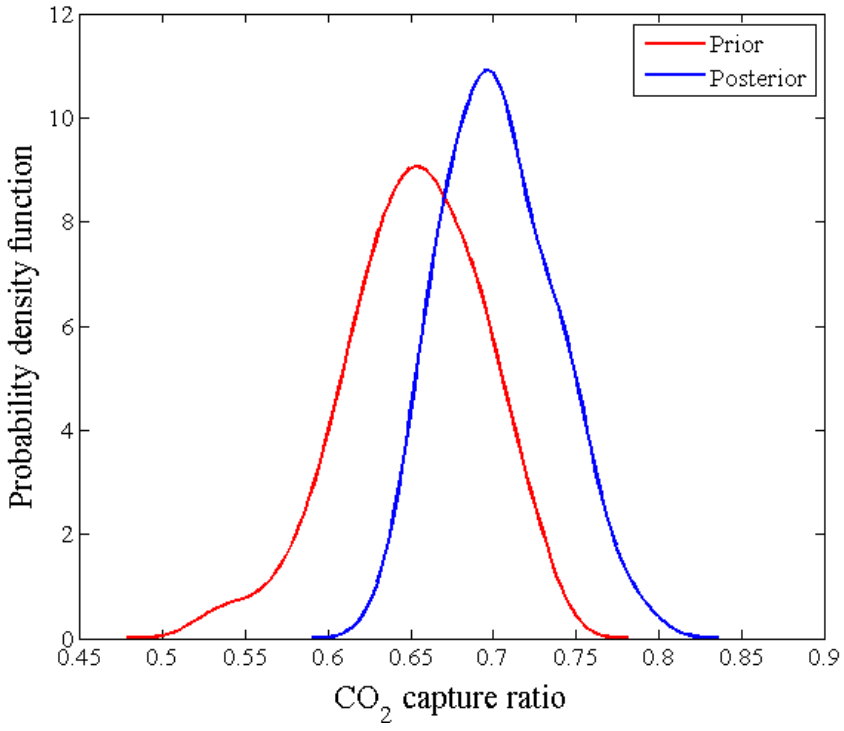

Figure 2.17 - Probability density function for the fractional CO2 capture for a particular operating condition

2. 4. Conclusion

Obtaining rigorous pressure drop and holdup models is essential for a process model especially for process models intended for pressure-driven dynamic simulations. Therefore, hydraulic models for a relatively newer packing type, Mellapak™ plus 252Y, is developed utilizing data from the literature. The regressed Tsai (2010) model is found to be the best model for this packing. It was observed that while selecting the pressure drop model, the holdup model plays a key role due to the dependency of pressure drop on holdup. The final models selected for the MellapakPlus™ 252Y are the regressed Billet and Schultes (1999) model for pressure drop while the regressed Tsai (2010) model is used for holdup calculations.

As opposed to the sequential approach in the literature for obtaining the mass transfer model and estimatisng their parameters, this paper proposes a sequential approach where simultaneous parameter regression of the mass transfer coefficients model, diffusivity model, interfacial area model, and kinetic model is carried out by simultaneously using the experimental data from multiple scales. Since such regression is not feasible in the framework of leading process smulation software platforms, the FOQUS toolbox developed by U.S.

DOE's CCCSI is leveraged. The final integrated mass transfer model comprises of the regressed Billet and Schultes (1999) model for mass transfer coefficient, the regressed Tsai (2010) model for interfacial area along with the regressed diffusivity and kinetic models given by Equations 2.28-33. It was observed that the model/parameters eobtained using the simultaneous approach have better predictive capability than those obtained using the sequential aparoach as tested on a set of data that are not 'seen' by either of the approaches.

Uncertainty in the parameter space is quantified by the Bayesian approach. The approach resulted in reduced uncertainty for the pressure drop model parameter while no or negligible change is observed in the parametric uncertainty of the holdup model. It is observed that there is still relatively high uncertainty in the hydraulic models that could be improved if additional experimental data were available. The authors would like to acknowledge the scarcity of the data in the open literature for the relatively newer packing types such as the one considered in this work.

For down-selecting the parameter space of the mass transfer model, Sobol indices are leveraged. It is observed that the prediction uncertainty for CO_2 capture gets reduced due to Bayesian uncertainty quantification of the mass transfer models.

Chapter 3. Dynamic Model

Properties models and the chemistry model corresponding to the steady-state model that is used for developing the dynamic model is described in details in the PhD thesis of Morgan (2017). Mass transfer models and hydraulic models for that steady-state model are described in the previous chapter. Therefore, only a brief summary of the steady-state model is provided below.

Models for the density, viscosity, and surface tension have been developed as function of temperature and composition using large amount of datasets available in the literature for the MEA-H_2O-CO_2 system (Morgan et al., 2015). The thermodynamic model has been developed using the e-NRTL thermodynamic framework (Morgan et al., 2017) where the Akaike Information Criterion (AIC) (Han et al., 2011) has been used for parameter selection. The thermodynamic model was developed by using both binary (MEA-H_2O) and ternary (MEA-H_2O-CO_2) data for the vapor-liquid equilibrium (VLE), enthalpy data, and heat capacity data. The reaction kinetics was modeled to ensure consistency with the thermodynamic framework by making it a function of activity coefficients, instead of the typical power laws that does not capture the nonlinearity of the chemical equilibrium for this electrolyte system. The reaction set and their corresponding rate equations are given by Equations 2.33-34 and Equations 2.35-36, respectively.

The final hydraulic model is represented by Equation 2.6-7 (Billet & Schultes, 1999) for pressure drop calculations combined with Equations 2.18 (Tsai, 2010) for holdup calculations. The mass transfer model comprises of the models for the liquid-side and gas-side mass transfer coefficients (Equations 2.22-23), interfacial area (Equation 2.30), and diffusivity (Equation 2.31-32). Validation of the steady-state model and uncertainty quantification of the individual properties models as well as the plant-wide models have also been presented in various publications (Morgan et al., 2018; Morgan et al., 2017; Morgan et al., 2015). The model has been found to predict the steady-state data from the NCCC for various key variables, such as CO_2 capture efficiency and CO_2 loading, satisfactorily over a wide operating range.

3. 1. Dynamic model development

The dynamic model is developed in Aspen Plus Dynamics (APD) platform. However, the APD platform does not support the rate-based tower model, but only an equilibrium model. One of the possible

methodologies to obtain a reasonable approximation of the rate-based model is to use a correlation for the Murphree efficiency in the equilibrium model (Zhang et al., 2016b).

In this work, the equation is used in the work of Zhang et al. (2016) is modified by incorporating additional terms by taking into consideration the effects of the MEA concentration and CO_2-loading of the lean solvent. The modified equation is given by Equation 3.1 where the multiplication factor and exponents are regressed using the benchmark model described earlier.

A random sample of 100 operating conditions are generated with due consideration of the expected operating ranges of the key process variables in NCCC as shown in Table 3.1 - Key variables ranges considered for the Murphree efficiencies modelthe Murphree efficiency is calculated for each discretization of the packing, a total of 8900 points is generated. Figure 3.1 shows the equilibrium model with modified Murphree efficiency yields a reasonable approximation of the equilibrium model.

Table 3.1 - Key variables ranges considered for the Murphree efficiencies model

Variable	Minimum	Max
Liquid flowrate (kg/hr)	5100	6250
MEA (w%)	25.4	29.3
CO_2 loading (mol/mol)	0.15	0.26
Flue gas flowrate	2020	2470

$$\epsilon_{CO_2,i} = 1.245\epsilon_{CO_2 o,i}\left(\frac{F_{gas}}{F_{gas\,o}}\right)^{-0.42}\left(\frac{F_{CO_2}}{F_{CO_2\,o}}\right)^{-0.42}\left(\frac{F_{liq}}{F_{liq\,o}}\right)^{0.64}\left(\frac{F_{MEA_w}}{F_{MEA_w\,o}}\right)^{-1.01}\left(\frac{\alpha_{CO_2}}{\alpha_{CO_2\,o}}\right)^{1.06} \quad (3.1)$$

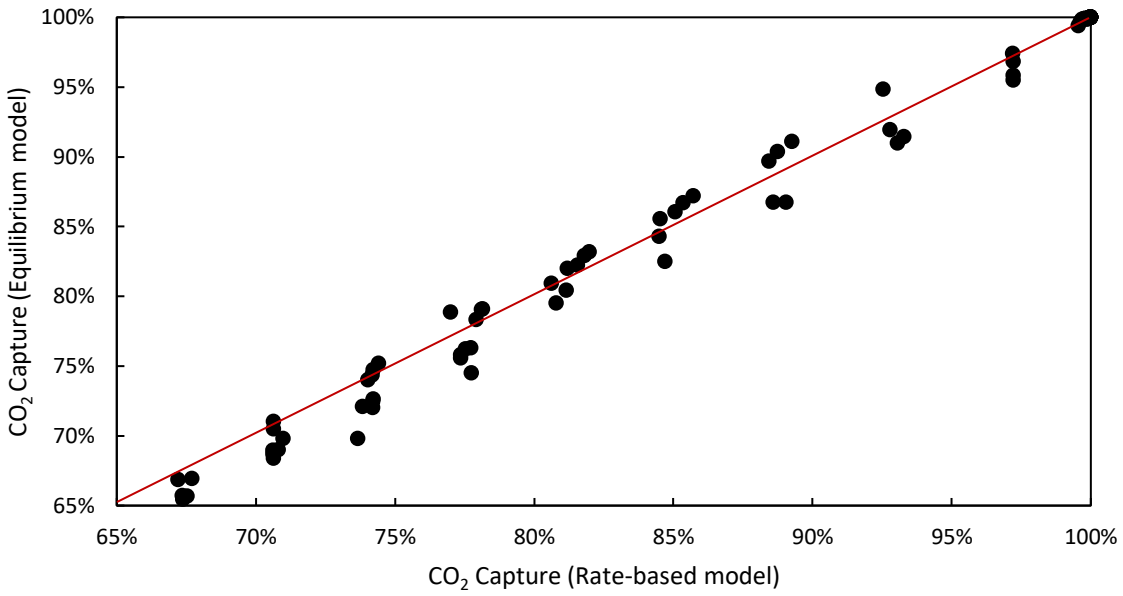

Figure 3.1. Equilibrium model and rate-based model comparison

Dimensions of the buffer and storage tanks as well as the column sumps at NCCC are shown in Table 3.2. These dimensions are inserted in the Aspen Plus model before exporting it to APD. The pressure drop and holdup models presented earlier are implemented as scripts in APD. As discussed in this chapter, while pressure drop is not expected to vary much under a wide range of operating conditions, it can significantly change as the tower approaches the flooding condition. Also, the holdup plays an important role in affecting the plant transient response.

Table 3.2 - Dimensions of Various Equipment Items in the NCCC pilot-plant

Equipment	Diameter (m)	Height (m)
Absorber	0.641	18.51
Absorber sump	0.641	4.15
Wash tower	2.44	2.44
Buffer tank	2.44	2.44
Stripper	0.59	12.1
Stripper Sump	0.59	1.22
Storage Tank	2.44	2.44

In accordance with the NCCC control strategy, PID controllers are implemented for controlling the lean solvent flowrate, flue gas flowrate, and steam flowrate. Figure 3.2 presents a simplified version of the NCCC PFD with the key controllers.

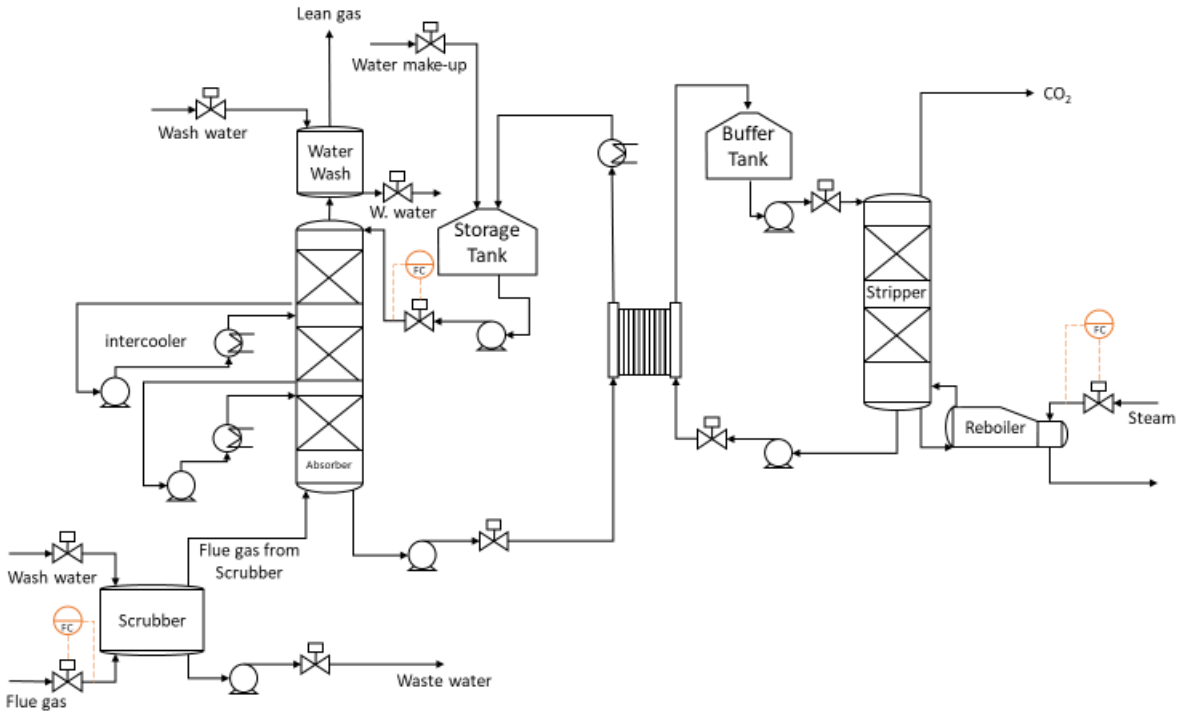

Figure 3.2 - Simplified PFD of the NCCC pilot-plant

3. 2. NCCC pilot-plant test runs

3. 2. 1. Test Protocol

Details of the NCCC pilot-plant have been thoroughly discussed in other publications (Morgan et al., 2017; Morgan et al., 2018). Dynamic experiments were conducted using an absorber configuration of 3 beds with 2 intercoolers. The stripper had a fixed configuration of 2 beds during all the dynamic experiments. The objective of the test protocol was to keep the process excited during the entire run. One method to achieve this is to use the PRBS signals (Gaikwad & Rivera, 1996). The PRBS is a two-level signal that depends on two parameters: the number of shifts (n_r) and the switching time (t_{sw}) that require a prior knowledge of

the process, or a model that can accurately represent it. However, these dynamic test runs were conducted during 8/20/2014-8/21/2014 when a process model was not available. Therefore these parameters were estimated through a series of preliminary step changes in the key variables of process in NCCC prior to the test runs. By analyzing the results from these step tests, it was realized that it would not be possible to run the entire PRBS signal, as it would require a number of shifts N_S equal to $2^{n_r} - 1$, if all 4 variables are investigated simultaneously. Due to the limited time-availability to run these tests and due to the time required to program the control system for implementing these tests, a modified signal, that will be called pseudo-PRBS signal here, is designed that could be implemented manually by the plant operators.

First of all, for a nonlinear process, the process gain and time constant is expected to vary depending on the step magnitude. For example, if the step magnitude is doubled, i.e. if the step magnitude is changed from *x* to 2*x*, it may not result in two-times change in the output variable; nor the time constant remains the same. Additionally, the gain can vary depending on the conditions the step is introduced and whether it is a step increase or decrease to the nominal value. Therefore, a test protocol as given in Table 3.3 is implemented. Similar to the PRBS signal, each successive step is introduced before the process has reached steady-state. It should be noted that although this signal does not have all the properties as a full PRBS design, it provides more information than the usual single step tests that are currently available in the literature. Moreover, this simplified protocol was implemented for 3 variables, namely solvent flowrate, inlet flue gas flowrate, and reboiler steam flowrate while dynamic data are typically found in the literature for 1 or 2 variables.

Table 3.3 - Example set of dynamic step tests in a given input or disturbance

Test#	Test Condition
1	Datum
2	+*x*% of datum
3	-*x*% of datum
4	+2*x*% of datum
5	-2*x*% of datum
6	+*x*% of datum
7	-*x*% of datum
8	Datum

The specific test plan for each of the input variables is shown in Table 1.4. Each variable was investigated independently to avoid a worst case dynamic response that could introduce safety issues for the pilot-plant.

This was done as timely investigation of these worst case responses could not be evaluated earlier in absence of a dynamic model when the test runs were conducted.

Table 3.4 - Dynamic step tests that were completed in the NCCC pilot-plant

Test#	Solvent Flow (lb/hr)	Comment
1	5675	Datum
2	6015.5	value of x_1= 340.5 lb/hr
3	5334.5	this step results in $2x_1$% decrease from the existing state
4	6353	this step results in $3x_1$% increase from the existing state
5	4994	this step results in $4x_1$% decrease from the existing state
6	6015.5	this step results in $3x_1$% increase from the existing state, note that even the final value is same as dynamic Test#2, the magnitude is different
7	5334.5	this step results in $2x_1$% decrease from the existing state, same as test#3, but introduced at different state of excitation
8	5675	return to datum, but doesn't need to settle to datum, next step introduced while the process is through transient
Test#	**Inlet Flue Gas (kg/hr)**	**Comment**
9	2497	value of x_2= 227 kg/hr of flue gas

10	2043	this step results in $2x_2$% decrease from the existing state
11	2724	this step results in $3x_2$% increase from the existing state
12	1816	this step results in $4x_2$% decrease from the existing state
13	2497	this step results in $3x_2$% increase from the existing state, note that even the final value is same as dynamic Test#9, the magnitude is different
14	2043	this step results in $2x_2$% decrease from the existing state, same as test#10, but introduced at different state of excitation
15	2270	return to datum

Test#	**Reboiler Steam Flow (kg/hr)**	**Comment**
16	726.4	value of x_3=227 kg/hr
17	454	this step results in $2x_3$% decrease from the existing state
18	862.6	this step results in $3x_3$% increase from the existing state
19	317.8	this step results in $4x_3$% decrease from the existing state
20	726.4	this step results in $3x_3$% increase from the existing state, note that even the final value is same as dynamic Test#16, the magnitude is different

21	454	this step results in $2x_3$% decrease from the existing state, same as test#17, but introduced at different state of excitation
22	590.2	return to datum

3. 2. 2. Sampling and Data Analysis

In NCCC, there is a lean solvent storage tank in between the stripper and the absorber and typically, the lean solvent samples are collected after the lean solvent storage tank, which can cause a large damping of the dynamics of the stripper. While this may be a desired operational strategy, for validation of the dynamic model, it was desired to collect sample at the stripper outlet so that the stripper outlet dynamics (mainly the rate of change of the solvent composition) can be adequately observed. Additional sampling line was laid out in NCCC for this purpose and samples were collected manually during the dynamic test run. These liquid samples were later manually analyzed to measure the CO_2 and amine concentrations. Due to the presence of the storage tank between the stripper and absorber and because of the recycling solvent, it results in slower dynamics of the integrated absorber-stripper process while the stripper itself has much faster response. Therefore, to observe the dynamics of the stripper as well as the integrated system, separate dynamic tests with shorter and longer time periods between introductions of step changes in the reboiler steam flow rate were conducted. The relative change in the steam flowrate remained same for these tests as given in Table 3.4 but only switching times were different.

While evaluating the dynamic data, it is important to consider time delay of the measured samples especially when the measurement samples are taken further from their source. During the experimental runs, MEA samples were collected at the lab that were at a considerable distance from the sample sources. measured data, this is especially critical for the laboratories analysis conducted in the collected liquid samples. If the measurements are not properly synched with the changes, the dynamic responses will not be observed correctly. For instance, in the specific case of measuring concentrations of the lean and rich loadings leaving the columns, the samples were transported, through piping, from the plant to the laboratory (where the MEA concentration and CO_2 loading are measured). Therefore, the time delay between the column and the laboratory needs to be calculated using hydraulic information.

The calculation was performed using the Fanning friction factor and the Darcy-Weisbach equation for the calculation of the average velocity using Churchill correlation (Churchill, 1977), shown below:

$$f = 2\left(\left(\frac{8}{Re}\right)^{12} + (A+B)^{-1.5}\right)^{\frac{1}{12}} \tag{3.2}$$

$$\Delta p = f_D \frac{L}{D} \rho \frac{v^2}{2} \tag{3.3}$$

$$f_D = 4\, f \tag{3.4}$$

where A and B are given by the following relations:

$$A = \left(2.457 \ln\left(\left(\left(\frac{7}{Re}\right)^{0.9} + 0.27\frac{\varepsilon}{D}\right)^{-1}\right)\right)^{16} \tag{3.3}$$

$$B = \left(\frac{37530}{Re}\right)^{16} \tag{3.4}$$

In these equations, f is the fanning friction factor, *Re* is the Reynolds number, ε is the roughness of the pipe, *D* is the pipe inner diameter, f_D is the Darcy friction factor, *L* is the length of the pipe, ρ is the liquid density and *v* the liquid velocity. As pressure drop (calculated from the sample take-off and return line pressures) and the length of the tubes were available (by using the sensor data and isometric drawings of the pump inlet and outlet lines), the delay time could be estimated. Typical delay times for the sampling of the lean and rich solvents were found to be 20.32 seconds and 20.87 seconds, respectively.

The liquid samples were used to determine both the MEA wt% and CO_2 loading from the dynamic test runs. The MEA wt% was measured using a conductometric equivalence point titration using 0.1 M HCl acid. The CO_2 loading was determined using a similar titration technique to obtain the total CO_2 concentration in the solution, with the solvent sample dissolved in excess methanol and using 0.1 M NaOH base as the titration agent. As mentioned, Morgan (Morgan, 2017) has reported that a significant uncertainty is present in the liquid composition measurements. There, the liquid composition measurements from the dynamic test runs were used mainly for qualitative comparison

The data collected from the pilot plant are typically noisy, do not necessarily satisfy mass and energy balances. In addition certain important variables may not be measured. First the noise in the raw data are removed by using a Butterworth filter, which is a bandpass filter, followed by a moving average filter. The filters are implemented in MATLAB. As an example, Figure 3.3 presents the raw and filtered measurements of the gas flue gas flowrate. The pre-processed data are considered to be adequate for the next step, which is dynamic data reconciliation, to satisfy the mass and energy balances.

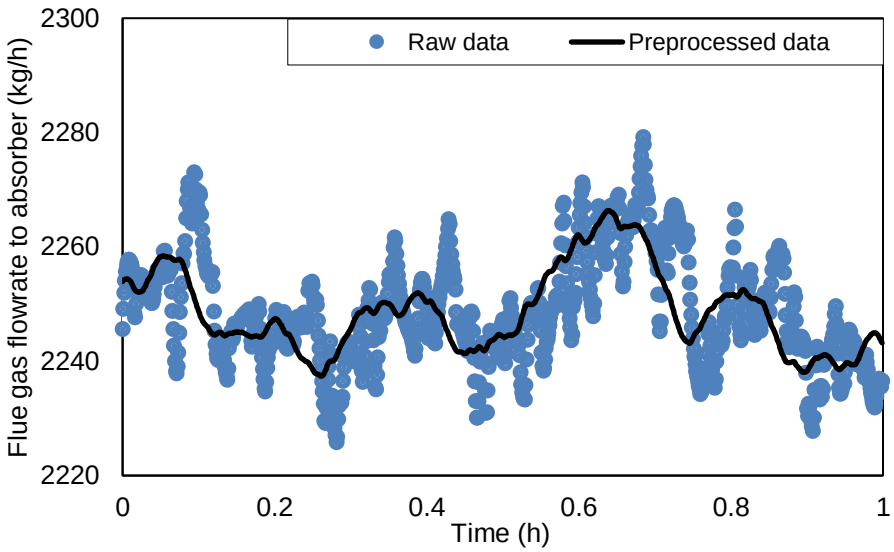

Figure 3.3. Raw and preprocessed flue gas flowrate data

3. 3. Dynamic Data Reconciliation (DDR)

An optimization problem is solved for DDR. The problem is set up in Aspen Plus® Dynamics as shown in Figure 3.4. The optimization objective is shown in Equation 3.5. Following variables are considered as decision variables- flowrate and CO_2 concentration of the flue gas to the absorber, lean solvent flowrate to the absorber, steam flowrate to the reboiler. These variables are also included in the objective function in Equation 3.5. One of the important variables with missing measurement is the water make-up to the storage tank between the stripper and absorber. During the test runs, whenever the storage tank's level would decrease below 30%, a pump would turn on automatically providing make-up water to the tank. Since the water make-up was not provided continuously, it can result in considerable variation in the lean solvent and therefore, providing an estimate of this variable was important. An estimate of the make-up water flow was obtained by using the make-up water pump performance curve and the information available for the pump on-off status. Due to uncertainty in the water make-up flowrate estimate, this variable is also reconciled. Overall, following variables are reconciled:

- Lean CO_2 loading
- Gas flowrate from the absorber
- Lean solvent temperature to absorber
- Lean solvent temperature from regenerator

- Lean solvent flowrate to absorber
- Flue gas flowrate and its CO_2 concentration
- Steam flowrate
- Water make-up

The dynamic data reconciliation problem was solved by specifying the objective function described in Equation 3.5 in the Aspen Plus® Dynamics flowsheet environment and using the optimizer to minimize a pre-determined number of discrete data at specific time instants. The optimizer algorithm 'FEASOPT' in Aspen Plus® Dynamics, which uses a feasible path SQP algorithm, is used. The computational time increases considerably depending on the number of discrete time instants considered for optimization. About 4 hours were necessary to find an optimal solution corresponding to the solvent step tests, using 15 discrete points. For solving the DDR problem corresponding to the gas flow and steam flow step tests, 45 and 90 discrete points were used, respectively, with the solution times increasing to about 14 and 20 hours, respectively.

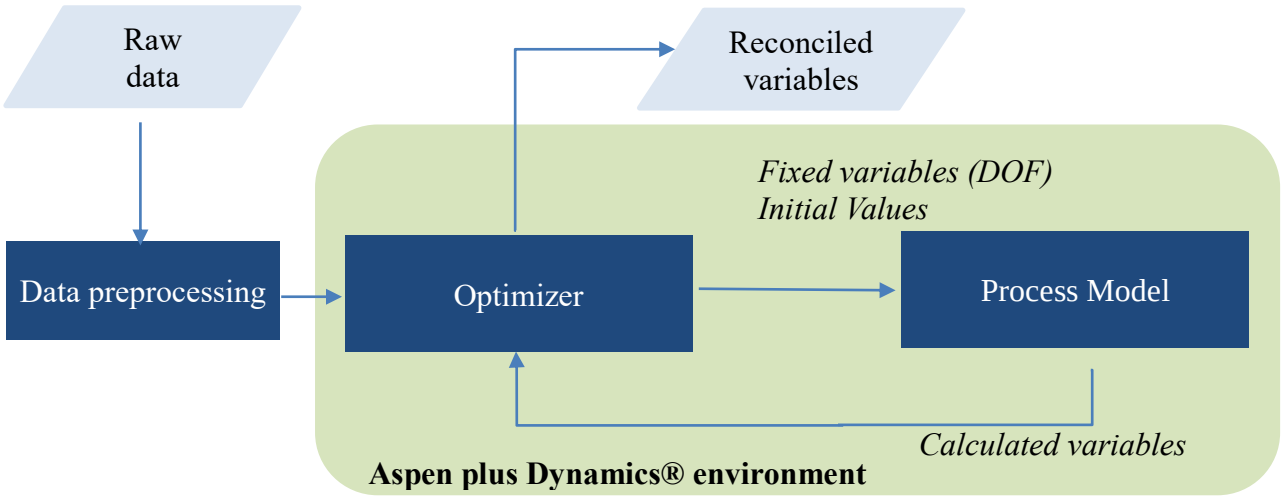

Figure 3.4 - DDR algorithm followed by raw data processing

$$\min \left(y_{exp} - y\right)' \sum^{-1} \left(y_{exp} - y\right) \tag{3.5}$$

s.t.

$$H(\eta, y, u) = f(\eta, y, u)$$

$$g(\eta, y, u) \leq 0$$
$$u^L < u < u^U$$
$$y^L < y < y^U$$

3. 4. Results and discussions

3. 4. 1. Step Tests in Solvent Flowrate:

Figure 3.5 and Figure 3.6 shows the raw versus reconciled lean solvent flowrate and CO_2 capture rate calculated from the gas side, respectively. It can be observed in Figure 3.6 that at the beginning of this test run, the plant is not at the steady state, which was undesired. Since the initial values of all state variables including the holdup was not known, it was practically impossible to match this initial transient. However, despite this initial transient, it can be observed that the model results match closely with the reconciled transient data.

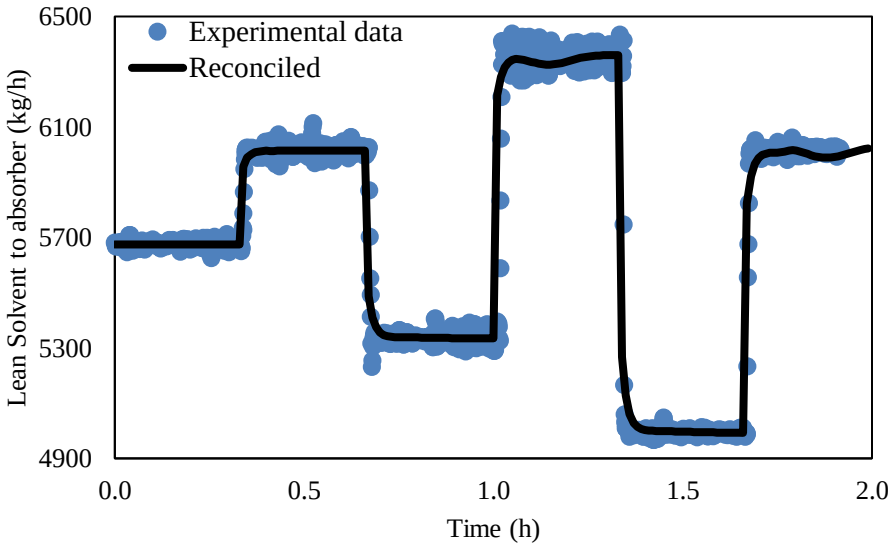

Figure 3.5. Reconciled Lean solvent flowrate from the solvent test

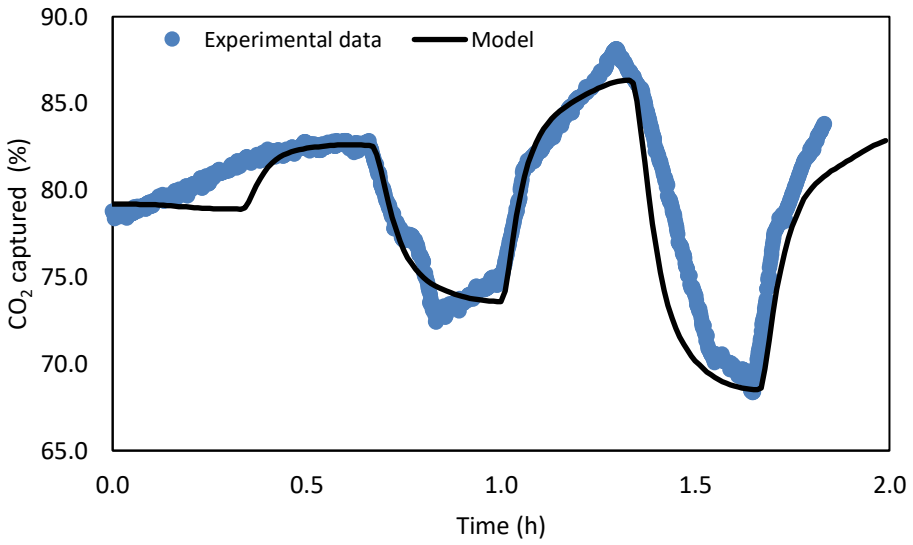

Figure 3.6. Reconciled CO_2 capture calculated from the gas side measurements for the solvent test

Figure 3.7 show the results for the reconciled CO_2 loading of the lean solvent at the stripper outlet. This sample was collected not at the mixing tank outlet, but immediately downstream of the stripper from where extra liquid samples were collected during the test run. Here the reconciled model results are qualitatively show the right trend, but the experimental data show much more variability that what is reflected in the model results. Figure 3.8 shows the results for the reconciled CO_2 loading of the rich solvent at the absorber outlet. Here the experimental data exhibit more variability than that in the model results. Uncertainty in liquid sample measurements have been documented in the work of Morgan (2017). It should be noted that these liquid samples capture mass balance closures of CO_2 from the liquid side while Figure 3.6 captures CO_2 mass balance from the gas side. Since the gas side measurements have far less uncertainty and Figure 3.6 shows a satisfactory fit to the experimental data, discrepancies between the liquid side measurements and model predictions are attributed to the errors in the experimental measurements, as discussed in Morgan et al. (2018) and Morgan (2017). Uncertainties in the liquid side measurements in NCCC were estimated by comparing the measurements with more accurate methods. The MEA concentration measurements were compared to a gas chromatography with thermal conductivity and flame ionization detectors (GC-TCD+FID). The CO_2 concentration was compared to a Total Inorganic Carbon (TIC) method with an IR detector. Both MEA and CO_2 concentrations are found to have an average error of about 4% with higher discrepancies for the rich solvent than for the lean solvent measurements.

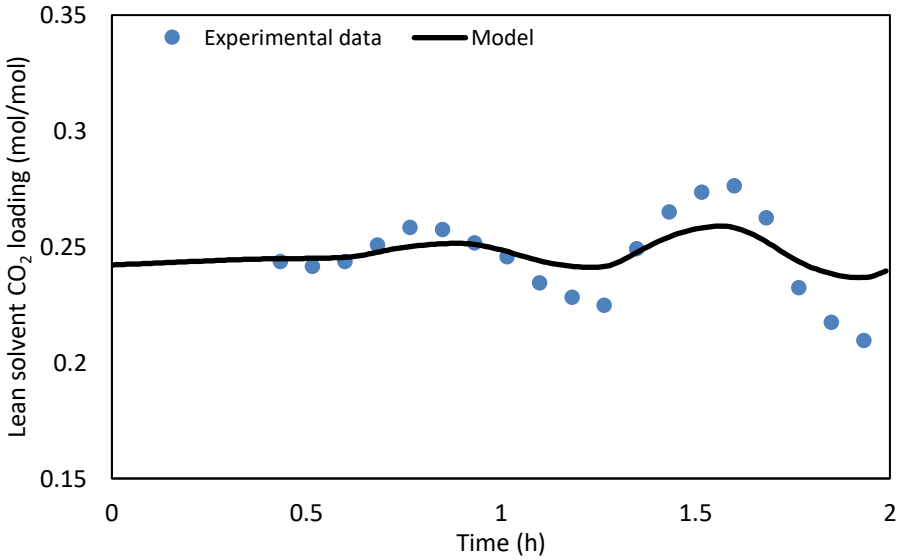

Figure 3.7. Reconciled lean CO_2 loading from the solvent test

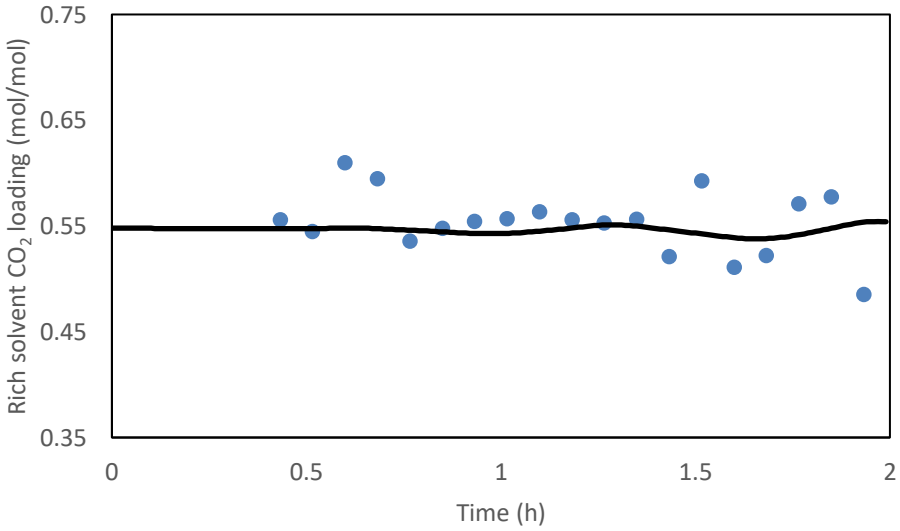

Figure 3.8. Reconciled rich CO_2 loading from the solvent test

3. 4. 2. Step Tests in Steam Flowrate:

When the steam flowrate to the stripper is changed, it takes longer to affect the absorber CO_2 capture due to the holdup in the downstream equipment items such as the lean/rich heat exchanger, storage tank, and the absorber. Therefore, for studying the dynamics of the stripper, it was desired to introduce step change in the steam flowrates and compare the dynamics in the CO_2 flowrate from the stripper top and lean loading composition from the stripper bottom. Figure 3.9 shows the reconciled steam flowrates when the step tests in the reboiler steam flowrates are introduced. Figure 3.10 shows the comparison of the CO_2 flowrate from the stripper top. Model results are in good agreement with the data.

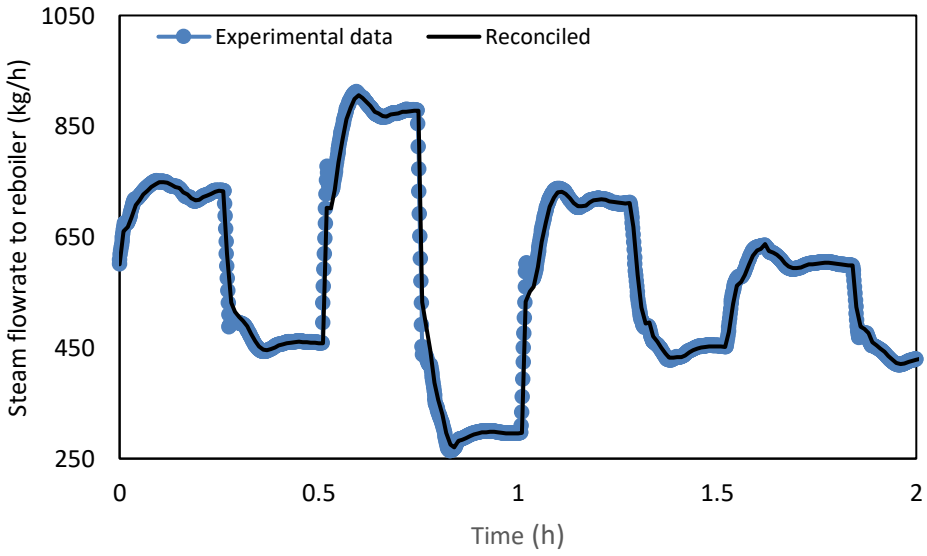

Figure 3.9. Reconciled steam flowrate

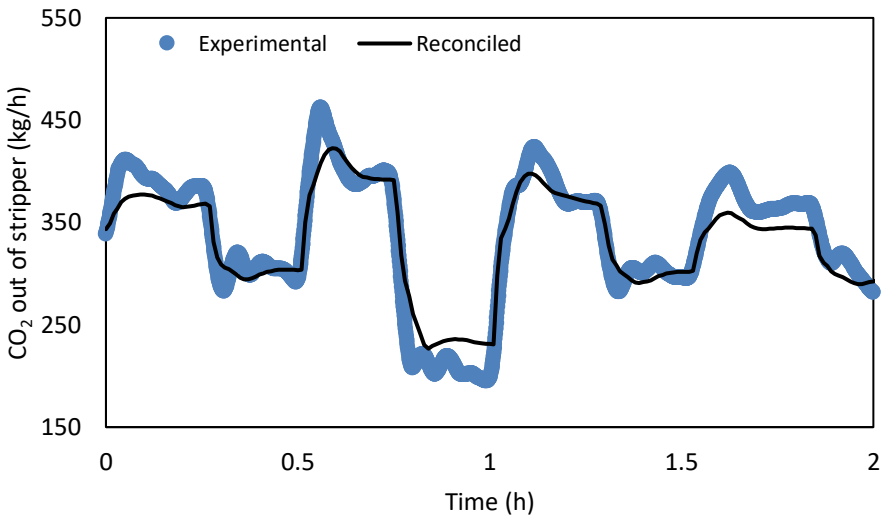

Figure 3.10. Reconciled regenerated CO_2 flowrate from the steam test

Figure 3.11 shows the comparison between the model results and the experimental data of the lean solvent CO_2 loading. Similar to the results when the solvent flowrate was changed, the experimental data show much more variability than the model results. Again, as gas flowrate and composition from the stripper are considered to have lower uncertainty in measurements and a reasonable fit to the gas side measurements were obtained, the discrepancy is attributed to the liquid-side measurements.

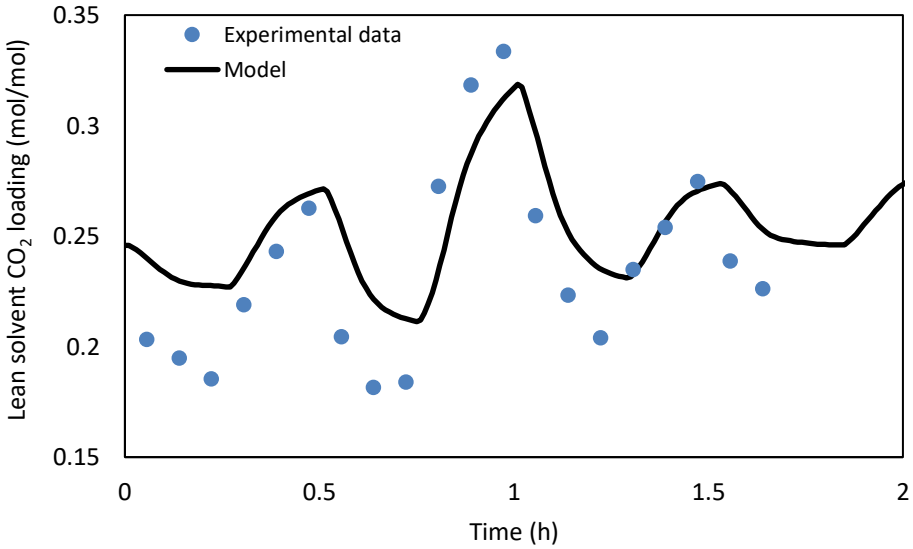

Figure 3.11. Lean solvent CO_2 loading from the steam test

3. 4. 3. Step Tests in Flue Gas Flowrate:

Figure 3.12 presents the reconciled flue gas flowrate to the absorber. Figure 3.13 presents the reconciled CO_2 capture percentage in comparison to the experimental data. It is observed that while the model prediction for some of the undershoots, especially around 1.1. hr and 1.6 hr, can be improved, generally the comparison is reasonably satisfactory. In general, it is it is believed that the model results could have improved further if the water make-up flowrate was a measured variable and liquid sample measurements would have better accuracy.

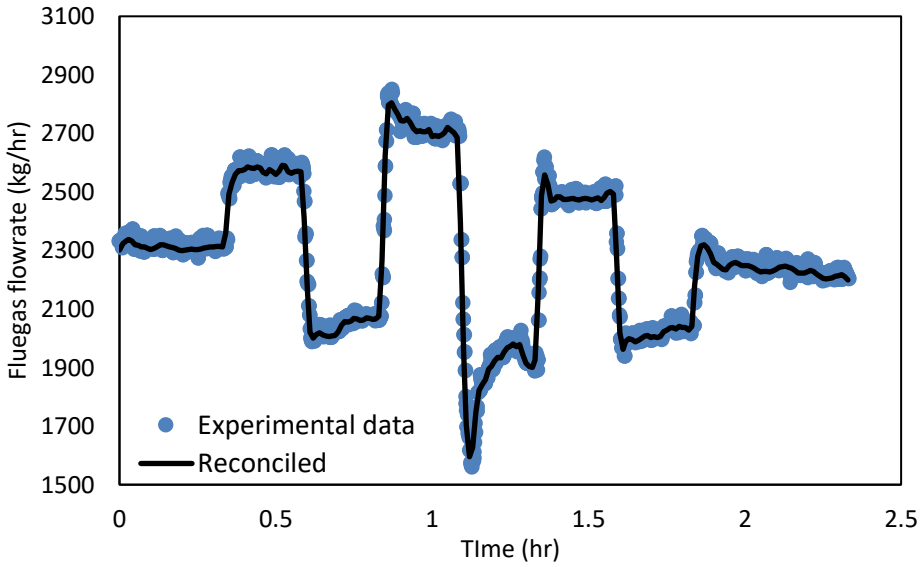

Figure 3.12. Reconciled flue gas flowrate

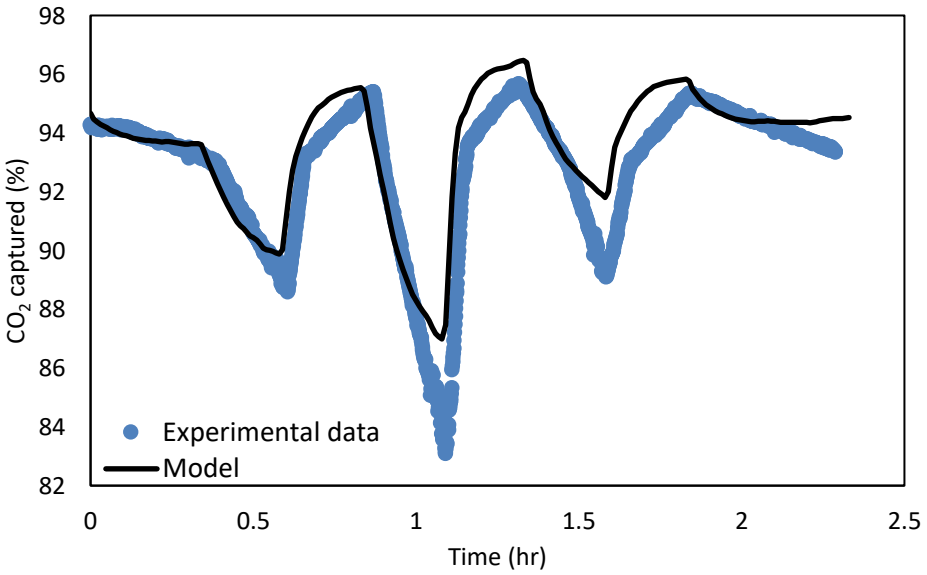

Figure 3.13. Reconciled CO_2 capture calculated from the gas side measurements for the flue gas test runs

3. 5. Transient studies

Two transient studies are conducted here by using the transient model of the NCCC pilot. The first study is similar to the typical single step change studies. In this case study, 5% step changes in the flue gas flowrate, lean solvent flowrate, and steam flowrate are simulated. In the second, a variable capture scenario is simulated and under these scenario, performance of traditional PID controllers are evaluated. In this scenario, the desired CO_2 capture rate is set by a scheduler at an upper level that maximizes the plant profit by taking into consideration the real-time price of the electricity, the real-time demand of the electricity, CO_2 capture target over a base period, and the carbon taxation described in Scenario 2 of Bankole et al. (2018). In this scenario, a penalty is imposed on CO_2 emissions above an allowable limit during the base period. However, there is no reward for capturing more CO_2 beyond this set limit. This scenario provides incentive to CO_2-emitting plants to capture at least the carbon target set by the regulatory agencies.

3. 5. 1. Case 1 results

The purpose of this case study is to evaluate the process gain and time constant for similar percentage change in some of the key variables from their nominal value. In a CO_2 capture unit, flue gas flowrate is a disturbance variable while the solvent and steam flowrates are manipulated variables. Therefore the transients can be helpful in designing the controllers. The nominal conditions considered for this study is similar to the dynamic test runs conducted at NCCC, with a lean solvent flowrate of 5675 kg/hr, a flue gas flowrate of 2270 kg/hr, and a steam flowrate of 663 kg/hr. All the step changes in this case study are introduced at the 2^{nd} hour and utilized the same control scheme as the NCCC pilot-plant. $\pm$5% step changes in the lean solvent flowrate and flue gas flowrate are introduced only to the absorber model so that the transient response of only the absorber can be studied as opposed to the integrated system that takes much longer to settle due to the circulating solvent. Corresponding CO_2 capture rates are presented in Figure 3.14. $\pm$5% step changes in the steam flowrate are introduced only to the stripper model, with the corresponding flowrates of the CO_2 released presented in Figure 3.15.

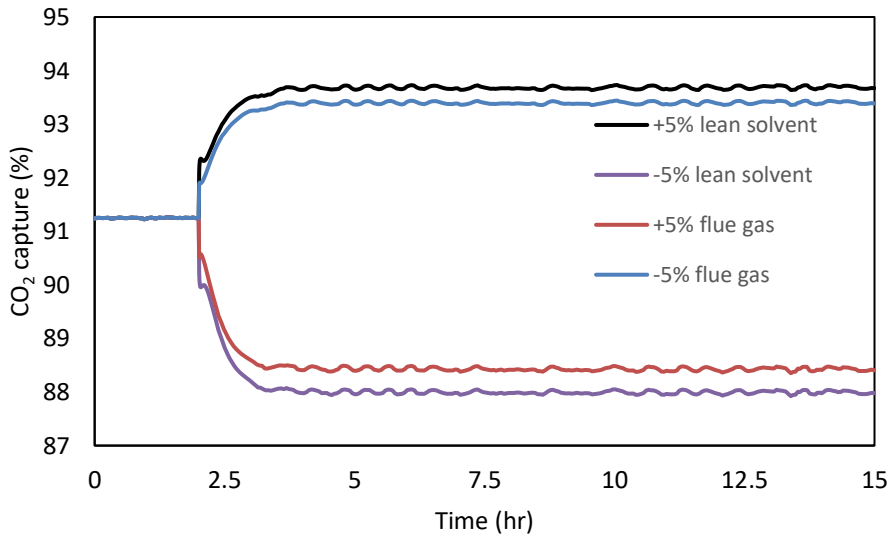

Figure 3.14 - Absorber-only case study step tests

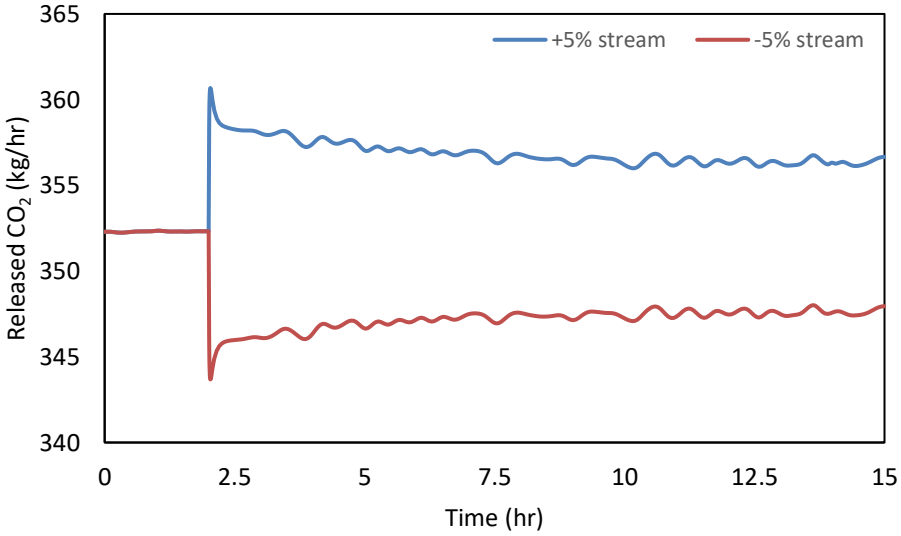

Figure 3.15 - Stripper-only case study step tests

The CO_2 capture rates for the whole pilot-plant, i.e. when the absorber and stripper are coupled, are presented in Figure 3.16. Case 1a, 1b, 1c, 1d, 1e, and 1f represent a +5% step change in the steam flowrate, a -5% step change in the steam flowrate, a +5% step change in the flue gas flowrate, a -5% step change in the flue gas flowrate, a +5% step change in the lean solvent flowrate, and a -5% step change in the lean solvent flowrate, respectively.

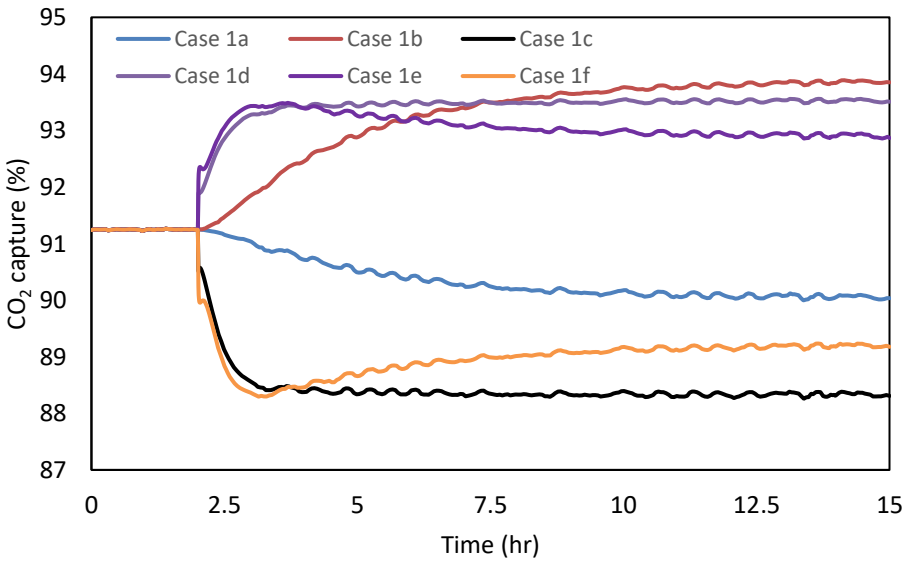

Figure 3.16 - CO_2 capture response in Case 1

First of all, the responses for the change in the solvent flowrate is similar to the flue gas flowrate in the isolated absorber study. This is expected for an absorber since it essentially changes L/G ratio by similar magnitude. The slight differences are due to the nonlinearity in the absorber and properties models. Furthermore, the gain is different when the flue gas flowrate or the solvent flowrate is increased in comparison to when they were decreased further demonstrating nonlinearity of the process.

In the integrated plant studies (Figure 3.16), when the flue gas flowrate and solvent flowrate are changed, the steam flowrate to the stripper remains unchanged therefore resulting in a change in the lean solvent composition. Due to this couple effect, the plant takes longer to settle in comparison to the absorber only and stripper only cases. It is observed that when only the solvent step changes are introduced it takes longer for the process to settle than when the flue gas flowrate is changed. It is expected since there is higher change in the solvent concentration when the solvent flowrate is changed in comparison to when the flue gas flowrate is changed.

Finally, it is observed that the time constant of the CO_2 release flowrate for the stripper only case is smaller than the time constants for the CO_2 capture rate for the absorber only cases. The time constants for CO_2 capture rate are ~18 minutes for the absorber and ~170 minutes for the stripper in the full pilot-plant cases, which are close to the value estimated at NCCC through step tests (21 minutes for absorber side and 90 minutes for stripper side). The time constant for CO_2 capture rate for the absorber model only cases and stripper model only cases are ~17 minutes, and ~173 minutes, respectively. Table 3.5 presents the individual time constants and gains observed for each case.

Table 3.5 - Gains and time constants observed in the case studies

Case	gain	τ(min)
Case a	0.24	179
Case b	0.52	164
Case c	-0.45	19
Case d	-0.59	16
Case f	0.41	19
Case g	0.33	16
+5% solvent	0.49	17
-5% solvent	0.65	18
+5% flue gas	-0.57	15
-5% flue gas	-0.43	17
+5% steam	0.20	167
-5% steam	0.24	178

3. 5. 2. Case 2 results

The optimal schedule for the CO_2 capture setpoints were taken from (Bankole et al., 2018). The flue gas flowrate was scaled down to a 0.5 MW equivalent pulverized coal power plant size and its composition was also changed accordingly to match the pilot-plant model presented in this work. However the variability in the flue gas flowrate was similar to the work of Bankole et al. (2018). For this study, the control strategy was changed from the previous process models: using the scheduled CO_2 capture as set-points controlled by the lean solvent flowrate, while the lean solvent CO_2 loading was controlled by the steam flowrate. Figure 3.17 presents the scheduled CO_2 capture. A zoomed version between 4.5-6 hr comparing the scheduler setpoint versus the actual CO_2 capture is shown in Figure 3.17satisfactorily achieved. The flue gas flowrates schedule used in this study and its model implementation are presented in Figure 3.19.

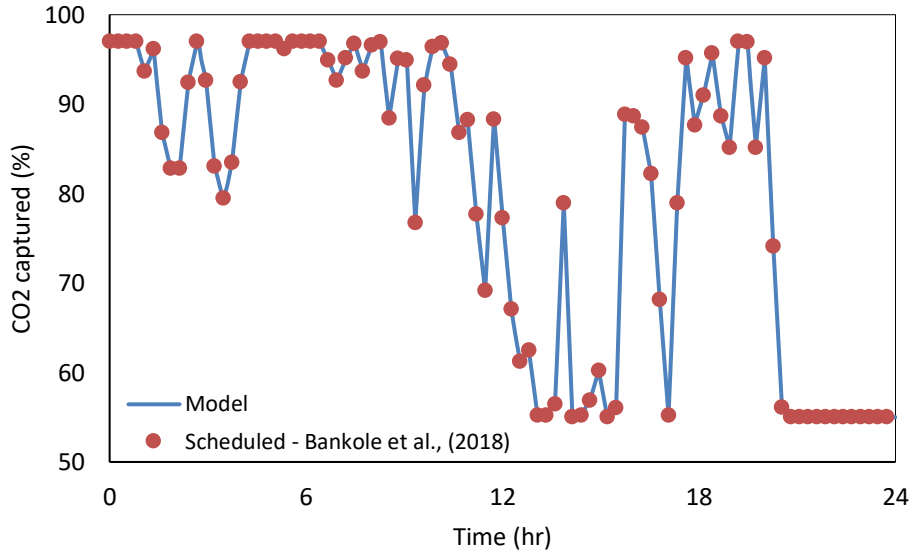

Figure 3.17 – Schedule of CO_2 capture rate in Case 2

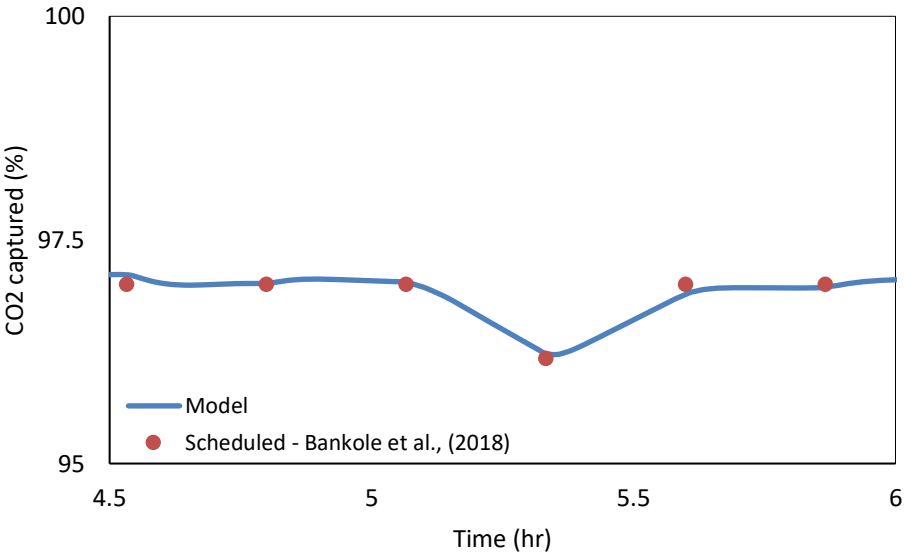

Figure 3.18 – Zoomed Schedule of CO_2 capture rate in Case 2

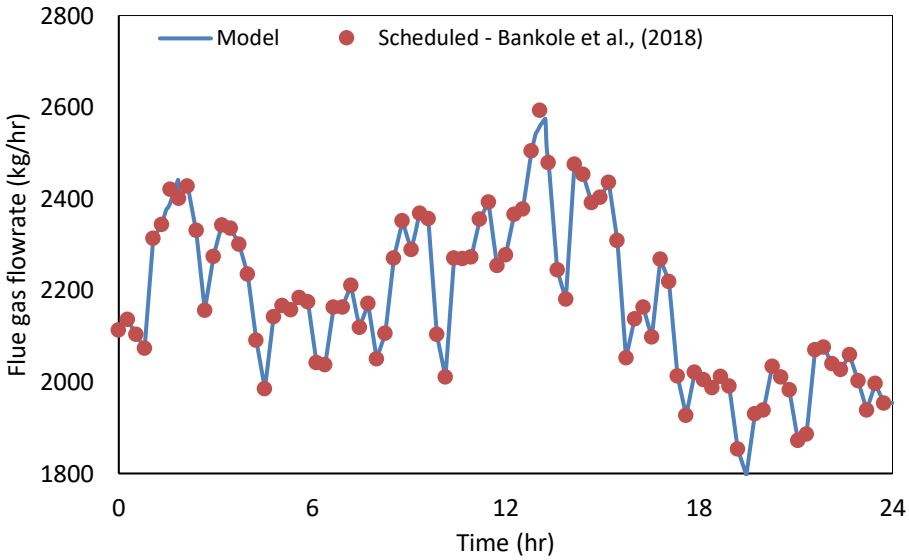

Figure 3.19 – Schedule of the flue gas flowrate in Case 2

Figure 3.20 presents the lean solvent flowrate. As expected, the flowrate increases for higher CO_2 capture percentage, and vice versa. Figure 3.21 presents the steam consumption in the reboiler, used to control the lean loading. As expected, it has an increased flowrate when the CO_2 capture percentage is higher and vice versa. Significant variation in these two flowrates, especially in the steam flowrate, is noticeable. The resulting transient in the lean solvent loading is presented in Figure 3.22. Significant discrepancies in the lean solvent loading from its setpoint is noticeable especially for the cases with high variation in the flue gas flowrate and CO_2 capture target. When the flue gas flowrate and the desired CO_2 capture both are at their low values such as between 21-24 hr, both the lean solvent flowrate and steam consumption are at their lowest values.

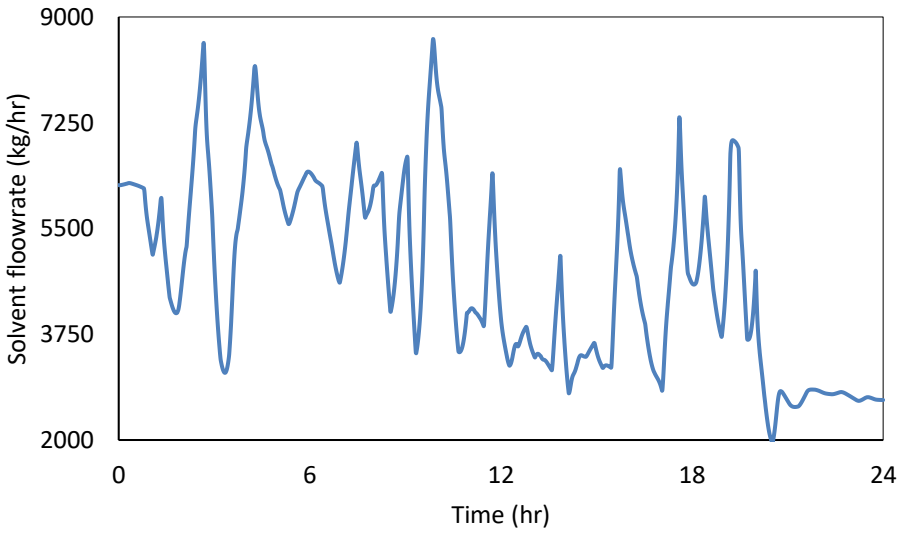

Figure 3.20 - Lean solvent flowrate in Case 2

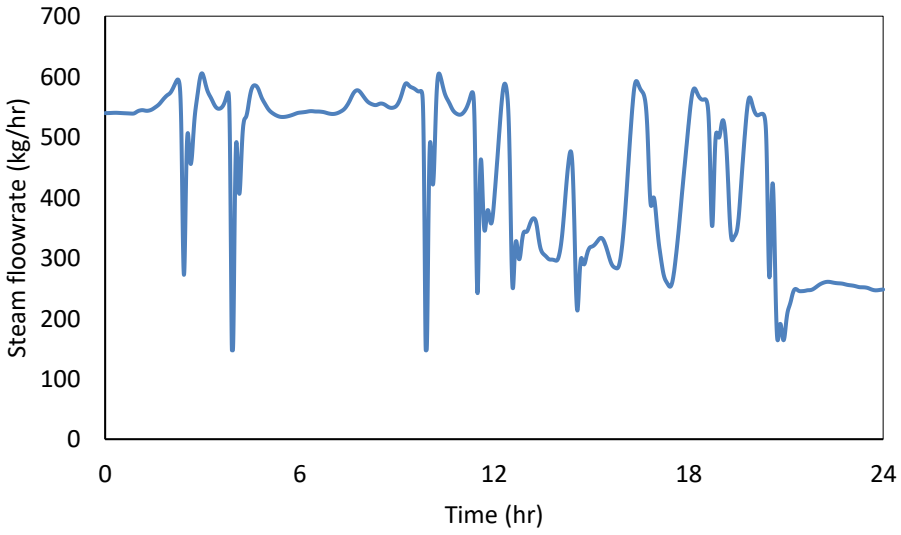

Figure 3.21 - Steam flowrate in Case 2

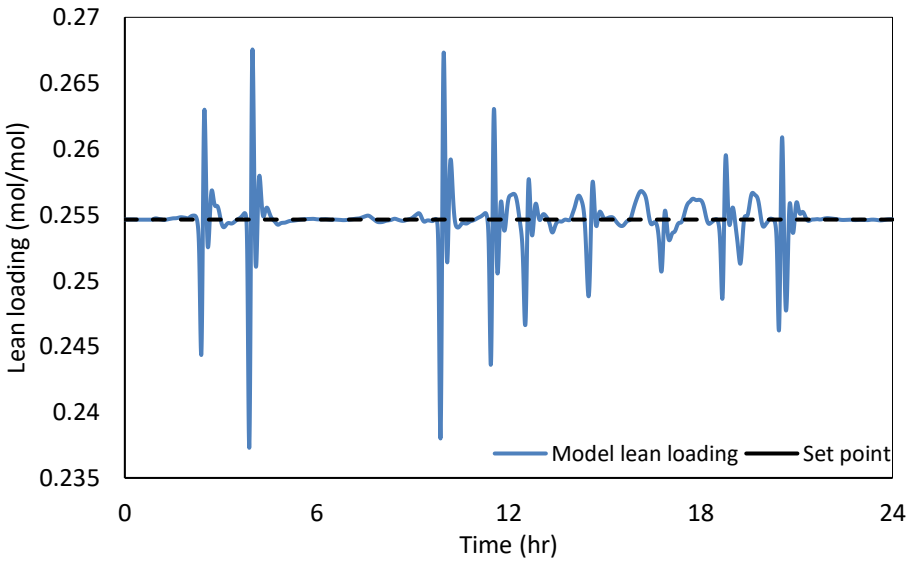

Figure 3.22 - Lean loading in Case 2

Figure 3.23 presents the stripper temperature profile in this case study. Even though the bottom temperature varies considerably, it still remains well below the solvent decomposition temperature. Considerably higher variability in the stripper top temperature is observed in comparison to the bottom. Figure 3.24 presents the instantaneous energy efficiency, which also shows considerable variability. Obviously, the variability can be correlated to the variability in the steam flowrate.

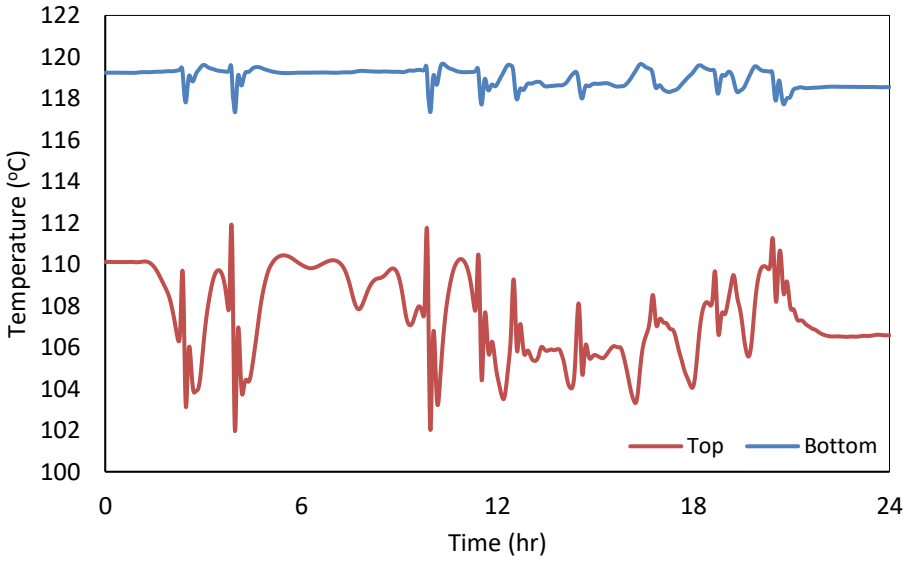

Figure 3.23 - Stripper bottom and top temperatures in Case 2

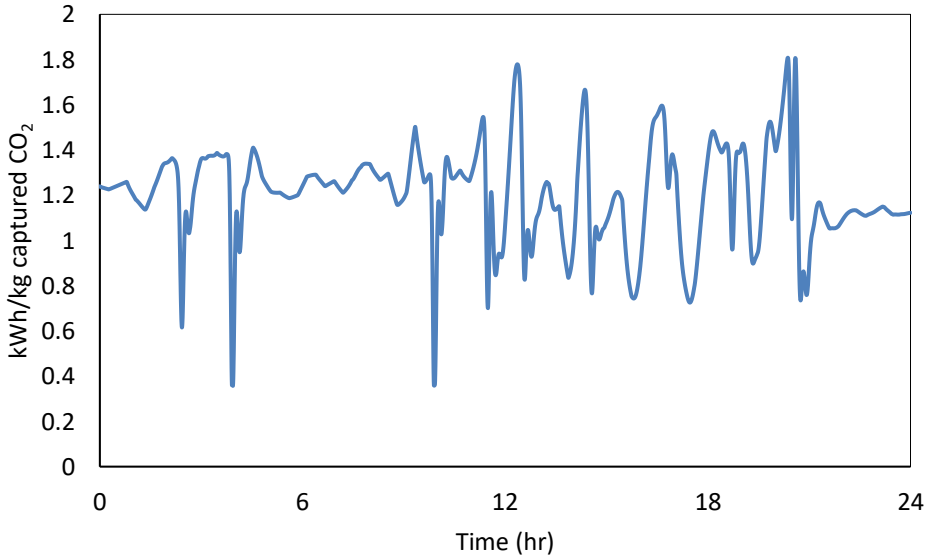

Figure 3.24 – Energy efficiency in Case 2

While conducting the studies presented above, the PID controllers were manually tuned. It was desired to analyze if the loop tuning techniques such as the IMC, Ziegler-Nichols, and Cohen-Coon rules, could lower the variability in the manipulated variables especially in the steam flowrate and thereby the energy efficiency. The estimated tuning parameters are presented in Table 3.6. The CO_2 capture rate in each of these cases had little variability in comparison to the manually tuned controller results, as presented in Figure 3.25. Figure 3.26 presents a zoomed view of the comparison between the CO_2 capture target and the actual CO_2 capture for various loop tuning techniques.

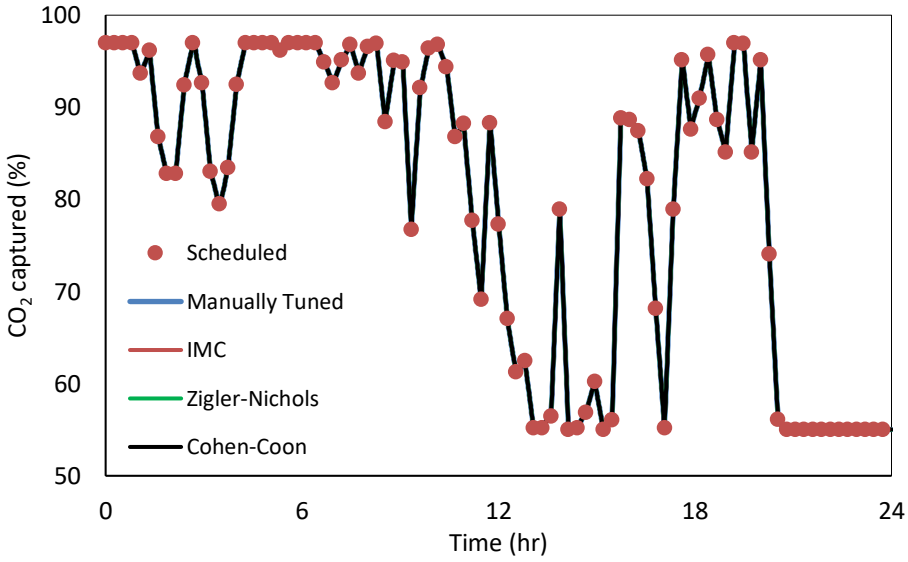

Figure 3.25 - CO_2 capture in Case 2 for various tuning methods

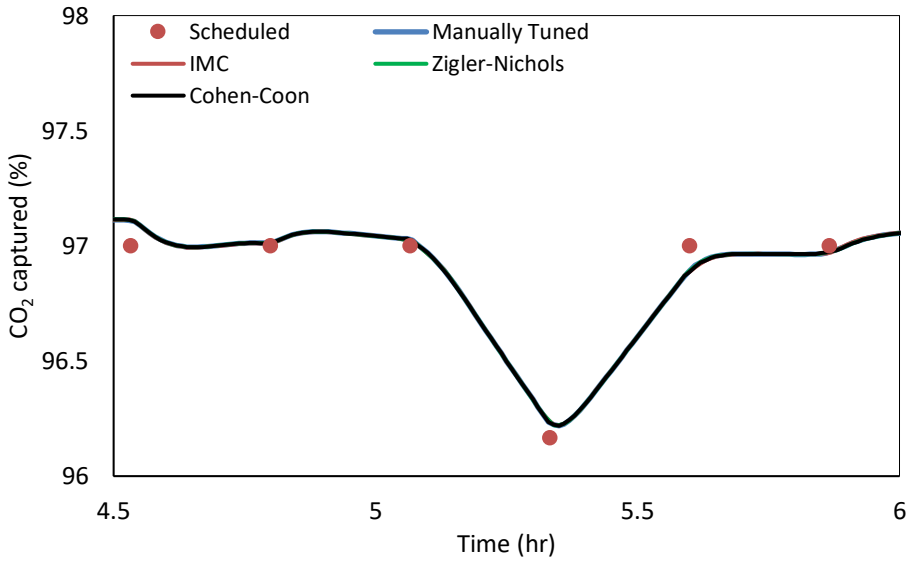

Figure 3.26 - Zoomed CO_2 capture in Case 2 for various tuning methods

Figure 3.27 presents the simulation results for the various controller tuning methods for the steam flowrate. Figure 3.28 and 3.29 shows that the variability in the lean loading could be lowered considerably by using the Ziegler-Nichols, and Cohen-Coon rules, while the IMC method introduced more variability in the steam flowrate in comparison to the manually-tuned controller. The high variability observed in the lean solvent, however, did not affect the CO_2 capture percentage performance not only due to the upper-level controller that uses the solvent flowrate as a manipulated variable, but also for the dampening effects of the storage tank in between the stripper and absorber. Similarly, Figure 3.30 and 3.31 show that the variability in the stripper temperatures especially in the top temperatures got reduced significantly. Figure 3.32 shows that there is some improvement in the energy efficiency when the Ziegler-Nichols, and Cohen-Coon rules were used in comparison to when the loop was manually tuned or tuned using the IMC rule. However, there is still considerable opportunity to maintain the efficiency close to its optimum using advanced controllers.

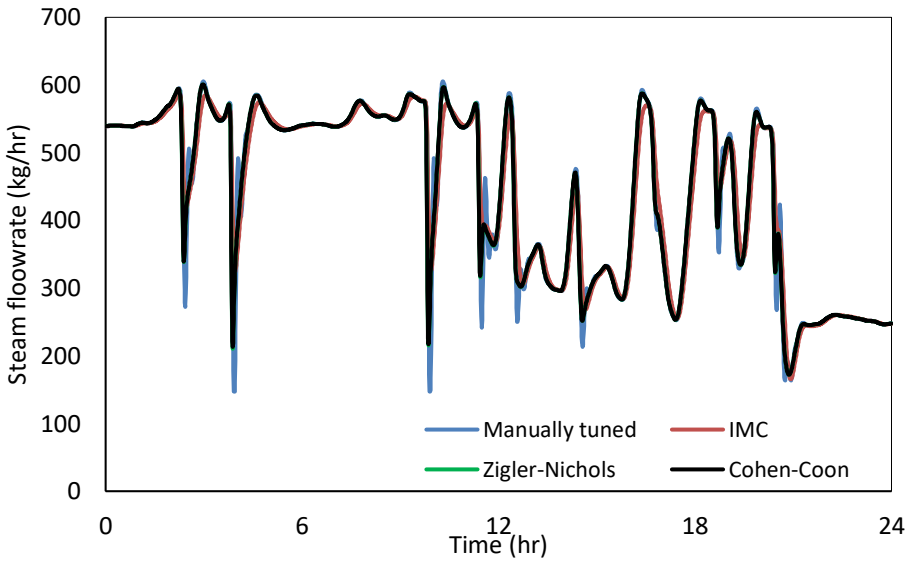

Figure 3.27 - Steam flowrate in Case 2 for various tuning methods

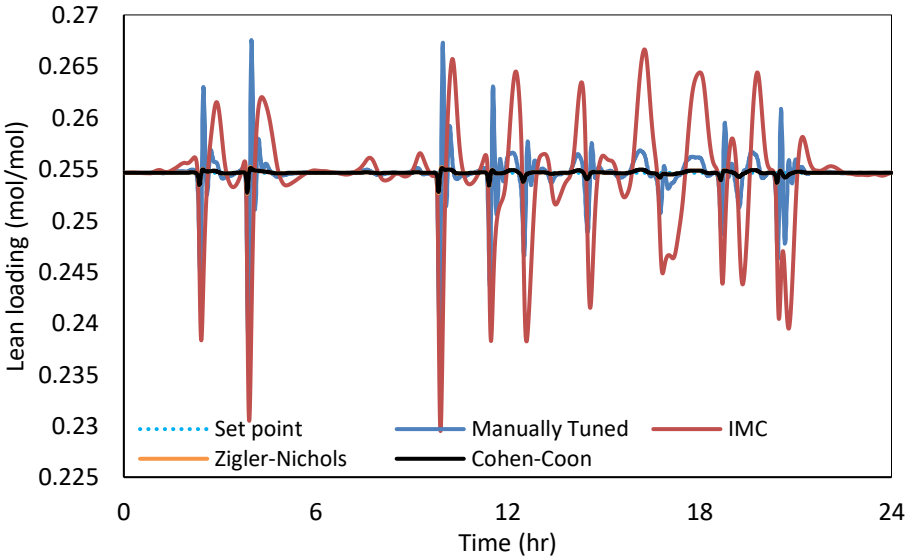

Figure 3.28 - Lean loading in Case 2 for various tuning methods

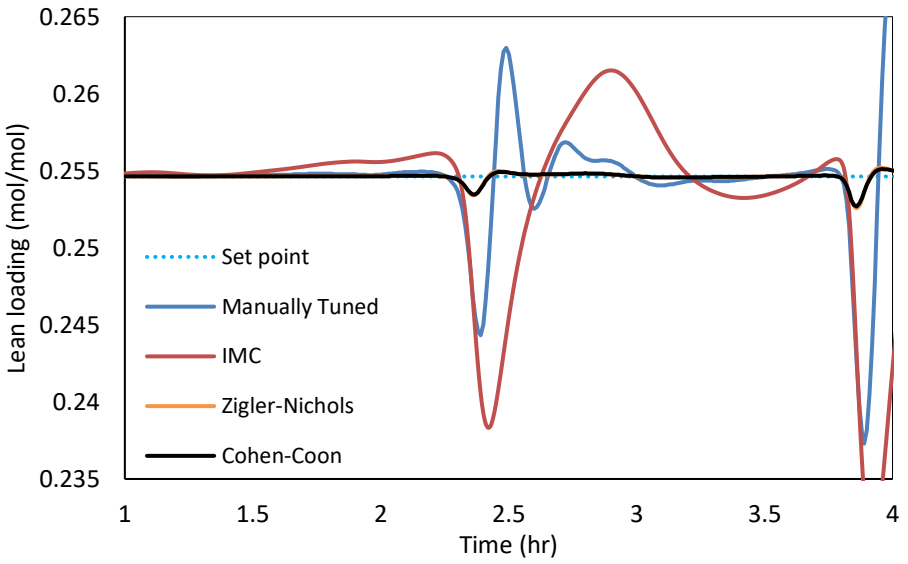

Figure 3.29 - Zoomed lean loading in Case 2 for various tuning methods

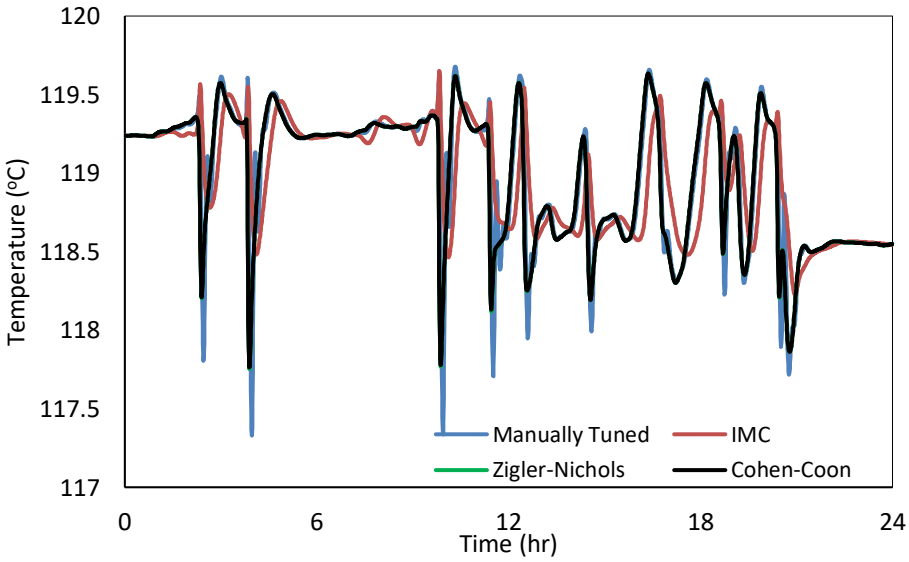

Figure 3.30 - Stripper bottom temperature in Case 2 for various tuning methods

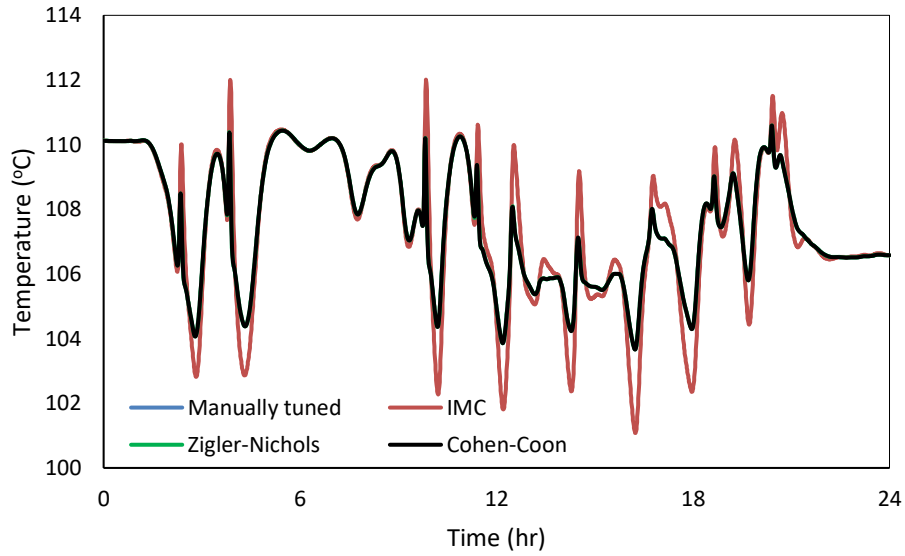

Figure 3.31 - Stripper top temperature in Case 2 for various tuning methods

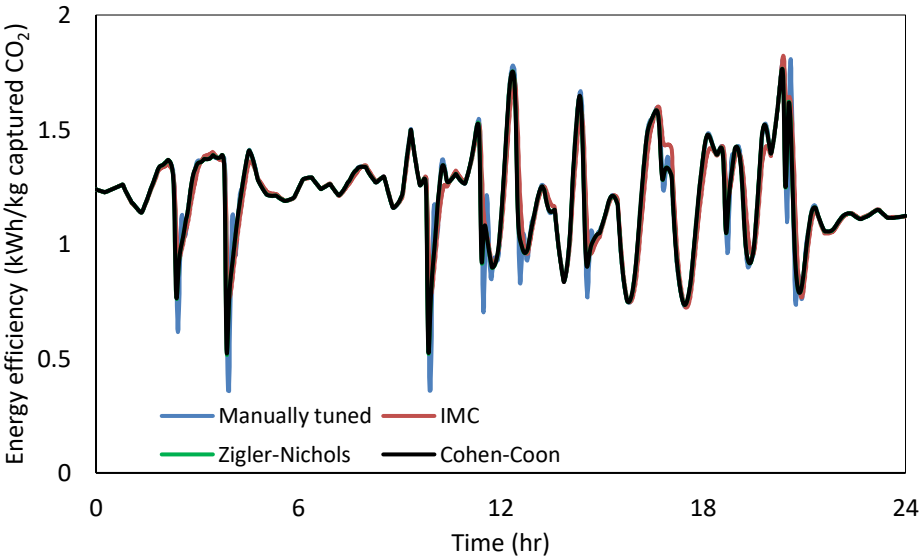

Figure 3.32 - Energy efficiency in Case 2 for various tuning methods

Table 3.6 – PID tuning parameters for the lean loading controller

Tuning method	Gain	Integral Time (min)	Derivative Time (min)

Manually tuned	2%	0.5	0
IMC	3.8%	6.87	0.37
Ziegler-Nichol	43.9%	1.56	0.39
Cohen-Coon	49.8%	1.82	0.28

3. 6. Conclusion

In this work, an APD model was developed starting with the Aspen Plus steady-state model by using a Murphree efficiency approach. A modified correlation for calculating the Murphree efficiency was developed where the parameters were estimated by using the results from the rate-based Aspen Plus model under varying operating conditions.

A pseudo-PRBS methodology was developed and implemented at the NCCC for performing dynamic test runs. The noisy data could be satisfactorily preprocessed using filtering technique. For satisfying the mass and energy balances, a DDR methodology was developed. This technique also helped to estimate the transient values of the variables that were not measured. The dynamic model was found to yield satisfactory estimates of transient CO_2 capture when steps changes in the solvent flowrate, flue gas flowrate, and steam flowrates were conducted. It was noticed that there is considerable discrepancies between the liquid side measurements and model predictions for all three cases. Considering the CO_2 balance of the system and based on the studies presented by Morgan (2017), these discrepancies are attributed to the errors in the experimental measurements of liquid loading and composition.

Two case studies were conducted that exhibit the nonlinearity of the process. It was noticed that depending on the change in the direction (increase or decrease) of the disturbance or manipulated variables, the process gain and time constants can change. It was observed that the time constant of the full plant can be considerably longer than the time constants of the absorber only or stripper only systems. It can be noted that the storage tank in between the absorber and stripper also resulted in an increase in the time constant. In another study, transient response to an optimal CO_2 capture schedule was studied. In this study, the flue gas flowrate also changes as the power plant optimally follows the load. It was observed that if the controllers are not optimally tuned, it can lead to considerable variations in the process variables especially in the steam flowrate to the reboiler that can affect the process efficiency. While the existing loop tuning techniques could improve the transient process efficiency, further improvement may be possible by using advanced controllers.

Lastly, it should be noted that the experiments conducted at NCCC were prepared without completing a full PRBS signal and, therefore, the data do not have the richness for parameter estimation. Moreover, one variables was changed at a time. Thus the process interaction due to simultaneous change in multiple variables are not captured in the data. A formal design of dynamic experiments methodology can, therefore, be useful to improve the outcome from the dynamic test runs.

Chapter 4. **Design of Dynamic Experiments**

Limitations of the dynamic design of experiments implemented at NCCC have been described in the previous chapter. The objective of the dynamic experiments described in this chapter is to estimate model parameters rather than validation of the dynamic model. For estimating n model parameters, the input signal should be designed to ensure persistence of excitation such that the signal has a spectrum of n nonzero distinct frequencies in its period. Various methods that vary in their frequency content, and waveforms can be used to design an input signal with the required properties. Each of these signal properties affect the following characteristics in the process as described below (Hjalmarsson, 2014):

- Variability: it is correlated to the level of excitation of the signal, and may cause the output being studied to reach an undesired value or specification.
- Frequency content: high frequency in the input signal may damage plant accessories and equipment items.
- Amplitude: a high values may be unacceptable and can also result in unrealistic values for the actuators whereas a low value may result in low signal-to-noise ratio for the output variables.
- Waveform: some waveforms may have difficult programming in the plant control system or can have large implementation error.

The power spectrum of a signal is an important criterion for design the input signals. It shows how the power of a signal is distributed over the frequencies. For a discrete-time signal $x(n)$ being applied to a process, the power spectrum can be calculated from its Discrete Fourier Transform (DFT):

$$X(k) = \frac{1}{N}\sum_{n=0}^{N-1} x(n) W_N^{kn} \tag{4.1}$$

$$W_N^{kn} = e^{-j2\pi kn/N} \tag{4.2}$$

This transformation is often called “forward DFT”, while a “backward DFT” differs by the sign of the exponent in Eq. (4.2), i.e. the exponent is given by $j2\pi\frac{nk}{N}$. It can be noted that the DFT can be readily

calculated by using the Fast Fourier Transform (FFT) algorithm. It should be noted that the designed input signals are always real. Because of that, the output signal $X(k)$ satisfies the symmetry:

$$X_m(k-n) = X^*(n) \tag{4.3}$$

, where * denotes complex conjugate. The power spectrum PS can then be generated by the following:

$$PS(f_m) = 2\frac{[X_m]^2}{f_S N}; \quad m = 0, \dots, N/2 \tag{4.4}$$

The power spectrum can be expressed in decibels (dB) to normalize its value and give an overall representation of its intensity, the conversion is defined as:

$$ratio[dB] = 10log_{10}\left(\frac{signal\ power}{reference\ power}\right) \tag{4.5}$$

Another important design criterion for the input signal is the sampling frequency. If a signal has its maximum frequency f_{Ny}, then as per the Nyquist theorem, its sampling frequency f_s, should be at least: $f_s = 2f_{Ny}$.

As mentioned earlier, the objective here is to estimate model parameters by optimal design of the dynamic experiments. Since large amount of data can be collected in a much shorter span of time as opposed to the steady-state test runs, it can help to reduce the time and resources for collecting the data. It is desired that the parameter estimates be unbiased, i.e. $E\{\hat{\theta}_N\} = \theta_N$ for a set of parameters $\hat{\theta}_N$ and consistent, i.e. $\lim_{n\to\infty} \hat{\theta}_N = \theta_N$. It is also desired that $\hat{\theta}_N$ has a small covariance. It is also desired that the estimator is efficient, i.e. its covariance is at least equal to the Cramér-Rao lower bound, which is given by:

$$CR = Fi^{-1}(\theta_N) \tag{4.6}$$

, where Fi is the Fisher information matrix, which is a measure of the information content in the experimental data.

With the objectives discussed above in mind, two signals, the pseudo-random binary sequence/signal (PRBS) and the Schroeder-phased input waveform signals are considered for the design of dynamic experiments (DoDE) at the NCCC pilot plant. Details of these signals are presented in details in the following sections.

4. 1. Pseudo-Random Binary Signal design of experiments

A PRBS is a two-level signal, represented by 0's or 1's generated with shift registers, which is given by Equation 4.7 (Miljković et al., 2011):

$$u(t) = rem(A(q)u(t), 2) \\ = rem(a_1 u(t-1) + \cdots + a_n u(t-n), 2) \tag{4.7}$$

, where $rem(x, 2)$ is the remainder of x divided by 2, which provides a binary value.

A representation of a 3 bit shift register sequence is presented in Figure 4.1.

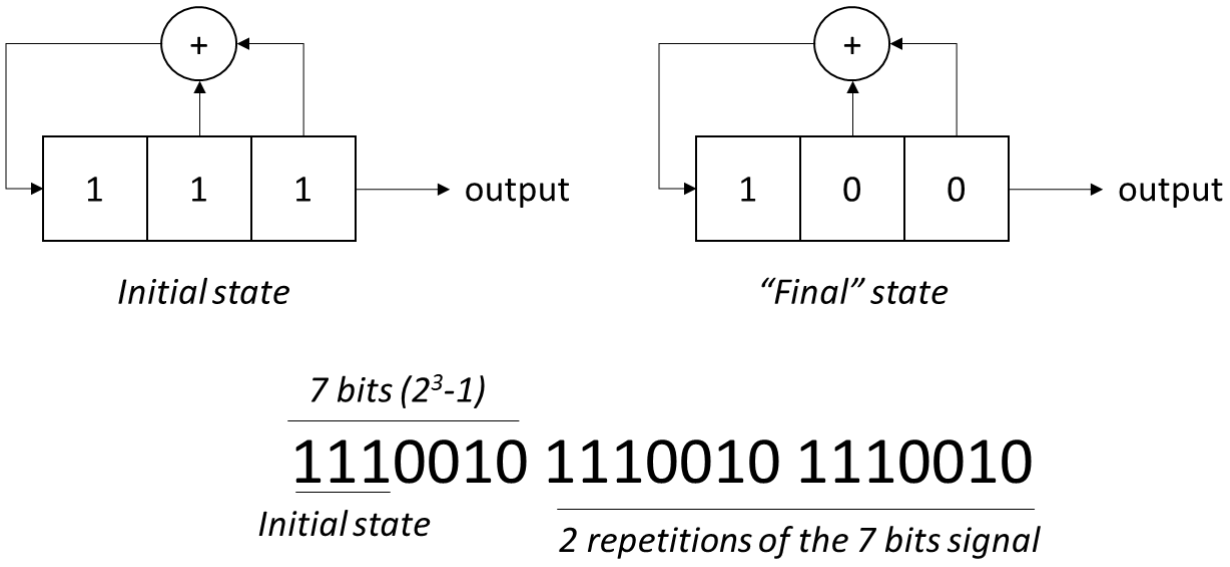

Figure 4.1 - 3 bit shift register example

The PRBS is a deterministic signal that has covariance similar to the white noise but its power spectrum is an impulse train while the while noise has flat spectrum. The signal has a length N_s, as described by Equation 4.8-11:

$$N_S = 2^{n_r} - 1 \tag{4.8}$$

$$N_{S_1} \geq \frac{\pi 6 \tau_{dom}^{H}}{T_{sw}} \tag{4.9}$$

$$N_{S_2} \geq p \times D \tag{4.10}$$

$$N_S = \max(N_{S_1}, N_{S_2}) \tag{4.11}$$

Here n_r, τ_{dom}^{H}, and τ_{dom}^{L} denote the number of shift registers, fastest and slowest time constants, respectively. It can be noted that the time constants can be estimated by using a process model, if available or through step tests. For example, during the 2014 NCCC test runs, the slowest ($\tau_{dom}^{H} = 0.15\ hr$) and fastest ($\tau_{dom}^{L} = 0.92\ hr$) time constants for the NCCC pilot plant were estimated through preliminary step tests. For multivariable PRBS design, it should be ensured that there is lack of cross-correlation between the signals (Gaikwad & Rivera, 1996). This is achieved by applying a delay D before implementing the subsequent variable till all p variables are exhausted. The delay can be calculated by taking into account the switching time T_{sw} as shown in Eq. 4.12. The overall time required to implement the signal for a single variable can be obtained by multiplying the signal length N_s with the switching time, $t_{final} = T_{sw} N_s$.

$$D = \frac{T_{settle}^{max}}{T_{sw}} \tag{4.12}$$

$$T_{sw} \leq \frac{2.8 \tau_{dom}^{L}}{2} \tag{4.13}$$

A persistently exciting input signal with high signal to noise ratio may not be acceptable to the plant operators due to its possible impact on equipment wear and tear, product quality violation, safety hazards and violation of environmental hazards. Therefore, the signals need to be designed such that the sequence is 'plant friendly' (Narasimhan et al., 2011; Rivera et al., 2009). While the friendliness of the input signal

can be quantified by considering the crest factor that can be represented by the ratio of the L_∞ norm to the L_2 norm of the signal, it was determined that the desired magnitudes and switching times of the bi-level signals were acceptable for all inputs, but it was desired that the output plant friendliness be considered as reflected in variability of the CO_2 capture percentage. It can be noted that large variability in CO_2 capture rate can not only cause considerable noise in the gas composition sensor measurements, it can cause loss in the solvent from the absorber due to large variations in the pressure. Due to the high nonlinearity of the process, it was desired that the magnitudes of the bi-level signals be adjusted to ensure the desired boundedness in the output. All other parameters as discussed above for PRBS design were determined by simulating the Aspen Plus dynamics® model described earlier. Due to inaccuracies in the model, the designed signals were implemented in the NCCC control system in such a way that the signal magnitude for each bi-level signal can be readily changed if it violates plant friendliness criteria. Figure 4.2 presents the designed PRBS in its general form.

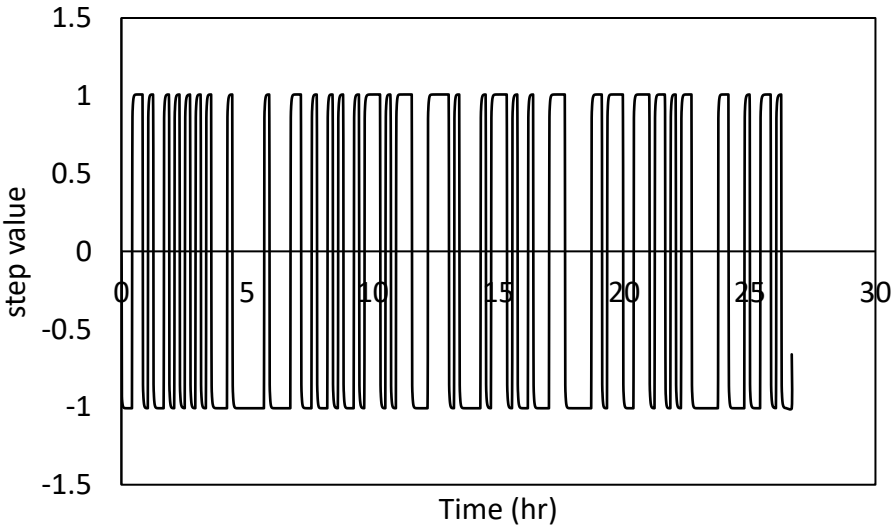

Figure 4.2 - PRBS designed signal

The signal magnitudes of each PRBS input were determined to ensure the signal would be constrained in the following operating conditions:

- Lean solvent flowrate: 5400 kg/hr – 5950 kg/hr
- Flue gas flowrate: 2130 kg/hr – 2360 kg/hr

- Flue gas CO_2 concentration: 10%w – 17.5%w
- Steam flowrate: 465 kg/hr – 515 kg/hr

Figure 4.3-4.6 present the designed signals already taking into consideration each of the delays necessary for the experimental implementation for the mentioned variables. Figure 4.7 presents the combined signals as designed to be implemented in NCCC. While plotting in Figure 4.7, individual signals are scaled so that the relative time delay can be clearly seen on the same figure. The gas flowrates, solvent flowrates, steam flowrates, and flue gas CO_2 concentration are scaled between -1 to 1, 2 to 4, 5 to 7, 8 to 10, respectively. It should be noted that this scaling is done only for illustration purpose and does not indicate relative intensity of the signals.

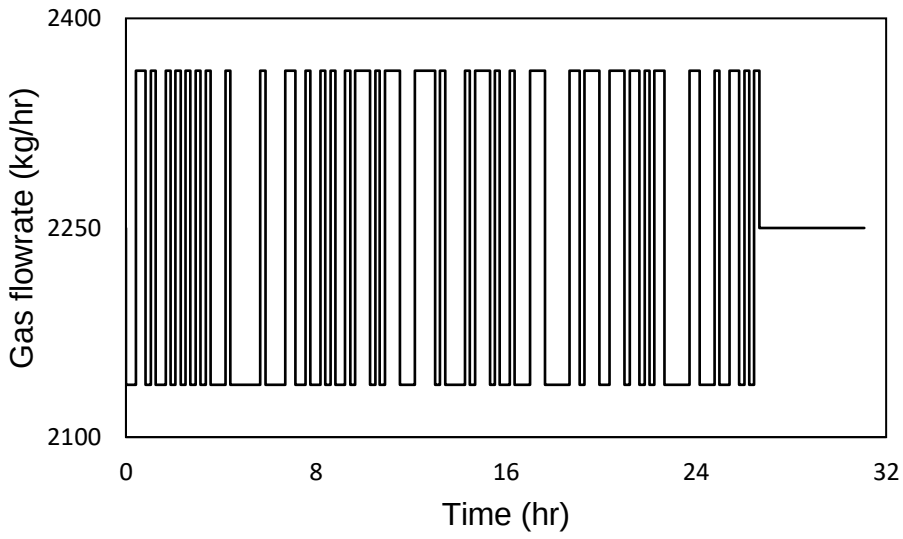

Figure 4.3 - Designed PRBS for gas flowrate

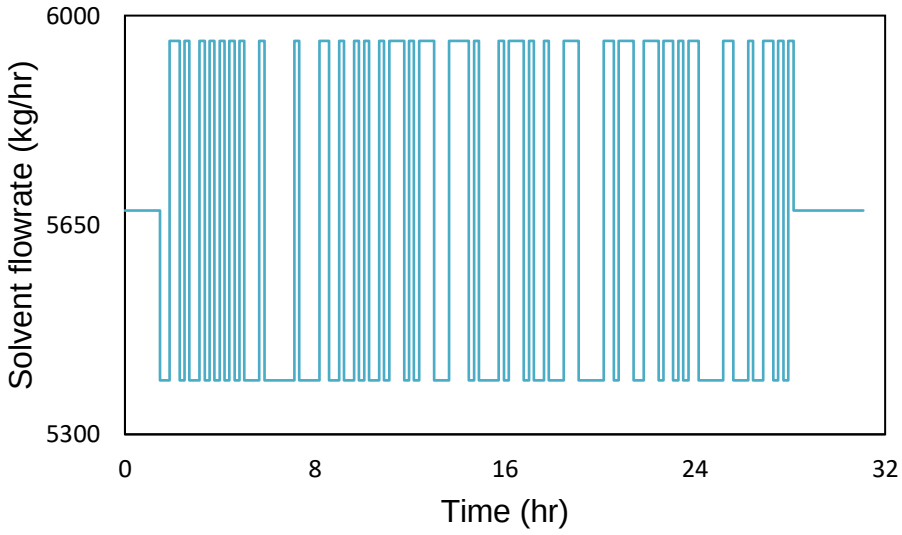

Figure 4.4 - Designed PRBS for solvent flowrate

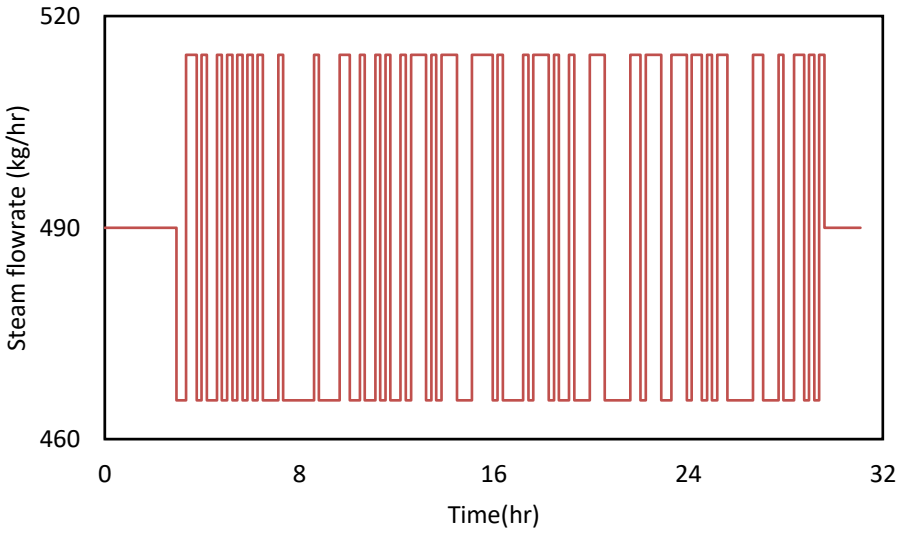

Figure 4.5 - Designed PRBS for steam flowrate

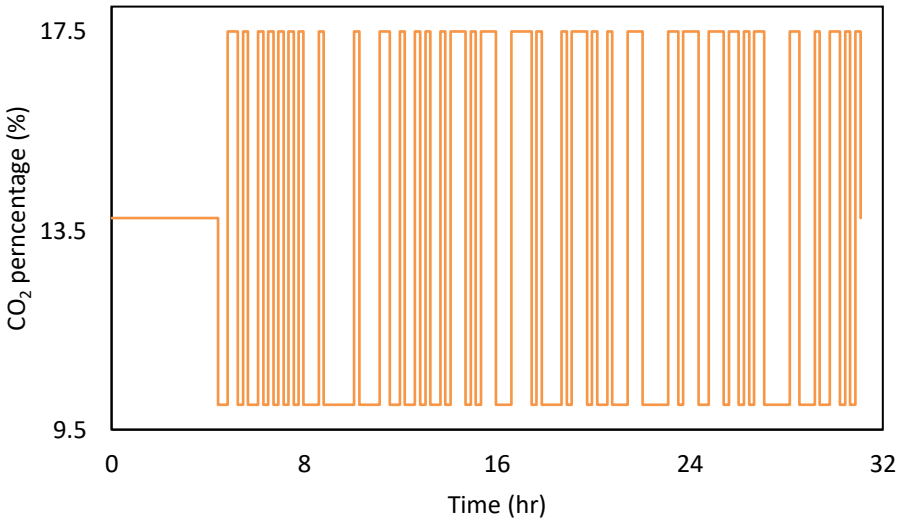

Figure 4.6 - Designed PRBS for CO_2 percentage in the flue gas

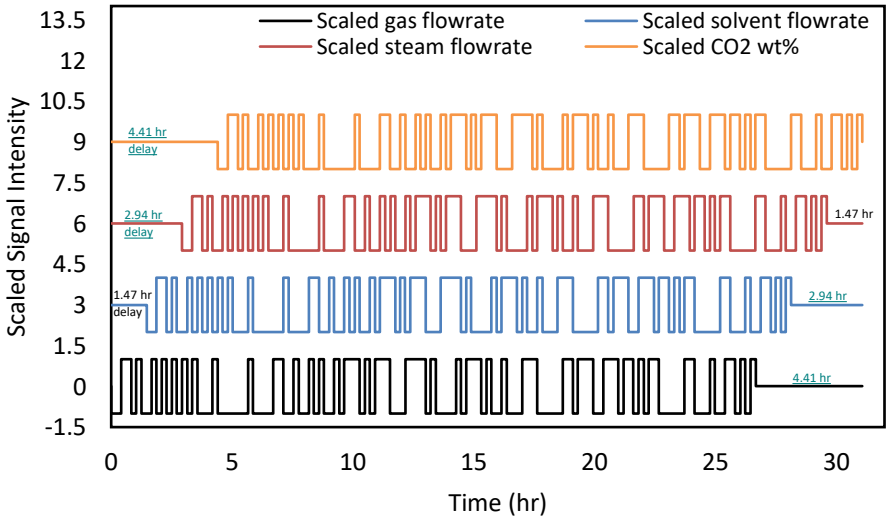

Figure 4.7 - Combined scaled PRBS design for implementation in the pilot plant (Signals are scaled so that the signals and the time delay can be distinct; scaled values do not mean to show the relative intensity of the signals)

The output plant-friendliness analysis that was done before the implementation at NCCC by using the Aspen Plus Dynamics model is shown in Figure 4.8. Based on the switching time, it was determined that if the maximum change in the CO_2 capture is constrained between about 65-90%, it will result in an acceptable

rate of change in the pilot plant and the plant will not reach mass transfer pinch. As seen in Figure 4.7, the design inputs signals were considered to be acceptable. It can be noted that in reality, no other changes were made in the input signals during the actual implementation in NCCC.

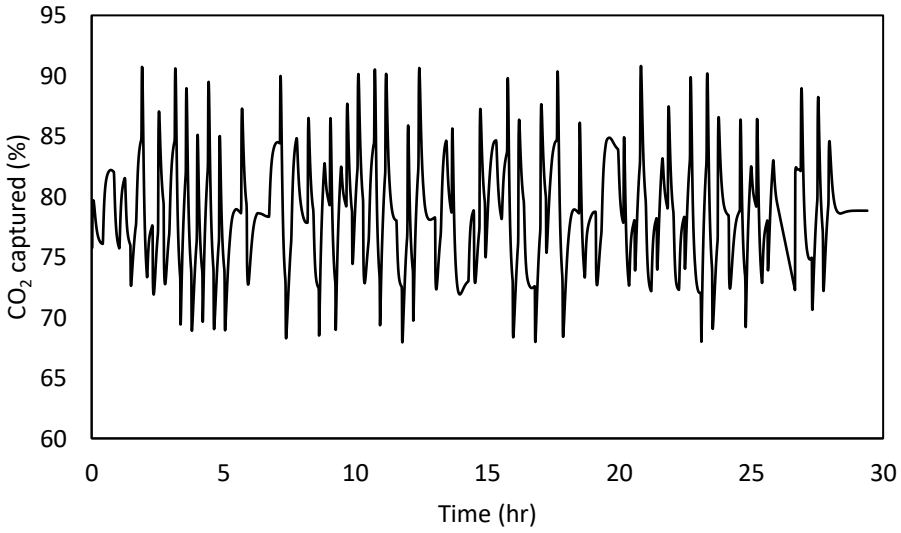

Figure 4.8 - CO_2 capture prediction from the PRBS designed signals

Figure 4.9 presents the power spectrum for the designed PRBS signal and Figure 4.10 presents the power spectrum for the CO_2 capture output signal. It can be observed that the power of the signals is reasonably uniformly distributed over the entire frequency range of interest.

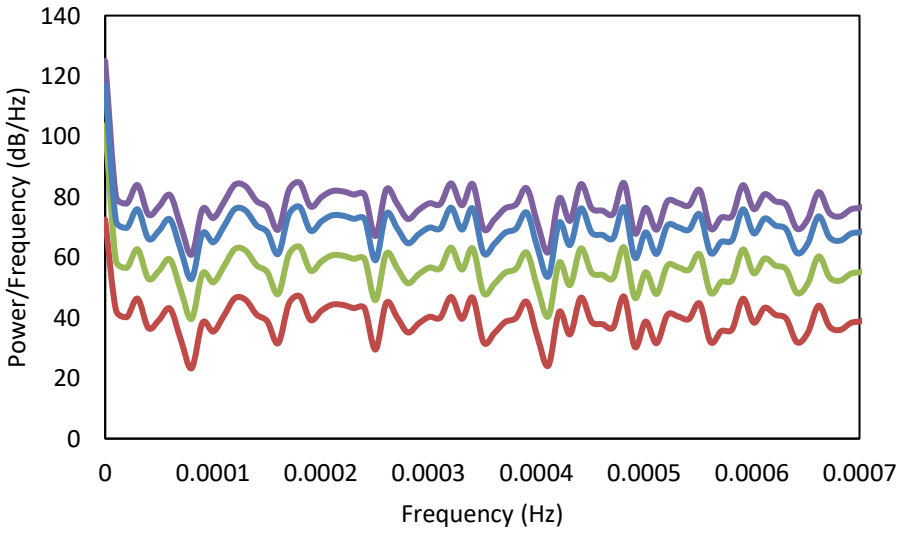

Figure 4.9 - Power spectrum of the PRBS DoDE

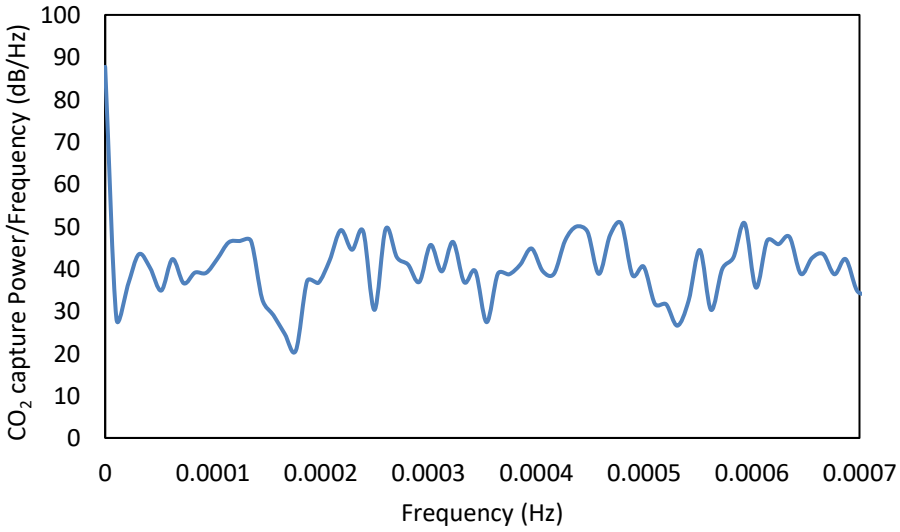

Figure 4.10 - Power spectrum of the PRBS DoDE response

4. 2. Schroeder-phased input signal

The Schroeder-phased input is a periodic and deterministic multisine input. It has a flexible spectrum that can be designed based on the specific requirement of a given process, as the input energy can be placed in

discrete frequency points. Thus low peak-factors, or crest factors can be attained, often associated with the Schroeder phased signals. The signal is given by Eq. 4.14:

$$u_n = \lambda_n \sum_{j=1}^{N_s/2} \sqrt{2\alpha_{[n,j]}} cos\left(\omega_j kT + \Phi_{[n.j]}\right) \quad (4.14)$$

$$\omega_j = \frac{2\pi j}{N_s T}, k = 1,2 \ldots., N_s$$

$$\alpha_{[n,j]} = \begin{cases} 1, & if\ j = L_u(i-1) + n \\ 0, & otherwise \end{cases} \quad (4.15)$$

$$\frac{2\pi}{N_s T} \leq \omega \leq \frac{2\pi n_s L_u}{N_s T} < \frac{\pi}{T} \quad (4.16)$$

$$\max\left(2n_s L_u, \frac{2\pi}{\omega_* T}\right) \leq N_s \leq \frac{2\pi n_s L_u}{\omega^* T} \quad (4.17)$$

$$\frac{1}{3\tau_{dom}^H} = \omega_* \leq \omega \leq \omega^* = \frac{2}{\tau_{dom}^L} \quad (4.18)$$

$$n_s \geq \frac{1}{L_u} \frac{\omega^*}{\omega} \quad (4.19)$$

In the equations above, λ_n is a scaling factor, N_s is the signal period, T is the sampling time. Each sinusoid has a coefficient $\alpha_{[n,j]}$ that is used to specify the power of each one of them, ω_j specifies the sinusoid frequency and $\Phi_{[n.j]}$ its phase. The coefficients $\alpha_{[n,j]}$ are determined by assuming that the signals are orthogonally excited in frequency. In this work a "zippered" design is used for the coefficients (Mart et al., 2015), which means that for a specific non-zero Fourier coefficient frequency, all other signals have a zero-valued Fourier coefficient. The total number of harmonics is determined by the number of excited sinusoids n_s and the number of input variables L_u by using the equation: $n_h = n_s L_u$.

The phase matrix $\Phi_{[n.j]}$ provides considerable flexibility to the design of the Schroeder-phased signal. A simple general form for specifying the phases requires consideration of the relative power p_j of the j[th] harmonic (Rivera et al., 2009):

$$\sum_{j=1}^{N} p_j = 1 \quad (4.20)$$

$$\Phi_j = 2\pi \sum_{k=1}^{j} p_k \tag{4.21}$$

The design parameters such as the signal period, N_s, the lower and the upper frequency bounds ω_* and ω^*, were calculated by simulating the dynamic model of the NCCC pilot plant described in Chapter 3. The corresponding signals for four inputs are presented in Figure 4.11. It can be noted that Figure 4.11 is generated using $\lambda = 1$, for demonstrating the issue with the high crest factor, if the signals are properly designed. The final values of λ_n are determined to ensure the signal would be constrained in the same operating conditions as described earlier for the PRBS signal design. The high peaks, i.e. high crest factors, observed at $t = \{6,12,18\}$ hr are not acceptable. To make the signals plant friendly, the phases $\Phi_{[n.j]}$ can be designed appropriately.

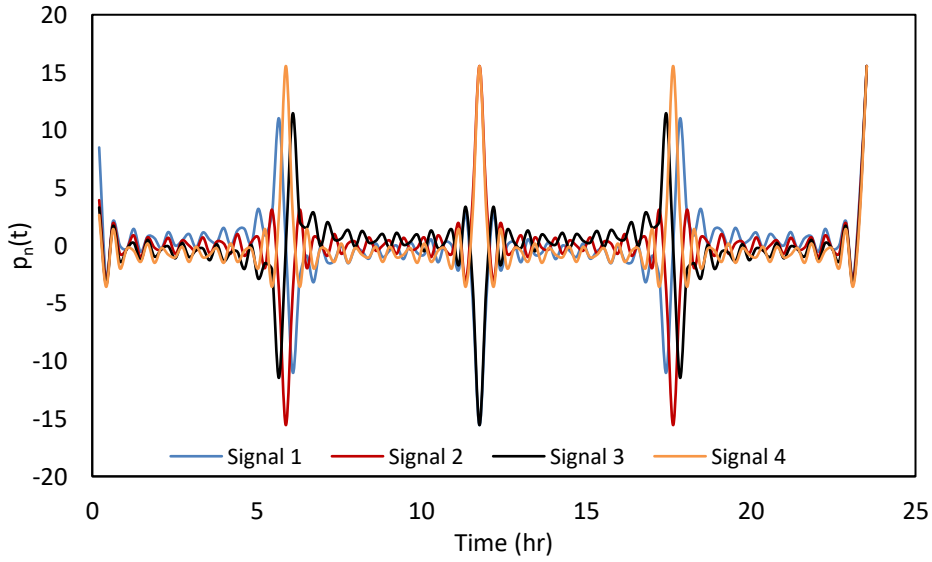

Figure 4.11 - Non optimized Schroeder-phased design signals

To avoid the issue with high crest factor, $\Phi_{[n.j]}$ were determined by minimizing the crest factor (CF) defined in Equation 4.22-24 (Guillaume et al., 1991).

$$CF = \frac{L_\infty(p_n)}{L_2(p_n)} \tag{4.22}$$

$$L_\infty(p_n) = \max|p_n| \tag{4.23}$$

$$L_2(p_n) = \left[\frac{1}{T}\int_0^T |p_n(T)|^2 dT\right]^{1/2} \tag{4.24}$$

The signals obtained for each of these variables is presented in Figure 4.12 - 4.15. While designing the signal for the CO_2 concentration in the flue gas, its variability is kept constrained based on what could be achieved using the existing control strategy in NCCC, where the flue gas CO_2 concentration is controlled by diluting it with N_2. It should be noted that these signals are simultaneously implemented as shown in Figure 4.16.

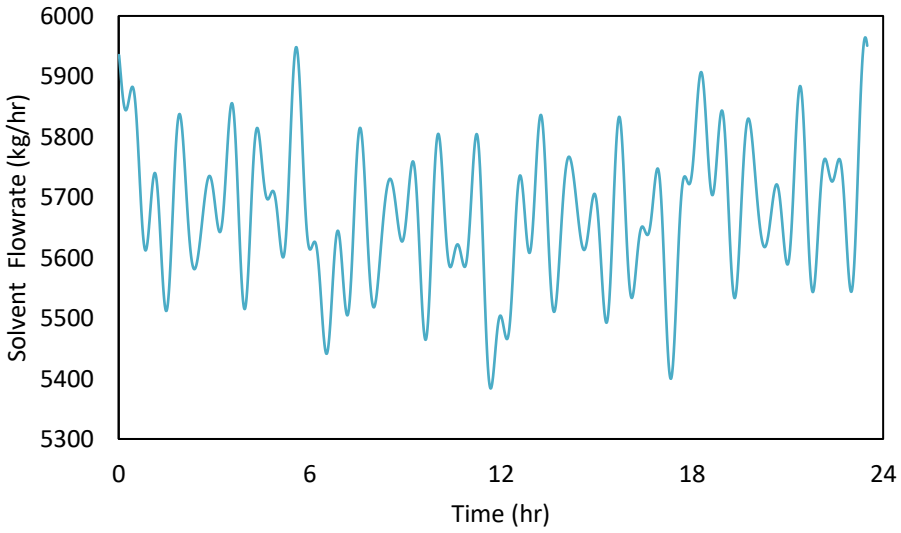

Figure 4.12 - Designed Schroeder-phased input for Solvent flowrate

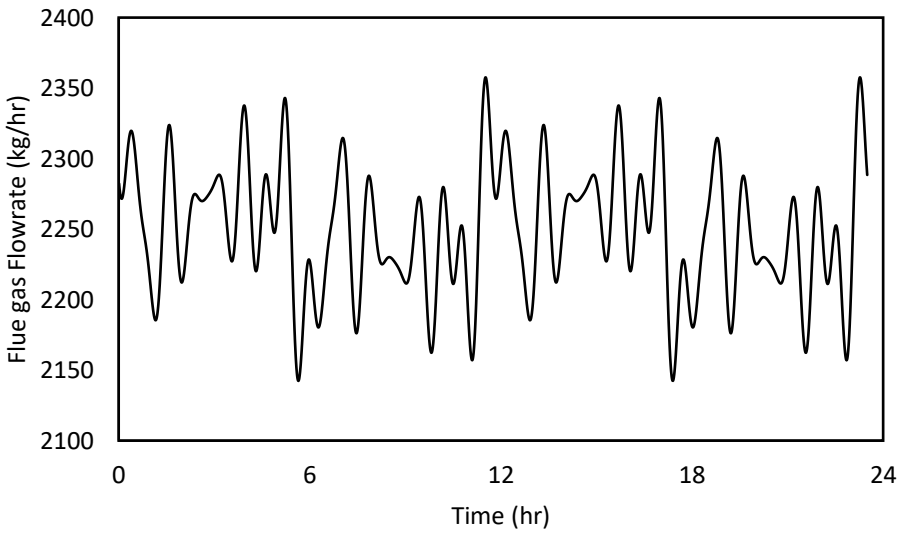

Figure 4.13- Designed Schroeder-phased input for flue gas flowrate

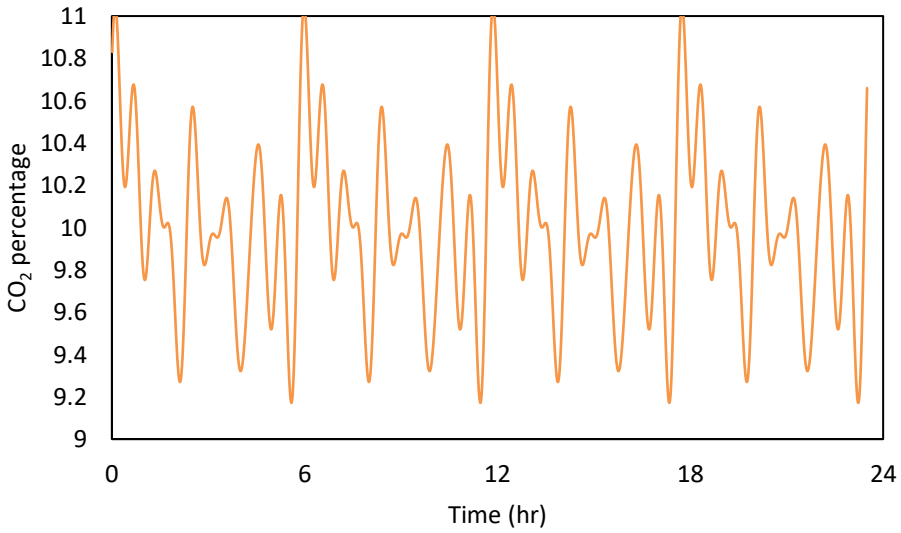

Figure 4.14- Designed Schroeder-phased input for CO_2 concentration in the flue gas

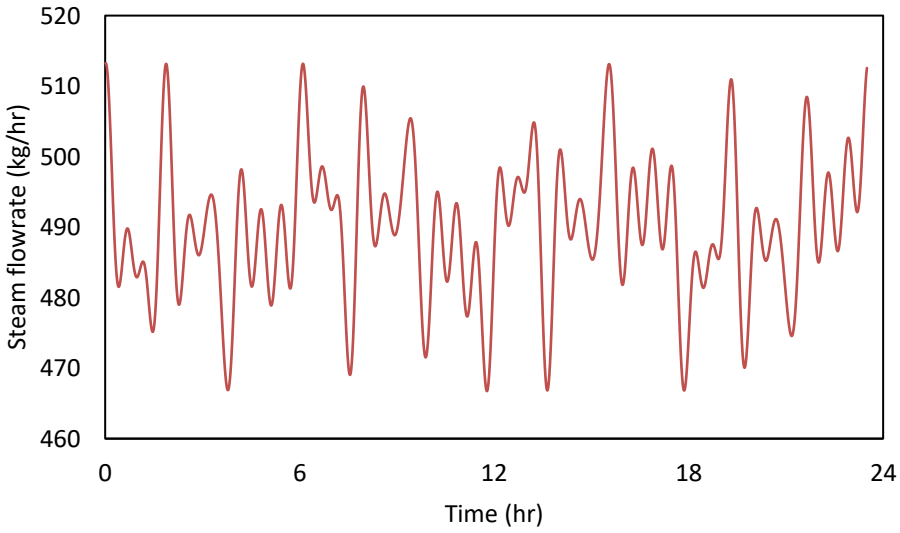

Figure 4.15 - Designed Schroeder-phased input for steam flowrate

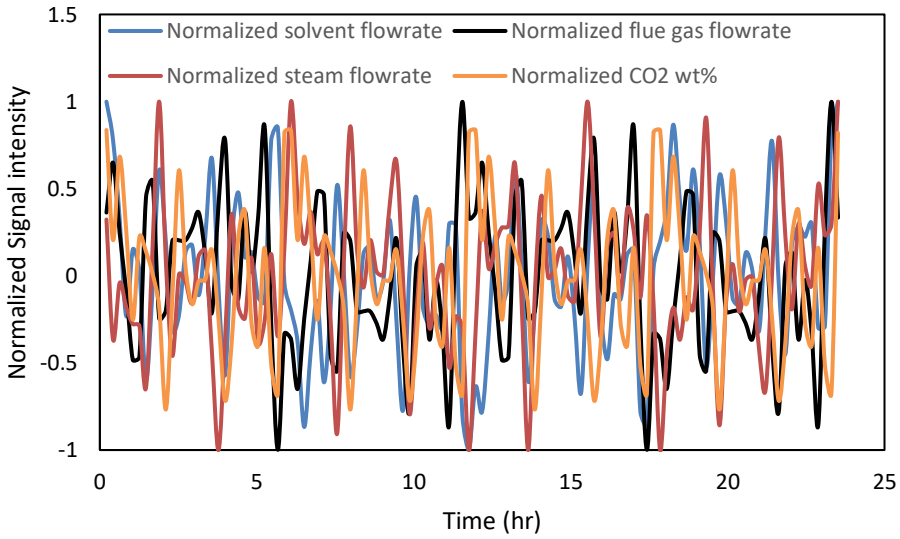

Figure 4.16 - Combined normalized signals for the Schroeder-phased design

Figure 4.17 presents the estimated CO_2 capture percentage from the Schroeder-phased input signal design of experiments. It can be observed that the CO_2 capture would remain constrained within the bounds 65-90% as discussed earlier.

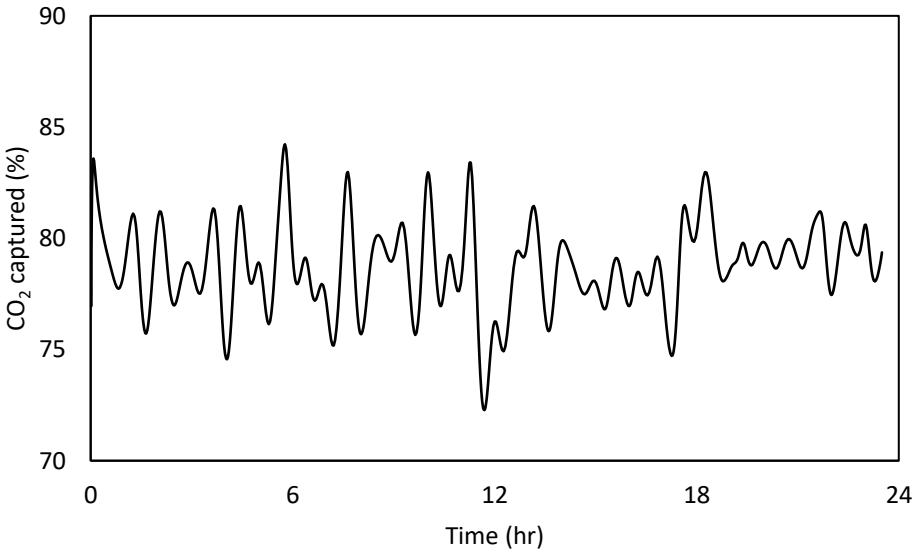

Figure 4.17 - CO_2 capture prediction from the Schroeder-phased input signals

The power spectrum of the input signals designed from the Schroeder-phased input guidelines are presented in Figure 4.18. As observed in that figure, the main characteristics of the signals can be verified in this plot, as the power spectrums present the same behavior and shape, but with different relative powers and phases.

Figure 4.19 presents the power spectrum for the simulated Schroeder-phased inputs signal response, which exhibits high and reasonably flat power in the entire frequency range of interest. It can be observed that the designed Schroeder-phased inputs have better properties in comparison to the PRBS signals as they yield higher power with less variability in the entire frequency range in comparison to the PRBS signal. In addition, as noted earlier, the Schroeder-phased input can be implemented in shorter time span than the PRBS signal. For this case, the PRBS signal took about 32 hrs while the Schroder-phased inputs took less than 24 hr to implement the entire sequence.

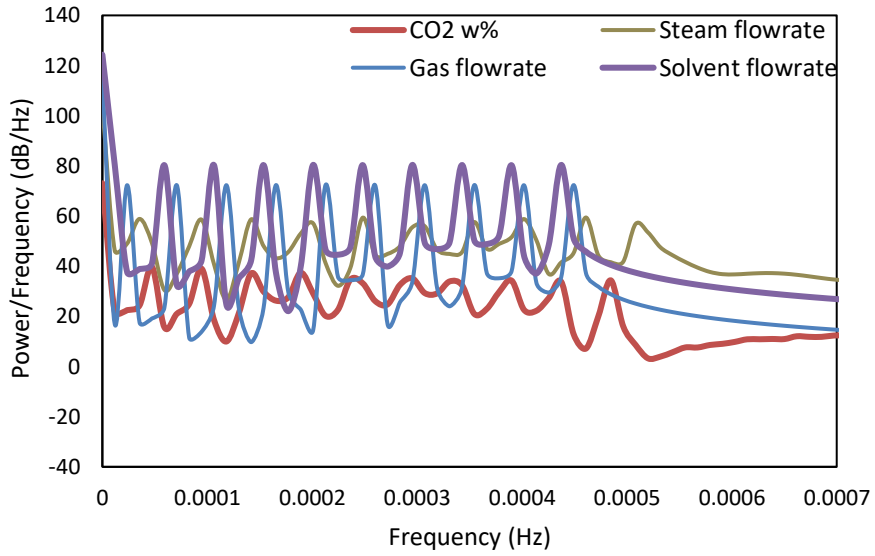

Figure 4.18 - Power spectrum density of the designed Schroeder-phased signals

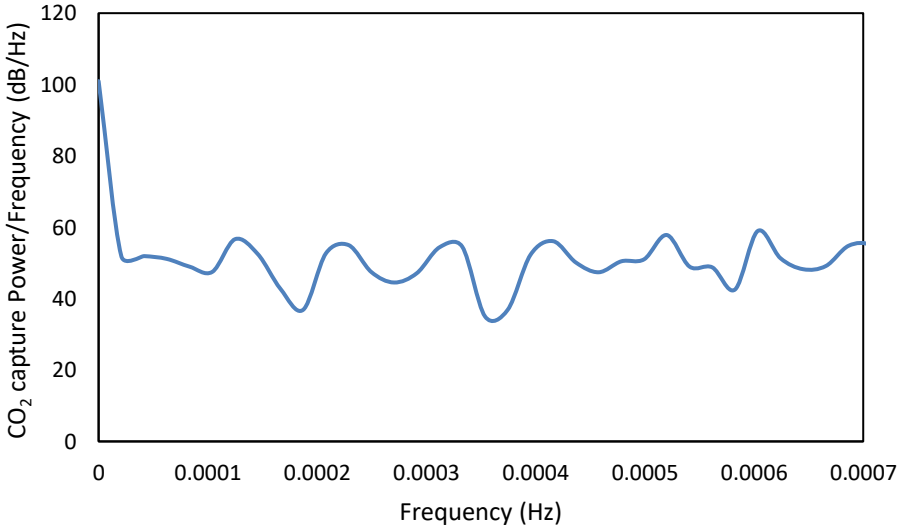

Figure 4.19 - Power spectrum density of the simulated CO_2 capture

4. 3. Summary of the overall methodology

A summary of the approach taken in this work can be described by the algorithm presented in Figure 4.20. For each input signal design technique, various information need to be obtained and decisions need to be made as listed below:

- Number of input variables
- Feasible ranges of input variables
- Rate of change of input variables
- Maximum settling time
- Lowest dominant time constant
- Highest dominant time constant
- Factors and variables for plant-friendliness analysis

For information such as feasible range of design variables and plant friendliness analysis, plant operating personnel needs to be consulted to check with hardware limitations, plant control system constraints, operating constraints based on the plant design and the solvent-type and impurities present in the flue gas and circulating solvent, safety constraints, environmental emission issues, unmodeled phenomena, etc. Other information such as the time constants and settling time can be obtained by performing preliminary step tests in the plant or by simulating these steps in an existing process model with due consideration of the inaccuracies in that model. While input plant friendliness can be ensured, it is hard to ensure output plant friendliness especially if the plant is highly nonlinear. Once the preliminary design is obtained, if a preliminary dynamic process model is available, it can be used to check the output plant friendliness. In absence of a model, a worst case analysis can be made to determine the worst case change/rate of change in the output variables through tests in the plant.

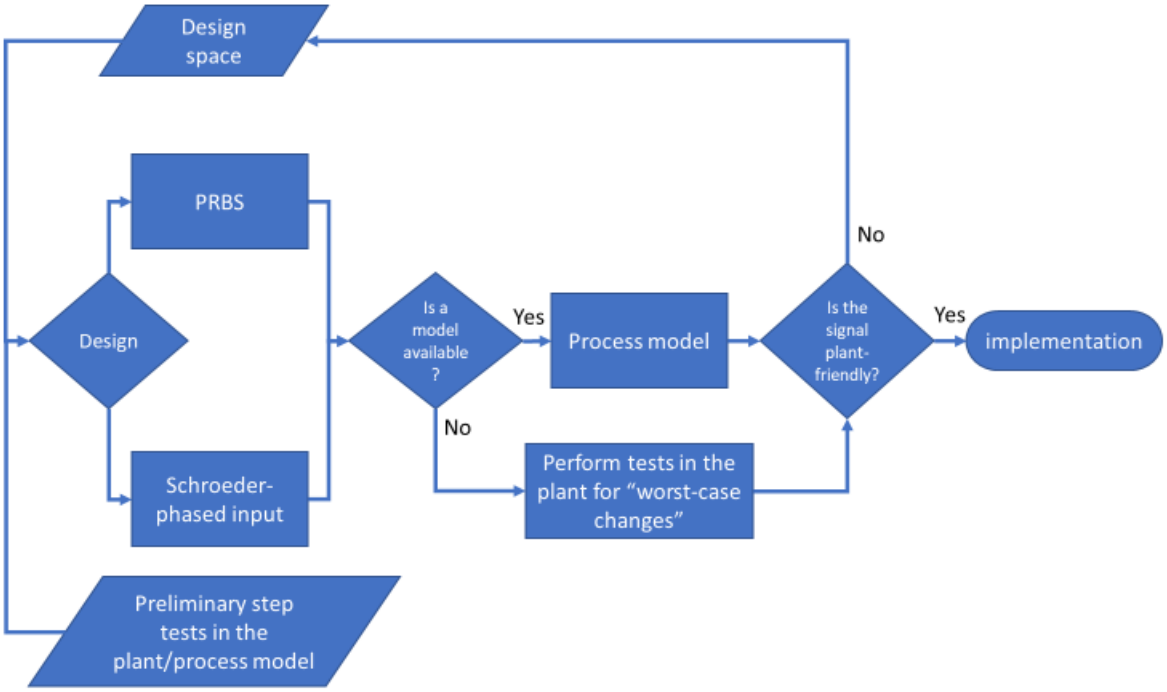

Figure 4.20 - DoDE Development Approach

4. 4. Implementation errors

The signals designed and presented in the previous sections were implemented in NCCC over the course of approximately 3 days (2 days for the PRBS DoDE and 1 day for the Schroeder-phased DoDE), where the tests were initiated after bringing back to the plant close to the desired steady state. Figure 4.21 to Figure 4.26 present the designed PRBS and the actual implementation/measured values for the main input variables discussed in Section 4.1. It is observed that there is low implementation error in the solvent flow rate (Figure 4.23) and steam flowrate (Figure 4.25), but there is high implementation error in the gas flowrate (Figure 4.21). The main issue is found in the implementation of the input signal for the wt% CO_2 as seen in Figure 4.26. The actual value did never reach below about 12.5 wt% CO_2 while the desired value was as low as 10 wt% CO_2. Looking at these signals, two other observations can be made: (1) the signals were noisy, (2) considering the relative large change in the input variables before the PRBS signals were implemented and based on our current knowledge about the settling time of the overall process, it can be anticipated that the plant was not at the steady-state. Therefore, dynamic data-reconciliation and estimation of the initial states and parameters become challenging and very important. Figure 4.27 compares the power spectrum of the actual vs design signals for the CO_2 weight percentage in the flue gas. It is observed that

the implemented signal still has reasonably high power in the entire range albeit low power at some frequency range.

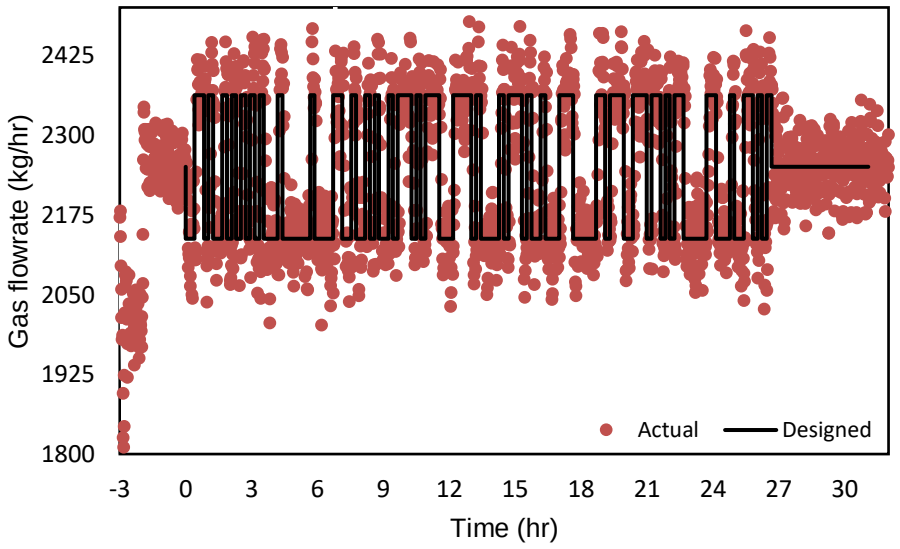

Figure 4.21 - Comparison between design and implementation for the PRBS for the gas flowrate

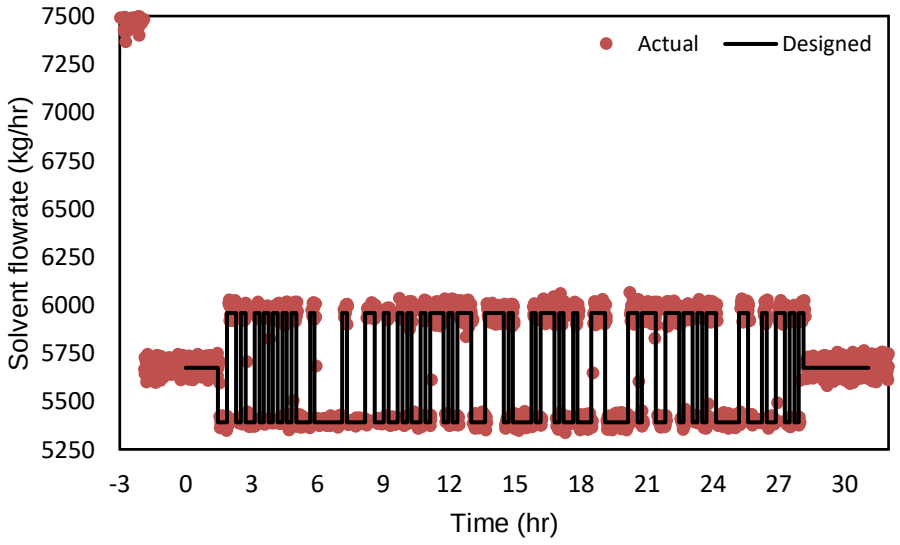

Figure 4.22 - Comparison between design and implementation for the PRBS for the solvent flowrate

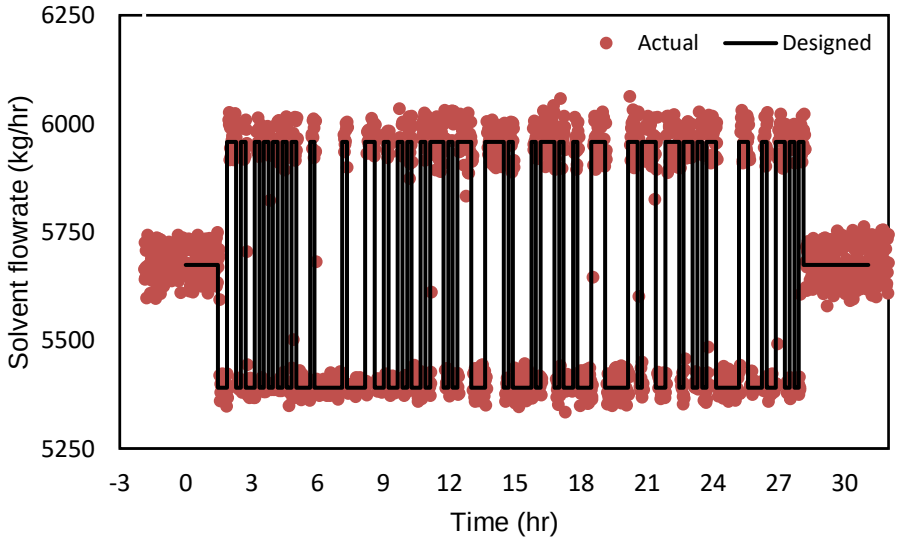

Figure 4.23 - Zoomed comparison between design and implementation for the PRBS for the solvent flowrate

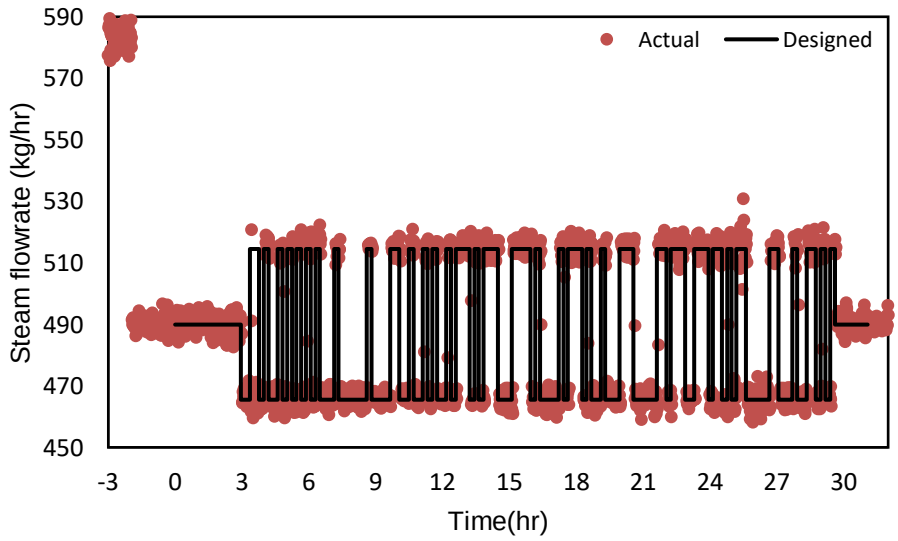

Figure 4.24 - Comparison between design and implementation for the PRBS for the steam flowrate

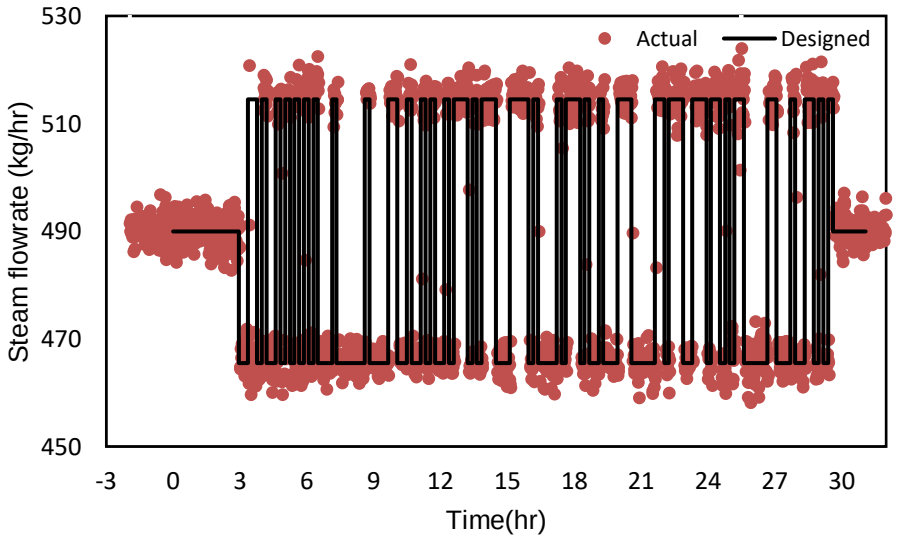

Figure 4.25 - Zoomed comparison between design and implementation for the PRBS for the steam flowrate

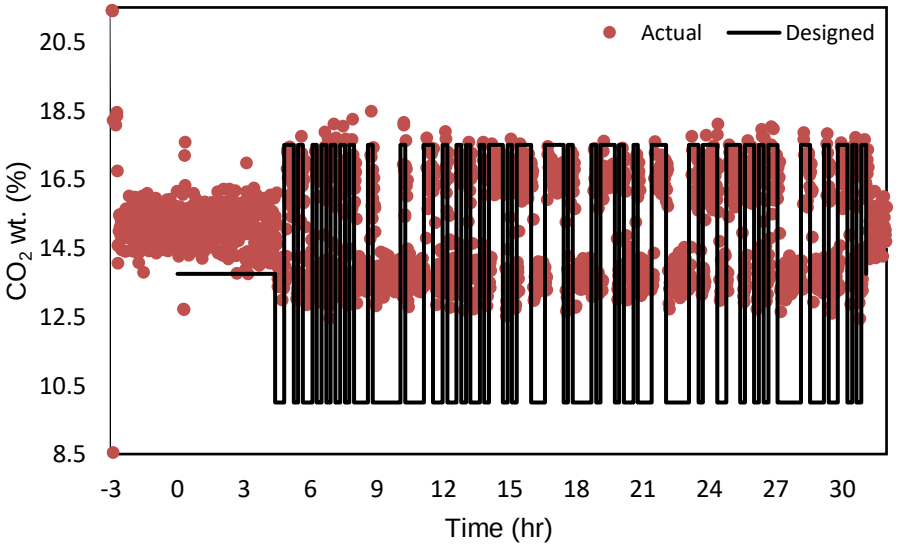

Figure 4.26 - Comparison between design and implementation for the PRBS for CO_2 wt% in the inlet flue gas

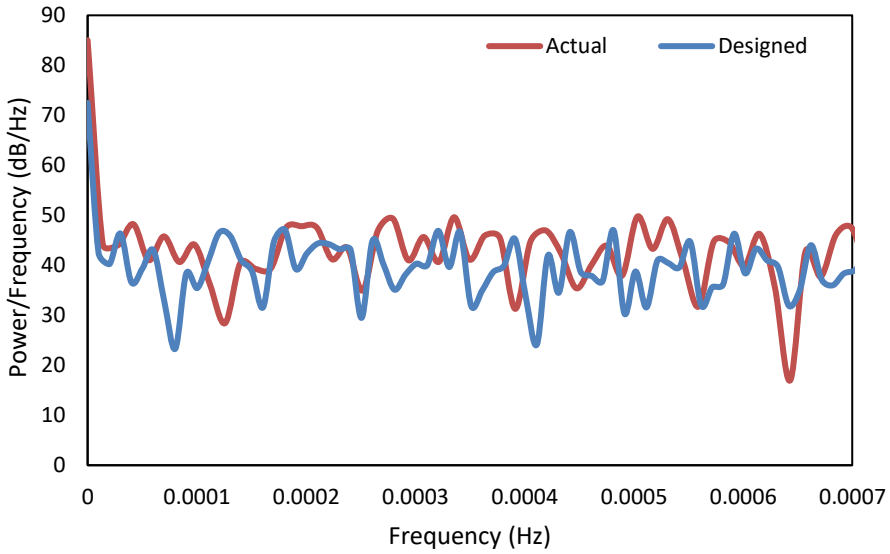

Figure 4.27 - PRBS power spectrum density for the CO_2 w%

Figure 4.28 to Figure 4.31 show that the implementation error in the Schroeder-phased input signals is far less than the PRBS signals with the exception of the CO_2 wt% in the flue gas, even though presence of noise in all signals especially in the flue gas flowrate is still observed. Figure 4.32 compares the power spectrum of the actual vs design signals for the CO_2 weight percentage in the flue gas. It is observed that the implemented signal still has reasonably high power in the entire range albeit low power at some frequency range.

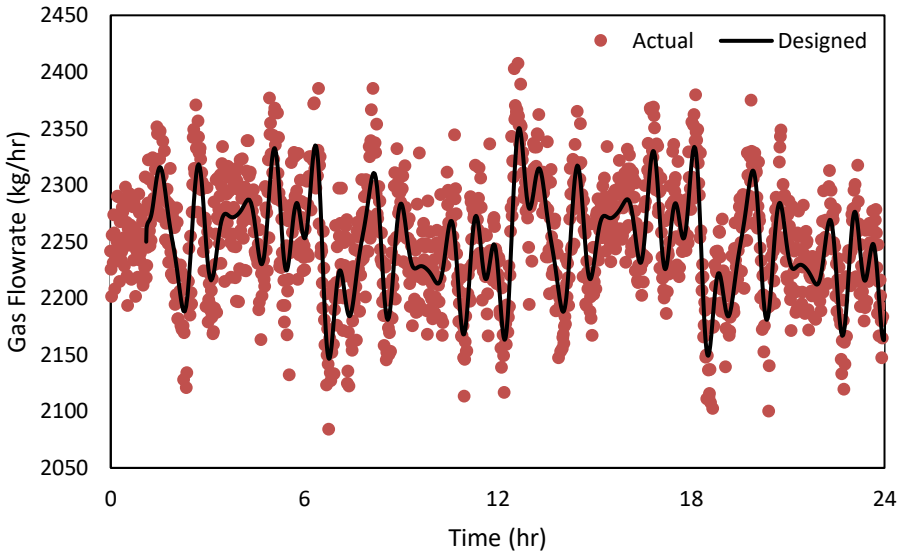

Figure 4.28 - Comparison between design and implementation for the Schroeder-phased input for the gas flowrate

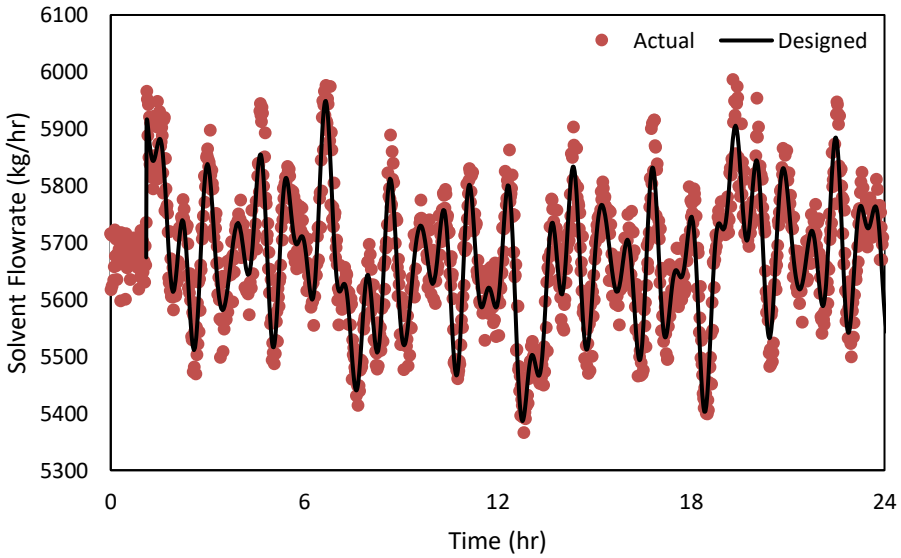

Figure 4.29 - Comparison between design and implementation for the Schroeder-phased input for the solvent flowrate

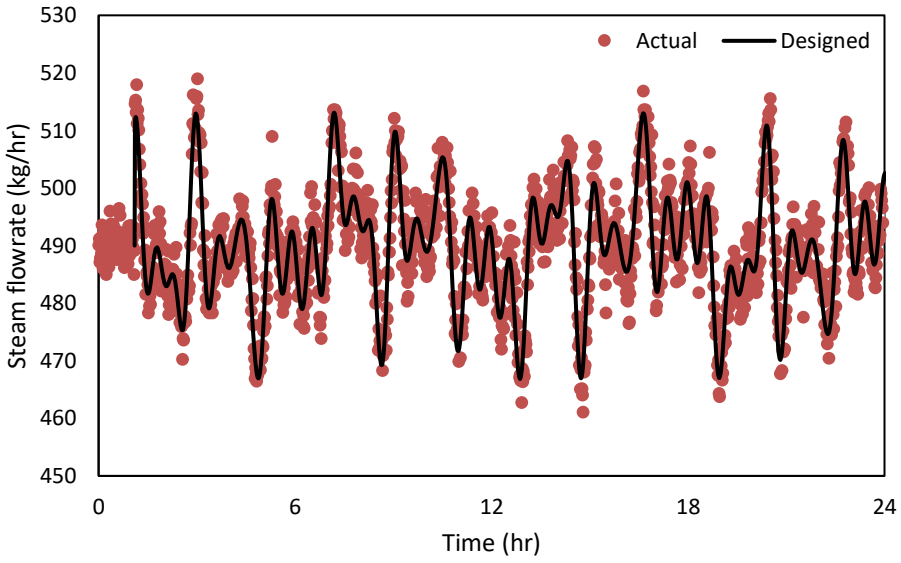

Figure 4.30 - Comparison between design and implementation for the Schroeder-phased input for the steam flowrate

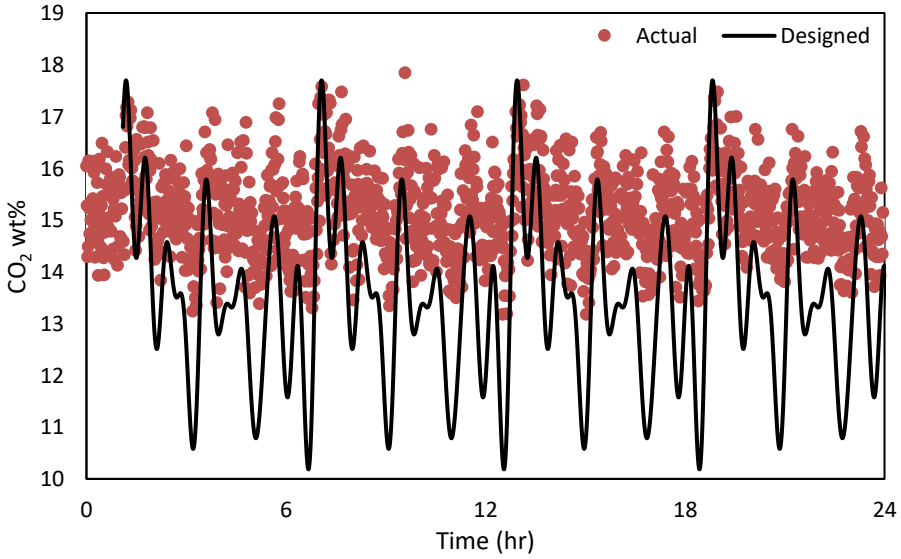

Figure 4.31 – Comparison between design and implementation for the Schroeder-phased input for CO_2 wt%

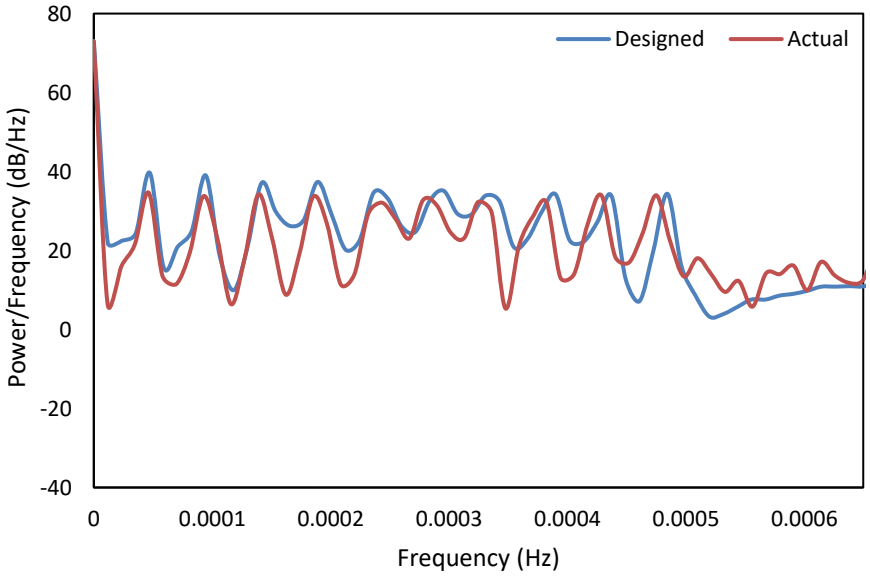

Figure 4.32 - Schroeder-phased input power spectrum density for the CO_2 wt%

4. 5. Dynamic Data Reconciliation (DDR) with parameter estimation

After implementing the presented signals at the NCCC pilot-plant, the data was preprocessed by applying a Butterworth filter (a band-pass filter) followed by a moving-average filter to remove noise from the data. The clean data were then utilized for DDR with parameter estimation. The DDR methodology is similar to Chapter 3, but in addition to that, it was desired that a parameter estimation problem is solved since the data are rich for such estimation. It was desired that parameters of the mass transfer coefficients, interfacial area, and holdup be estimated. However, since the optimization have to be solved in Aspen Plus Dynamics platform using the optimizers available there, only a sequential strategy could be implemented where the differential algebraic equation (DAE) solver works in tandem with the nonlinear programming (NLP) codes to solve the optimization problem. In this strategy, the decision variables from the NLP code is passed on to the Aspen Plus Dynamics DAE solver to solve an initial value problem for the entire time domain. Transient profiles of state and algebraic variables from the DAE solver is then used to calculate the objectives and constraints. The DAE solver then calculates the next update for the decision variable s, which is then passed on to the DAE solver. This continues till the convergence is obtained. There are several issues that need to be addressed here. First, the test runs took place over large number of hours (about 24 hr for the Schroeder-phased input signal and about 33 hr for the PRBS signals). This led to significant

computational cost for the DAE solver. Second, since a data reconciliation problem was solved, it led to large number of decision variables. Third, as discussed earlier, the plant was not necessarily at the steady state when the signals are initiated. Therefore, the initial value of some of the key state variables were also estimated leading to the large dimensionality of the problem. Fourth, there were some missing measurements such as the water makeup flowrate to the intermediate storage tank. These need to be estimated as well. Fourth, when the process model parameters noted above were included in the estimation problem, it led to a large dimensional optimization problem. One issue with the sequential approach with such problems is that the NLP solver cannot take advantage of the sparsity or structure of the underlying dynamic model, neither that of the KKT system (Biegler, 2010). Even with several days of simulation, parameter estimation problem for not even a single model could be successfully solved. It should be noted that in comparison to the dynamic DDR problem solved in Chapter 3, here the dimensionality and computational expense of the problem became significantly larger due to inclusion of the initial values of some of the state variables and because of the long time span of the test run data. Since dynamic data reconciliation, initial state estimation and missing measurement estimation must be considered, it was decided that the parameter estimation will be performed only for the holdup model since that has a strong impact on the transient response, but not so much on the steady state response. Also, the parameters were estimated manually through sensitivity studies. Furthermore, due to high implementation error and significant noise in the input data and due to the high noise in the output data corresponding to the PRBS design and due to high computational time required by the DAE solver for the PRBS design (the solver had to cut steps significantly where only very short integration steps could be successfully converged), it was desired that the parameter will be estimated by using the data corresponding to the Schroeder-phased input signal design. These estimated parameters are then tested on the data corresponding to the PRBS design.

4. 5. 1. Schroeder-phased input data DDR and parameter estimation

The DDR with parameter estimation was implemented as an optimization problem in Aspen plus Dynamics® as described by Equation 4.25.

$$\min \left(y_{exp} - y\right)' \sum^{-1} \left(y_{exp} - y\right)$$

s.t. (4.25)

$$H(\eta, y, u, \theta) = f(\eta, y, u, \theta)$$

$$g(\eta, y, u, \theta) \leq 0$$

The flue gas, lean solvent and steam flowrates and CO_2 concentration in the flue gas were used as decision variables. These variables were included while calculating the objective function as well. Overall, following variables were reconciled:

- Lean CO_2 loading
- Gas flowrate from absorber
- CO_2 concentration in flue gas
- Lean solvent temperature to absorber
- Lean solvent temperature from regenerator
- Lean solvent flowrate to absorber
- Flue gas flowrate
- Steam flowrate

These variables were selected as they are the key input and output variables that affects the plant mass and energy balance. The estimated parameters for the holdup model are presented in Table 4.1. These parameters correspond to the holdup correlation presented in Equation 2.18. The estimated value for the linear parameter H_{L1} did not change much, while H_{L2} got reduced from approximately 0.65 to 0.39. These column hydraulic parameters could be estimated from the dynamic data collected in about 24 hr. As discussed earlier in Chapter 2, data from air-water systems are generally used for estimating these parameters and these data are collected over the period of about four weeks for each packing type (Tsai, 2010). While the parameters are not too different, they are certainly superior as seen in Table 4.1, are for the actual MEA-H_2O-CO_2 system, and could be estimated using data collected from considerably lesser time.

Table 4.1 - Estimated holdup parameters

Parameter	Original value (Soares Chinen et al., 2018)	Estimated value
H_{L1}	11.45	11.5
H_{L2}	0.6471	0.39

The discrete-time cumulative root means squared error (DCRMSE) in % CO_2 capture, given by Equation 4.26, for the original versus regressed holdup model parameters corresponding to the PRBS and Schroeder-phased input signals are shown in Table 4.2. For both cases, a modest improvement could be observed.

$$DCRMSE = \sqrt{\frac{1}{N}\sum_{i=1}^{N} \varepsilon^2} \tag{4.26}$$

Table 4.2 - DCRMSE (% CO_2 capture) for original and regressed holdup parameters

	Original holdup parameters	Regressed holdup parameters
Pseudo Random Binary Signal	3.25	3.11
Schroeder-phased input signal	2.15	1.96

Figure 4.33 to Figure 4.36 show the experimental versus reconciled Schroeder-phased inputs for the solvent flowrate, flue gas flowrate, CO_2 concentration in the flue gas, and steam flowrates, respectively. Figure 4.37 presents the comparison between the model results and experimental data for the CO_2 capture percentage.

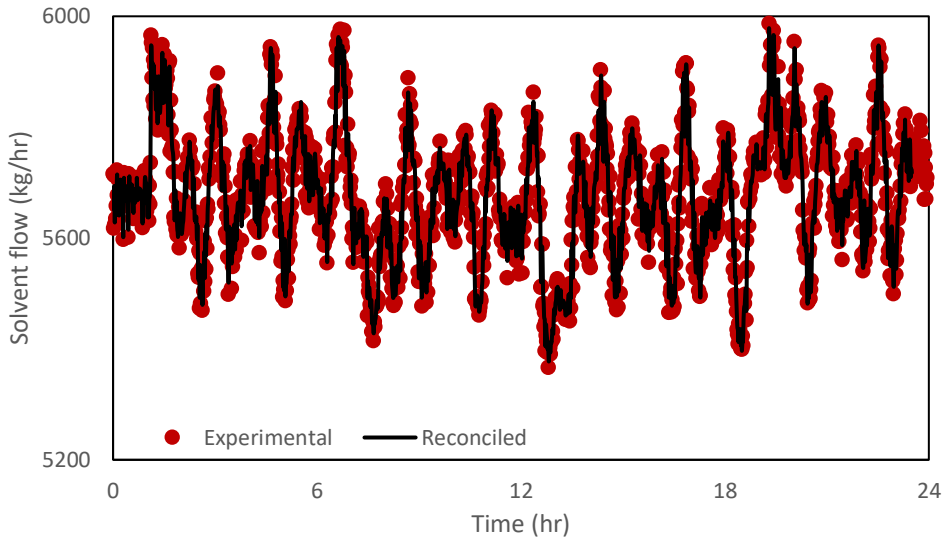

Figure 4.33 - Reconciled Schroeder phased input solvent flowrate

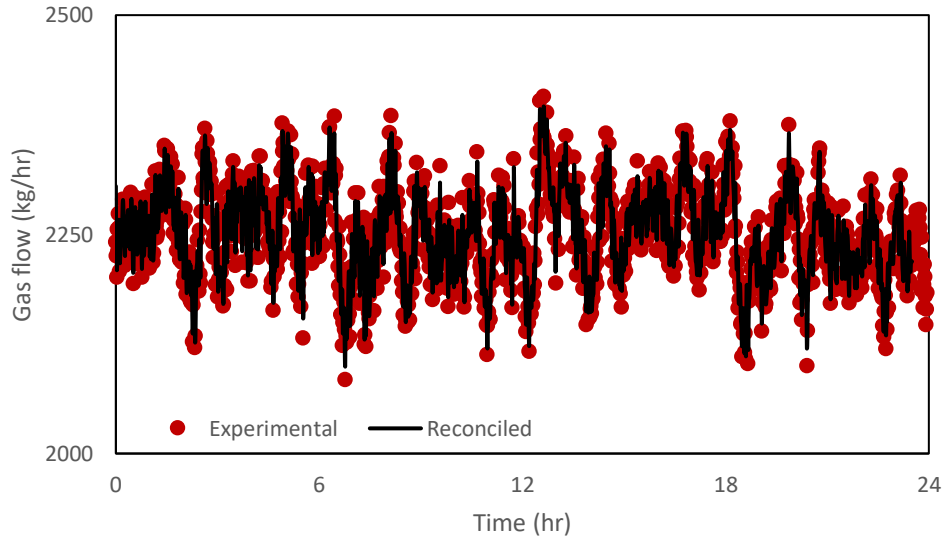

Figure 4.34 - Reconciled Schroeder phased input flue gas flowrate

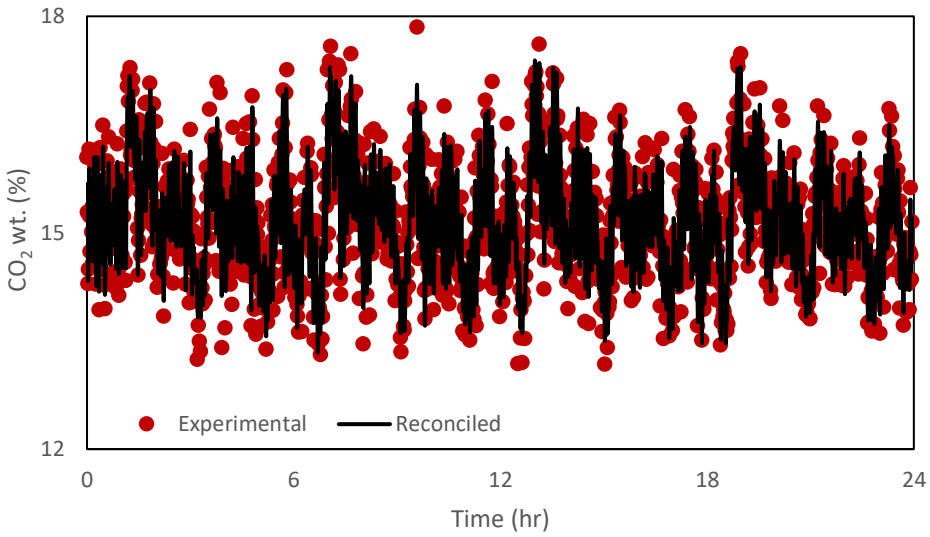

Figure 4.35 - Reconciled Schroeder phased input CO2 percentage in the flue gas

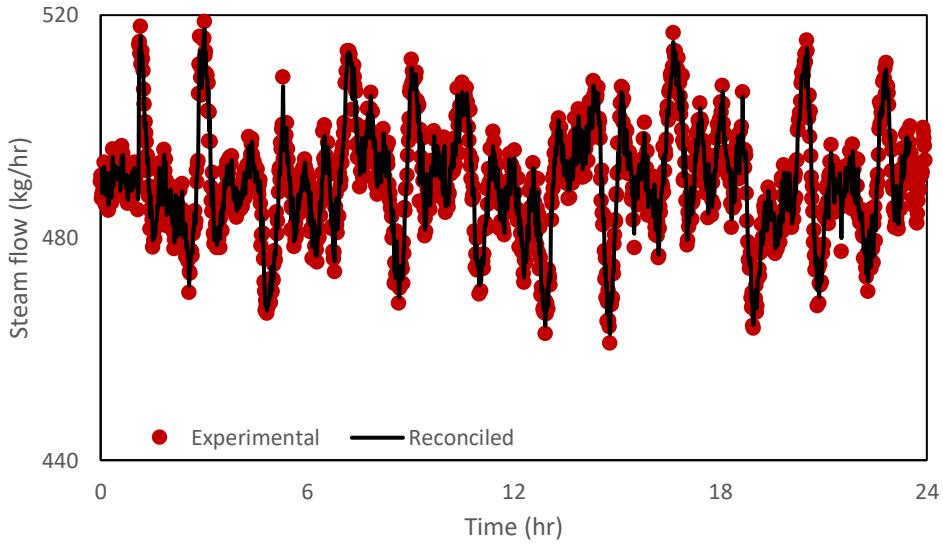

Figure 4.36 - Reconciled Schroeder phased input steam flowrate

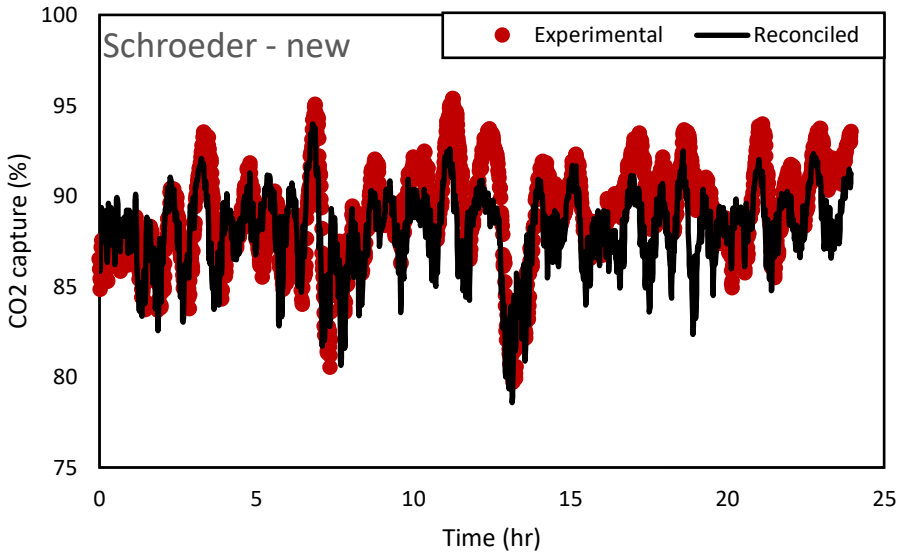

Figure 4.37 - Schroeder phased input CO_2 capture percentage

It is observed that while the model could capture general trend well, there are still peaks in the experimental data that could not be addressed by the model. It can be noted that both the solvent concentration and the absorber outlet gas flowrate are variables that have large impact, but are not reconciled due to the poor quality of its measurement data. Reconciling this variable and estimation of other model parameters could have improved the fit further.

4. 5. 2. Pseudo-random binary signal dynamic data reconciliation

Similar DDR problem is solved for the PRBS dataset using the holdup model parameter obtained through the Schroeder-phased input. One issue for these tests, as discussed earlier, is that the pilot plant was not in the steady-state when the PRBS test run is initiated. Therefore, initial values of some of the key variables were estimated. There is also considerable implementation error in the signal.

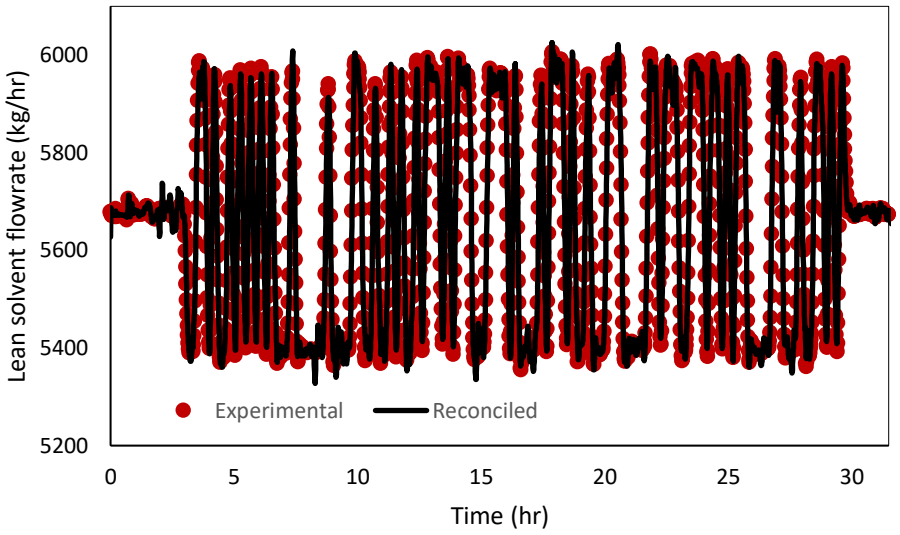

Figure 4.38 - Reconciled PRBS solvent flowrate

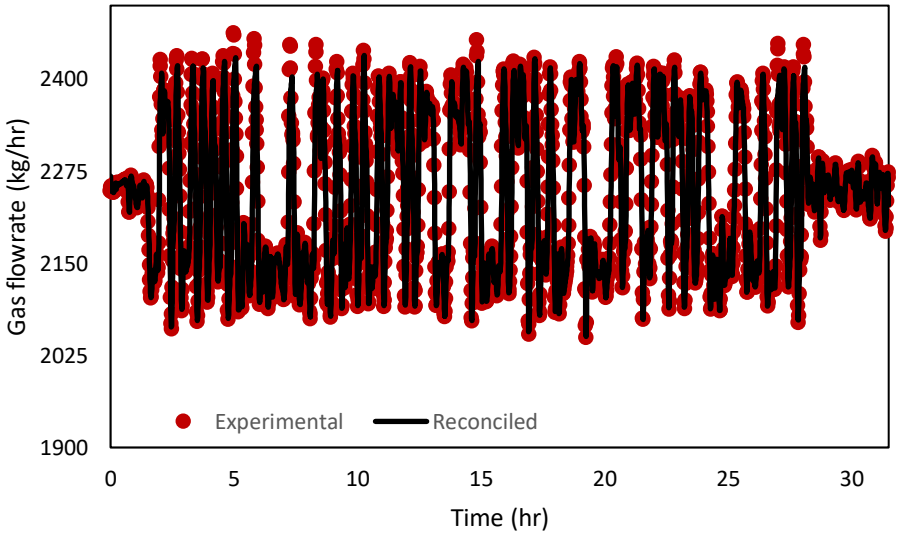

Figure 4.39 - Reconciled PRBS flue gas flowrate

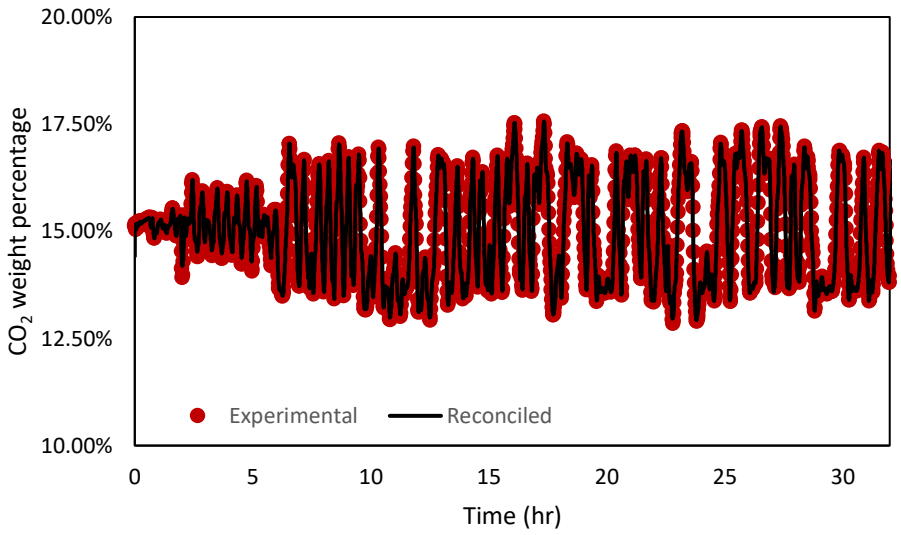

Figure 4.40 - Reconciled PRBS CO2 percentage in the flue gas

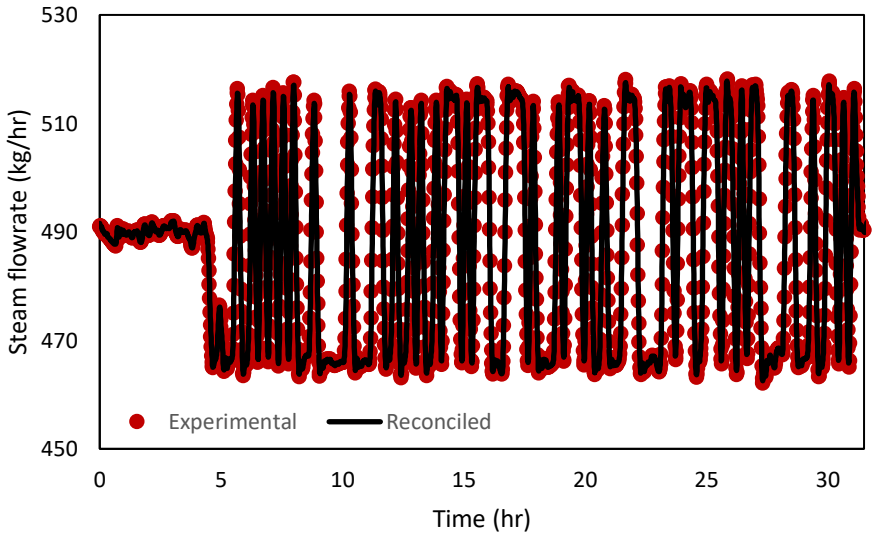

Figure 4.41 - Reconciled PRBS steam flowrate

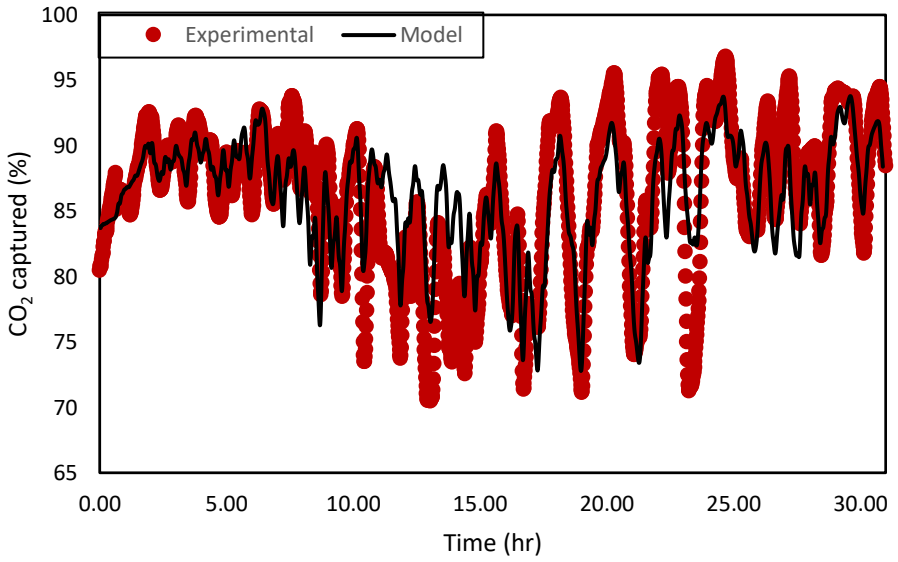

Figure 4.42 - Reconciled PRBS CO_2 capture percentage

Figure 4.38 to Figure 4.41 show the experimental versus reconciled PRBS signals for the solvent flowrate, flue gas flowrate, CO_2 concentration in the flue gas, and steam flowrates, respectively. Figure 4.42 presents the comparison between the model results and experimental data for the CO_2 capture percentage. Similar to before, while the model could capture the trend generally well except at a few time instants, the peaks could not be well addressed. It can be noted that there is considerable mismatch for the PRBS data when the CO_2 capture is calculated from the liquid side as opposed to the gas side. It is felt that reconciling the solvent concentration and absorber outlet gas flowrate, estimation of other model parameters, and initiation of the test run from the steady-state condition would have improved the fit.

4. 5. 3. Case studies

Similar case studies as Chapter 3 is presented by Figure 4.43, in which a study is conducted by introducing +/-5% step changes in the flue gas flowrate and the lean solvent flowrate, but by using the regressed holdup parameter. “Case a” presents a -5% solvent flowrate step change, and “case b” a +5% solvent flowrate step change. The same percent step changes were implemented for the flue gas flowrate in cases “c” and “d”, respectively.

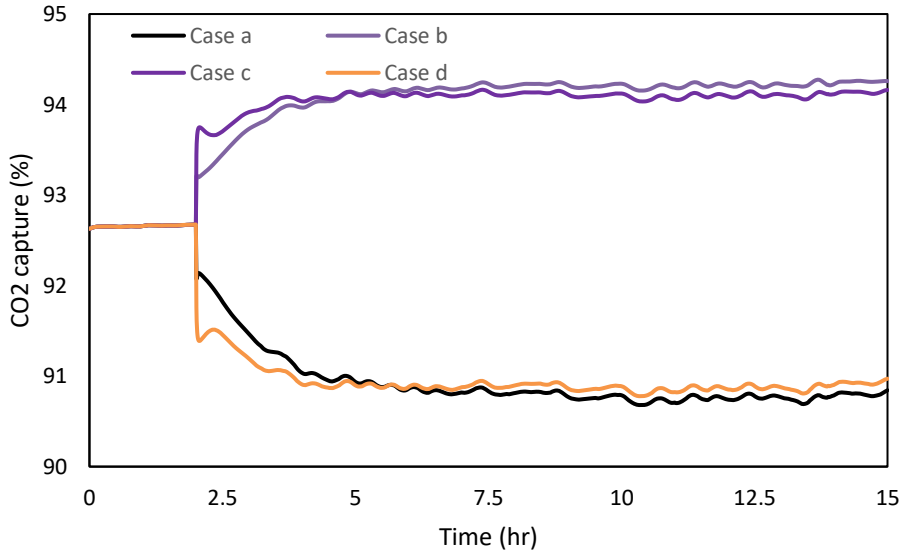

Figure 4.43 - Case study CO_2 capture response

First of all, the CO_2 capture response for the change in the solvent flowrate became closer to that of the flue gas flowrate in comparison to what was observed earlier with the original holdup model parameters in Chapter 3. The gains are found to be 0.36 and 0.33 % CO_2 capture/% solvent flowrate, respectively when the solvent flowrate is increased and decreased, respectively, as opposed to 0.58 and 0.46 % CO_2 capture/% solvent flowrate, respectively using the original holdup model parameters in Chapter 3. Similar observations are made for the response when the solvent flowrate is changed. There is practically no difference in the time constant between the earlier and current responses.

4. 6. Conclusions

For the first time, PRBS and Schroeder-phased input signals are designed and implemented for a CO2 capture pilot plant. Signals are designed for a multivariable system where the signals are designed to ensure output plant friendliness. As expected the Schroeder-phased input signal took shorter time to implement in comparison to the PRBS design. Both input signal designs result in the power of the signals reasonably uniformly distributed over the entire frequency range of interest. However, the designed Schroeder-phased inputs yield higher power with less variability in the entire frequency range in comparison to the PRBS

signal. Higher implementation error is observed for the PRBS signals. Considerable implementation error is observed in the signal for CO_2 concentration in the flue gas for both types of input signals. Instead of the implementation error, the power spectrum of the actual signal is still reasonably close to that of the designed signals albeit low power at some frequency range.

A sequential strategy is implemented for solving the DDR and parameter estimation problem where the DAE solver and the NLP codes are used sequentially to solve the optimization problem. A number of key input and output variables are reconciled so that plant mass and energy balances could be satisfied. A few key unmeasured input variables are also estimated. Due to computational intractability, the parameter estimation problem could not be solved. A sensitivity study is performed to obtain the optimal estimate of the parameters for the holdup model by using the data corresponding to the Schroeder-phased input signal design. The regressed parameter is then used while performing DDR for the PRBS data. While the model predicted the transient response well especially for the Schroeder-input signal, the peaks in the CO2 capture response could not be addressed. It is believed that the reliable liquid concentration measurement and parameter estimation could improve the model prediction. Further, initiation of the test runs under steady state would have also reduced the uncertainty in the estimates of the initial states.

Regression of parameters for the holdup model resulted in some differences in the transient response of the process, especially the gain, in comparison to the original parameters for same perturbations. Finally, it can be noted that even though only holdup model parameter could be estimated, it resulted in a slightly superior estimate of the parameters in comparison to the original values. As discussed in Chapter 2, the holdup parameters were obtained by regressing the steady-state holdup and pressure drop data collected over several weeks of test runs. It is worth noting that superior values for the model parameters could be obtained using the data collected for just a data. Further improvement in the results are anticipated if computational capability can be developed in the future for estimation of other model parameters.

Chapter 5. Final Remarks and Future Work

One of the main objectives of the CCSI was the development of a rigorous "gold-standard" process model for the solvent system for CO_2 capture. In this work, sub-models were developed for interfacial area, mass transfer coefficients, reaction kinetics, pressure drop, and holdup and implemented in Aspen Plus as FORTRAN user models. A novel simultaneous optimization technique was proposed for parameter regression. The technique results in a better predictive capability of the models. Predictive capability of the process model is evaluated further by using the steady-state data from the National Carbon Capture Center in Wilsonville, AL for an MEA-H_2O-CO_2 system over a wide operating regime (Morgan, 2017). The overall approach is generic and can be readily applied to other solvent systems, packings and column configurations, as demonstrated in appendix B for a high viscosity solvent system being developed by an industrial collaborator.

Obtaining an accurate model requires rigorous pressure drop and holdup models, especially for pressure-driven dynamic simulations. Most of these models are restricted to well-known packing types, while newly developed packings are overlooked. Therefore, hydraulic models were developed utilizing data from the literature for a relatively newer packing type, MellapakTM plus 252Y. During the selection of the most suitable pressure drop model, a strong dependency of pressure drop on holdup was observed. The final models selected for the MellapakPlusTM 252Y are the regressed Billet and Schultes (1999) model for pressure drop while the regressed Tsai (2010) model is used for the holdup calculations.

Opposed to the typical sequential approach in the existing literature for development of mass transfer models, a simultaneous optimization approach is proposed in this work where the optimal estimates of the parameters of the mass transfer coefficients model, diffusivity model, interfacial area model and kinetic model are obtained by using the data from multiple scales that span wide range of operating conditions and flow regimes. The FOQUS toolbox developed by the U.S. DOE's CCSI is utilized for the simultaneous regression, since the proposed approach is not feasible for implementation in the leading commercial process simulation platforms. The final integrated mass transfer model comprises of the regressed Billet and Schultes (1999) model for mass transfer coefficient, the regressed Tsai (2010) model for interfacial area along with the regressed diffusivity and kinetic models. An improved predictive capability was observed for the models developed using the simultaneous regression approach in comparison to those from the open literature, while applying them to a data-set "not previously seen" by neither of the methods.

A Bayesian uncertainty quantification methodology was implemented for both the mass transfer and hydraulics models. The approach resulted in a reduced uncertainty for the pressure drop model parameter while no or negligible change was observed in the parametric uncertainty of the holdup model. It is observed that there is still relatively high uncertainty in the hydraulic models that could be improved if additional experimental data were available. There is scarcity of the data in the open literature for the relatively newer packing types such as the one considered in this work. Sobol indices are leveraged for down-selecting the parameter space of the integrated mass transfer model. It is observed that the prediction uncertainty for CO_2 capture gets reduced due to Bayesian uncertainty quantification of the mass transfer models.

Using the results from the rate-based model, a modified Murphree-efficiency method is developed for an equilibrium-based Aspen Plus Dynamics model. A pseudo-PRBS signal design was developed for the steam flowrate, solvent flowrate, and flue gas flowrate by using information obtained from step tests in the NCCC pilot plant. Noisy signal are filtered and used for DDR to satisfy mass and energy conservation as well for estimating unmeasured variables. The dynamic model yielded satisfactory estimates of the CO_2 capture rates when solvent flowrate, flue as flowrate, and steam flowrate step changes were introduced. Notable discrepancies between the liquid side measurements and model prediction are observed for all cases. A previous investigation by Morgan (2017) shows that the discrepancies are a reflection of errors in the measurement of CO_2 loading and solvent composition.

Two case studies were conducted to study the nonlinearity of the process. It was observed that the process gain and time constants would change depending on the change in the direction of the perturbation. It was verified that the time constant of the full plant can be significantly longer than the time constants of the isolated absorber or stripper systems. The storage tank in between the absorber and stripper also resulted in an increase in the time constant and dampening of the effect of the stripper operation on the absorber operations. In another study, transient response to an optimal CO_2 capture schedule was studied. In this study, it was observed that if the controllers are not optimally tuned, it can lead to considerable variations in the steam flowrate to the reboiler, which may affect the process efficiency and solvent quality. While the existing loop tuning techniques could improve the transient process efficiency, further improvement may be possible by using advanced controllers.

It should be noted that the dynamic experiments conducted at NCCC in 2013 were executed without completing a full PRBS signal and, therefore, the data do not have the required information content for parameter estimation. Moreover, one variables was changed at a time. Thus the process interaction due to simultaneous change in multiple variables are not captured in the data. A formal design of dynamic experiments methodology, therefore, is proposed to improve the outcome from the dynamic test runs.

The systematic methodology developed for the Design of Dynamic Experiments was implemented successfully in the NCCC pilot plant to obtain a rich dataset. Both a full-length PRBS and a Schroeder-phased input signal designs were developed for the multivariable system. The data were filtered and used for DDR and parameter estimation. It was observed that the Schroeder-phased input signal could be implemented in shorter time than the PRBS signals, even though it yielded similar richness in the data. Considerable implementation error was observed in the signal for CO_2 concentration in the flue gas for both types of input signals. Instead of the implementation error, the power spectrum of the actual signal was found to be still reasonably close to that of the designed signals albeit low power at some frequency range.

The DDR and parameter estimation problem are solved using a sequential strategy where the DAE solver and the NLP codes are used sequentially to solve the optimization problem. Several key input and output variables are reconciled to ensure that mass and energy balances are satisfied. A few key unmeasured input variables are also estimated. A sensitivity study is performed to obtain the optimal estimate of the parameters for the holdup model by using the data corresponding to the Schroeder-phased input signal design. The regressed parameter is then used while performing DDR for the PRBS data. The model satisfactorily predicted the transient response, especially for the Schroeder-input signal, although the peaks in the CO_2 capture response could not be addressed.

A superior estimate of the holdup model parameters could be estimated using the dynamic data. The approach points to the promise of parameter estimation using the dynamic data that can be collected over much shorter period of time than the conventional steady-state test runs. The estimated parameters resulted in a slightly higher gain, in comparison to the original parameters presented in Chapter 2.

Future Work

It should be noted that the integrated mass transfer model was obtained when the mass transfer rate was modeled using the two film theory. Development of other mass transfer models such as those based on the penetration theory or the eddy diffusion theory and extension of the simultaneous regression approach to those mass transfer models that are inherently transient is a desired future work. Comparison of these mass transfer models for different scales and flow regimes for solvent-based capture systems can be a valuable contribution in the future.

One desired future work in the area of uncertainty quantification will be to evaluate scaleup uncertainty. Study on the impact of liquid distributions on the column hydraulic and mass transfer characteristics will

be very valuable. Investigation of various mass transfer models for commercial-scale applications and development of new mass transfer models, if needed, will be worthwhile.

A dynamic uncertainty quantification methodology would be a valuable future direction of research. This should take into consideration uncertainty in the process model and parameters along with the measurement uncertainty.

An equilibrium-based model with Murphree-efficiency approach is used in this work. Development of a rigorous rate-based dynamic model will be desired to improve the model accuracy especially when the plant transient drifts further from the nominal condition.

Due to computational intractability, the desired parameter estimation problem comparison all mass transfer and hydraulic submodels could not be solved. While it was desired to design the Schroeder-phased input signals for D-optimality, it could not be implemented due to computational challenge of the software platform of choice for this work, although plant-friendliness could be satisfied. It will be desired to develop Schroeder-phased input signal design that satisfies both the D-optimality and plant-friendliness criteria.

A software platform that can handle large-scale DDR and parameter estimation problem with large amount of transient data will be very valuable. The framework should also be capable of estimating initial states and missing parameters. Observability and identifiability of the states, missing measurements, and parameters should be evaluated. Additional measurements may be needed and should be evaluated.

In this work, parametric uncertainty in the mass transfer and hydraulic models could not be evaluated for the dynamic model due to the Murphree-efficiency approach and due to the considerable computational expense of solving the dynamic data reconciliation problem. Development of simultaneous approach to solving the dynamic data reconciliation (and parameter estimation) problem would be a valuable future capability.

References

Afkhamipour, M., & Mofarahi, M. Comparison of rate-based and equilibrium-stage models of a packed column for post-combustion CO2 capture using 2-amino-2-methyl-1-propanol (AMP) solution. International Journal of Greenhouse Gas Control 2013, 15, 186-199.

Afkhamipour, M., & Mofarahi, M. Sensitivity analysis of the rate-based CO2 absorber model using amine solutions (MEA, MDEA and AMP) in packed columns. International Journal of Greenhouse Gas Control 2014, 25, 9-22.

Aguilar, J. V., Langarita, P., Rodellar, J., Linares, L., & Horváth, K. (2016). Predictive control of irrigation canals – robust design and real-time implementation. Water Resources Management, 30(11), 3829–3843. https://doi.org/10.1007/s11269-016-1387-6

Austgen, D. M., Rochelle, G. T., & CHAU-CHYUN, C. H. E. N. Model of vapor− liquid equilibria for aqueous acid gas− alkanolamine systems. II, Representation of H2S and CO2 solubility in aqueous MDEA and CO2 solubility in aqueous mixtures of MDEA qwith MEA or DEA. Industrial & Engineering Chemistry Research 1991, 30(3), 543-555.

Backx, T. C. (2003). Model-based control of glass melting furnaces and forehearths: First principles-based model of predictive control system design. Ceramic Engineering and Science Proceedings, 24(1), 21–32. https://doi.org/10.1177/0192513X12437708

Bankole, T., Jones, D., Bhattacharyya, D., Turton, R., & Zitney, S. E. (2018). Optimal scheduling and its Lyapunov stability for advanced load-following energy plants with CO2capture. Computers and Chemical Engineering, 109, 30–47. https://doi.org/10.1016/j.compchemeng.2017.10.025a

Bhattacharyya, D., & Miller, D. C. (2017). Post-combustion CO 2 capture technologies — a review of processes for solvent-based and sorbent-based CO 2 capture. Current Opinion in Chemical Engineering, 17, 78–92. https://doi.org/10.1016/j.coche.2017.06.005

Biegler, L. (2010) Nonlinear Programming: Concepts, algorithms, and applications to chemical processes. SIAM, Philadelphia.

Biliyok, C., Lawal, A., Wang, M., & Seibert, F. (2012). Dynamic modelling, validation and analysis of post-combustion chemical absorption CO \n 2 capture plant. International Journal of Greenhouse Gas Control, 9, 428–445. https://doi.org/10.1016/j.ijggc.2012.05.001

Billet, R., & Schultes, M. (1999). Prediction of mass transfer columns with dumpled and arranged packings Updated Summary of the Calculation Method of Billet and Schultes. Chemical Engineering Research and Design, 77(6), 498–504. https://doi.org/http://dx.doi.org/10.1205/026387699526520

Billet, R., & Schultes, M. Predicting mass transfer in packed columns. Chemical engineering & technology 1993, 16(1), 1-9.

Billet, R., Schultes, M. Prediction of Mass Transfer Columns with Dumped and Arranged Packings: Updated Summary of the Calculation Method of Billet and Schultes. Chem. Eng. Res. Des. 1999 77 A6. 498-504.

Bravo, J. L., Rocha, J. A., & Fair, J. R. Mass transfer in gauze packings. Hydrocarbon processing 1985, 64(1), 91-95.

Bravo, J. L., Rocha, J. A., & Fair, J. R. Pressure drop in structured packings. Hydrocarbon Process 1986, 65(3).

Bui, M., Gunawan, I., Verheyen, V., Feron, P., Meuleman, E., & Adeloju, S. (2014). Dynamic modelling and optimisation of flexible operation in post-combustion CO2 capture plants-A review. Computers and Chemical Engineering, 61, 245–265. https://doi.org/10.1016/j.compchemeng.2013.11.015

Cormos, A. M., & Gaspar, J. Assessment of mass transfer and hydraulic aspects of CO2 absorption in packed columns. International Journal of Greenhouse Gas Control, 6, 201-209, 2012.

Dang, H., & Rochelle, G. T. CO2 absorption rate and solubility in monoethanolamine/piperazine/water. Separation science and technology 2003, 38(2), 337-357.

Darde, V., Van Well, W. J., Fosboel, P. L., Stenby, E. H., & Thomsen, K. Experimental measurement and modeling of the rate of absorption of carbon dioxide by aqueous ammonia. International Journal of Greenhouse Gas Control 2011, 5(5), 1149-1162.

Dugas, R. E. Carbon Dioxide Absorption, Desorption, and Diffusion in Aqueous Piperazine and Monoethanolamine" University of Texas at Austin, 2009 Ph.D. Dissertaion.

Enaasen Flø, N., Knuutila, H., Kvamsdal, H. M., & Hillestad, M. (2015). Dynamic model validation of the post-combustion CO2 absorption process. International Journal of Greenhouse Gas Control, 41, 127–141. https://doi.org/10.1016/j.ijggc.2015.07.003

Enaasen, N., Zangrilli, L., Mangiaracina, A., Mejdell, T., Kvamsdal, H. M., & Hillestad, M. (2014). Validation of a dynamic model of the brindisi pilot plant. Energy Procedia, 63(1876), 1040–1054. https://doi.org/10.1016/j.egypro.2014.11.111

Fair, J. R., & Bravo, J. L. Distillation columns containing structured packing. Chemical Engineering Progress 1990, 86(1), 19-29.

Faramarzi, L., Kontogeorgis, G. M., Michelsen, M. L., Thomsen, K., & Stenby, E. H.. Absorber model for CO2 capture by monoethanolamine. Industrial & Engineering Chemistry Research 2010, 49(8), 3751-3759.

Frailie, P. T. Modeling of carbon dioxide absorption/stripping by aqueous methyldiethanolamine/piperazine University of Texas at Austin 2014, Ph.D. Dissertation.

Fedorov, V. V. (1972). Theory of optimal experiments (XI). New York: Academic Press.

Gaikwad, S. V., & Rivera, D. E. (1996). Control-Relevant Input Signal Design for Multivariable System Identification: Application to High-Purity Distillation. IFAC Proceedings Volumes, 29(1), 6143–6148.

Gel A, Li T, Gopalan B, Shahnam M, Syamlal M. Validation and uncertainty quantification of a multiphase computational fluid dynamics model. Ind Eng Chem Res. 52 (2013), pp. 11424-11435.

Gel, A., Chaudhari, K., Turton, R., Nicoletti, P., Application of uncertainty quantification methods for coal devolatilization kinetics in gasifier modeling. Powder Technol. 265 (2014), 66-75.

Georgakis, C. (2013). Design of dynamic experiments: A data-driven methodology for the optimization of time-varying processes. Industrial and Engineering Chemistry Research, 52(35), 12369–12382.

https://doi.org/10.1021/ie3035114

Glasscock, D. A. Modeling and experimental study of carbon dioxide absorption into aqueous alkanolamines. University of Texas at Austin 1990. Ph.D. Dissertation.

Global Carbon Project. Carbon budget and trends, 2016. Available at www.globalcarbonproject.org/carbonbudget]

Guillaume, P., Schoukens, J., Pintelon, R., & Koll??i, I. (1991). Crest-Factor Minimization Using Nonlinear Chebyshev Approximation Methods. IEEE Transactions on Instrumentation and Measurement, 40(6), 982–989. https://doi.org/10.1109/19.119778

Hjalmarsson, H. (2014). Experiment Design and Identification for Control. Encyclopedia of Systems and Control. https://doi.org/10.1007/978-1-4471-5102-9

Jayarathna, S. A., Lie, B., & Melaaen, M. C. Dynamic modelling of the absorber of a post-combustion CO2 capture plant: Modelling and simulations. Computers & Chemical Engineering 2013, 53, 178-189.

Jiju, A. (2003). Design of experiments for engineers and scientists. Oxford: Butterworth-Heinemann.

Kale, C., Górak, A., & Schoenmakers, H. Modelling of the reactive absorption of CO2 using mono-ethanolamine. International Journal of Greenhouse Gas Control 2013, 17, 294-308.

Khan, F. M., Krishnamoorthi, V., & Mahmud, T. Modelling reactive absorption of CO2 in packed columns for post-combustion carbon capture applications. Chemical Engineering Research and Design 2011, 89(9), 1600-1608.

Körkel, S., Kostina, E., Bock, H. G., & Schlöder, J. P. (2004). Numerical Methods for Optimal Control Problems in Design of Robust Optimal Experiments for Nonlinear Dynamic Processes. Optimization Methods and Software Journal, 19(3–4), 327–338.

Kumar, A., & Narasimhan, S. (2013). Robust plant friendly optimal input design. IFAC Proceedings Volumes (IFAC-PapersOnline) (Vol. 10). IFAC. https://doi.org/10.3182/20131218-3-IN-2045.00110

Kvamsdal, H. M, Rochelle, G. T. Effects of the Temperature Bulge in CO2 Absorption from Flue Gas by Aqueous

Monoethanolamine. Ind. Eng. Chem. Res. 2008, 47. 867-875

Kvamsdal, H. M., & Hillestad, M. Selection of model parameter correlations in a rate-based CO2 absorber model aimed for process simulation. International Journal of Greenhouse Gas Control 2012, 11, 11-20.

Kvamsdal, H. M., Chikukwa, A., Hillestad, M., Zakeri, A., & Einbu, A. (2011). A comparison of different parameter correlation models and the validation of an MEA-based absorber model. Energy Procedia, 4, 1526–1533. https://doi.org/10.1016/j.egypro.2011.02.021

Kvamsdal, H. M., Jakobsen, J. P., & Hoff, K. A. (2009). Dynamic modeling and simulation of a CO2 absorber column for post-combustion CO2 capture. Chemical Engineering and Processing: Process Intensification, 48(1), 135–144. https://doi.org/10.1016/j.cep.2008.03.002

Lane W.A., Storlie C.B., Montgomery C.J., Ryan E.M. Numerical modeling and uncertainty quantification of a bubbling fluidized bed with immersed horizontal tubes. Powder Technology 2014 253, 733-743.

Lara, J. M. V., & Milani, B. E. A. (2003). Identification of neutralization process using multi-level pseudo-random signals. Proceedings of the 2003 American Control Conference, 2003., 5(1), 3822–3827. https://doi.org/10.1109/ACC.2003.1240431

Le Quéré, C., Andrew, R. M., Canadell, J. G., Sitch, S., Ivar Korsbakken, J., Peters, G. P., … Zaehle, S. (2016). Global Carbon Budget 2016. Earth System Science Data, 8(2), 605–649. https://doi.org/10.5194/essd-8-605-2016

Li, L. T. Carbon Dioxide Solubility and Mass Transfer in Aqueous Amines for Carbon Capture. University of Texas at Austin 2015, Ph.D. Dissertation.

Lin, Y. J., Pan, T. H., Wong, D. S. H., Jang, S. S., Chi, Y. W., & Yeh, C. H. (2011). Plantwide control of CO2 capture by absorption and stripping using monoethanolamine solution. Industrial and Engineering Chemistry Research, 50(3), 1338–1345. https://doi.org/10.1021/ie100771x

Lin, Y. J., Wong, D. S. H., Jang, S. S., & Ou, J.-J. (2012). Control Strategies for Flexible Operation of Power Plant

with CO2 Capture Plant. AIChE Journal, 58(9), 2697–2704.

Llano-Restrepo, M., & Araujo-Lopez, E. (2015). Modeling and simulation of packed-bed absorbers for post-combustion capture of carbon dioxide by reactive absorption in aqueous monoethanolamine solutions. International Journal of Greenhouse Gas Control, 42, 258–287. https://doi.org/10.1016/j.ijggc.2015.08.008

Mart, A., Rivera, D. E., & Hekler, E. B. (2015). An Identification Test Monitoring Procedure for MIMO Systems Based on Statistical Uncertainty Estimation. Conference on Decision and Control (CDC), (Cdc), 2719–2724.

Mathias PM. Sensitivity of process design to phase equilibrium- a new perturbation method based upon the Margules equation. J Chem Eng Data 2014, 59, 1006-1015.

Mathias, P. M., & Gilmartin, J. P. Quantitative Evaluation of the Effect of Uncertainty in Property Models on the Simulated Performance of Solvent-Based CO2-Capture. Energy Procedia 2014, 63, 1171-1185.

Mead, R. (1988). The design of experiments : statistical principles for practical applications. Cambridge: Cambridge Press.

Mebane DS, Bhat KS, Kress JD, Fauth DJ, Gray ML, Lee A, Miller DC. Bayesian calibration of thermodynamic models for the uptake of CO2 in supported amine sorbents using ab initio priors. Phys Chem Chem Phys. 2013;15:4355-4366.

Miller, D. C., Syamlal, M., Mebane, D. S., Storlie, C., Bhattacharyya, D., Sahinidis, N. V., … Dale, C. (2014). Carbon Capture Simulation Initiative: A Case Study in Multiscale Modeling and New Challenges. Annual Review of Chemical and Biomolecular Engineering, 5(1), 301–323.

Miller, D., Sun, X., Storlie, C., & Bhattacharyya, D. Using Advanced Modeling to Accelerate the Scale-Up of Carbon Capture Technologies (No. PNNL-SA-110092) 2015. Pacific Northwest National Laboratory (PNNL), Richland, WA (US).

Mobed, P., Maddala, J., Rengaswamy, R., Bhattacharyya, D., Turton, R., “Data Reconciliation and Dynamic Modeling of a Sour Water Gas Shift Reactor”, Industrial and Engineering Chemistry Research, 53 (51), pp

19855–19869, (2014)

Morgan, J. C., Chinen, A. S., Omell, B., Bhattacharyya, D., Tong, C., & Miller, D. C. (2015). Uncertainty Quantification of Property Models: Methodology and Its Application to CO2-Loaded Aqueous MEA Solutions. AIChE Journal, 61, 1822–1839. https://doi.org/10.1002/aic

Morgan, J. C., Chinen, A. S., Omell, B., Bhattacharyya, D., Tong, C., & Miller, D. C. (2017). Thermodynamic modeling and uncertainty quantification of CO 2 -loaded aqueous MEA solutions. Chemical Engineering Science, 168, 309–324. https://doi.org/10.1016/j.ces.2017.04.049

Morgan, J. C., Soares Chinen, A., Omell, B., Bhattacharyya, D., Tong, C., Miller, D. C., … Lucquiaud, M. (2018). Development of a Gold-Standard Model for Solvent-Based CO2 Capture. Part 2: Steady-State Validation with Pilot Plant Data.

Narasimhan, S., & Bombois, X. (2012). Plant friendly input design for system identification in closed loop. IFAC Proceedings Volumes (IFAC-PapersOnline) (Vol. 16). IFAC. https://doi.org/10.3182/20120711-3-BE-2027.00124

Nittaya, T., Douglas, P. L., Croiset, E., & Ricardez-Sandoval, L. A. (2014a). Dynamic modelling and control of MEA absorption processes for CO2 capture from power plants. Fuel, 116, 672–691. https://doi.org/10.1016/j.fuel.2013.08.031

Nittaya, T., Douglas, P. L., Croiset, E., & Ricardez-Sandoval, L. A. (2014b). Dynamic Modelling and Evaluation of an Industrial-Scale CO2 Capture Plant Using MEA Absorption Processes. Industrial & Engineering Chemistry Research, 11411–11426. https://doi.org/10.1021/ie500190p

Notz, R., Mangalapally, H. P., & Hasse, H. Post combustion CO 2 capture by reactive absorption: pilot plant description and results of systematic studies with MEA. International Journal of Greenhouse Gas Control 2012, 6, 84-112.

Piché, S., Grandjean, B. P., & Larachi, F. Reconciliation procedure for gas− liquid interfacial area and mass-transfer coefficient in randomly packed towers. Industrial & engineering chemistry research 2002, 41(19), 4911-4920.

Piché, S., Grandjean, B. P., Iliuta, I., & Larachi, F. Interfacial mass transfer in randomly packed towers: a confident correlation for environmental applications. Environmental science & technology 2001, 35(24), 4817-4822.

Plaza, J. M. Modeling of Carbon Dioxide Absorption using Aqueous Monoethanolamine, Piperazine, and Promoted Potassium Carbonate. University of Texas at Austin 2012, Ph.D. Dissertation.

Powell, M. J.. The BOBYQA algorithm for bound constrained optimization without derivatives. Cambridge NA Report NA2009/06 2009, University of Cambridge, Cambridge.

Puxty, G., Rowland, R., & Attalla, M. Comparison of the rate of CO2 absorption into aqueous ammonia and monoethanolamine. Chemical Engineering Science 2010, 65(2), 915-922.

Puxty, G., Rowland, R., Allport, A., Yang, Q., Bown, M., Burns, R., … Attalla, M. (2009). Carbon dioxide post combustion capture : a novel screening study of the carbon dioxide absorption performance of 76 amines. Environmental Science & Technology, 43(16), 6427–6433.

R. Jin, W. Chen, T.W. Simpson. Comparative studies of metamodelling techniques under multiple modelling criteria. Struct Multidisc Optim. 2001; 23: 1-13

Razi, N., Bolland, O., & Svendsen, H. Review of design correlations for CO2 absorption into MEA using structured packings. International Journal of Greenhouse Gas Control, 9, 193-219, 2012.

Razi, N., Svendsen, H. F., & Bolland, O. Assessment of mass transfer correlations in rate-based modeling of a large-scale CO2 capture with MEA. International Journal of Greenhouse Gas Control, 26, 93-108, 2014.

Rivera, D. E., Chen, X., & Bayard, D. S. (1993). Experimental Design for Robust Process Control Using Schroeder-Phased Input Signals. In American Control Conference (pp. 895–899). San Francisco: IEE

Rivera, D. E., Gaikwad, S. V., & Chen, X. (1994). CONTROL-ID: A demonstration prototype for control-relevant identification. Proceedings of the American Control COnference, 2055–2058. https://doi.org/10.1006/viro.2000.0344

Rivera, D. E., Lee, H., Mittelmann, H. D., & Braun, M. W. (2009). Constrained multisine input signals for plant-friendly identification of chemical process systems. Journal of Process Control, 19(4), 623–635.

https://doi.org/10.1016/j.jprocont.2008.08.006

Rivera, D. E., Zong, S., & Ling, W.-M. (1997). A Control-relevant Multivariable System Identification Methodology based on Orthogonal Multifrequency Input Perturbations. Proceedings of the 11th IFAC Symposium on Identification and System Parameter Estimation, 595–600. https://doi.org/10.1016/S1474-6670(17)42906-5

Rocha, J. A., Bravo, J. L., & Fair, J. R. Distillation columns containing structured packings: a comprehensive model for their performance. 1. Hydraulic models. Industrial and Engineering Chemistry Research 1993 32(4).

Rocha, J. A., Bravo, J. L., & Fair, J. R.. Distillation columns containing structured packings: a comprehensive model for their performance. 2. Mass-transfer model. Industrial & engineering chemistry research 1996, 35(5), 1660-1667

Saimpert, M., Puxty, G., Qureshi, S., Wardhaugh, L., & Cousins, A. A new rate based absorber and desorber modelling tool. Chemical engineering science 2013, 96, 10-25.

Sarkar S, Kosson DS, Mahadevan S, Meeussen JC, van der Sloot H, Arnold JR, Brown KG. Bayesian calibration of thermodynamic parameters for geochemical speciation modeling of cementitious materials. Cem Concr Res. 2012;42:889-902.

Sherman, B. J. Thermodynamic and Mass Transfer Modeling of Aqueous Hindered Amines for Carbon Dioxide Capture. University of Texas at Austin 2016, Ph.D. Dissertation.

Simon, L. L., Elias, Y., Puxty, G., Artanto, Y., & Hungerbuhler, K. Rate based modeling and validation of a carbon-dioxide pilot plant absorbtion column operating on monoethanolamine. Chemical Engineering Research and Design 2011, 89(9), 1684-1692.

Soares Chinen, A., Morgan, J. C., Omell, B., Bhattacharyya, D., Tong, C., & Miller, D. C. (2018). Development of a Gold-Standard Model for Solvent-Based CO2 Capture. Part 1: Hydraulic and Mass Transfer Models and Their Uncertainty Quantification.

Sobol, I. M. Sensitivity estimates for nonlinear mathematical models, Mathematical Modeling and Computational

Experiments 1993, 1, 407-414.

Stichlmair J., Bravo J. L., Fair J. R. General model for prediction of pressure drop and capacity of countercurrent gas/liquid packed columns. Gas Sep. Purif. 1989 3, 19-28.

Structured Packings. Winterhur, Switzerland. Sulzer Chemtech 2015.

Suess P, Spiegel L. Hold-up of Mellapak structured packings. Chem. Eng. Process. 31(2) (1992), pp. 119-124.

Tobiesen, A., Juliussen, O., Svendsen, H. F. Experimental validation of a rigorous model for CO2 postcombustion capture. AIChE Journal 2007 53, pp. 846–865,.

Tobiesen, F. A., Hillestad, M., Kvamsdal, H., & Chikukwa, A. (2012). A general column model in CO2SIM for transient modelling of CO2 absorption processes. Energy Procedia, 23(1876), 129–139. https://doi.org/10.1016/j.egypro.2012.06.071

Tönnies, I., Mangalapally, H. P., & Hasse, H. Sensitivity study for the rate-based simulation of the reactive absorption of CO2. Energy Procedia 2011, 4, 533-540.

Tsai, R. E. Mass Transfer Area of Structured Packing. University of Texas at Austin, 2010, Ph.D. Dissertation.

Versteeg, G. F., & Van Swaalj, W. Solubility and diffusivity of acid gases (carbon dioxide, nitrous oxide) in aqueous alkanolamine solutions. Journal of Chemical and Engineering Data 1988, 33(1), 29-34.

Versteeg, G. F., Blauwhoff, P. M. M., & Van Swaaij, W. P. M. The effect of diffusivity on gas-liquid mass transfer in stirred vessels. Experiments at atmospheric and elevated pressures. Chemical Engineering Science 1987, 42(5), 1103-1119.

Versteeg, G. F., L. A. J. Van Dijck, and W. P. M. Van Swaaij. On the kinetics between CO2 and alkanolamines both in aqueous and non-aqueous solutions. An overview. Chemical Engineering Communications 1996 144.1: 113-158.

von Harbou, I., Imle, M., & Hasse, H. Modeling and simulation of reactive absorption of CO2 with MEA: results

for four different packings on two different scales. Chemical Engineering Science 2014, 105, 179-190.

Walters, M. S., Edgar, T. F., & Rochelle, G. T. (2016a). Dynamic modeling and control of an intercooled absorber for post-combustion CO2capture. Chemical Engineering and Processing: Process Intensification, 107, 1–10. https://doi.org/10.1016/j.cep.2016.05.012

Walters, M. S., Edgar, T. F., & Rochelle, G. T. (2016b). Regulatory Control of Amine Scrubbing for CO2 Capture from Power Plants. Industrial and Engineering Chemistry Research, 55(6), 4646–4657. https://doi.org/10.1021/acs.iecr.5b04379

Walters, M. S., Lin, Y. J., Sachde, D. J., Edgar, T. F., & Rochelle, G. T. (2016). Control Relevant Model of Amine Scrubbing for CO2 Capture from Power Plants. Industrial and Engineering Chemistry Research, 55(6), 1690–1700. https://doi.org/10.1021/acs.iecr.5b04379

Weber CL, Vanbriesen JM, Small MS. A stochastic regression approach to analyzing thermodynamic uncertainty in chemical speciation modeling. Environ Sci Technol. 2006;40:3872-3878.

Whiting WB. Effects of uncertainties in thermodynamic data and models on process calculations. J Chem Eng Data. 1996;41:935-941.

Ying, J., & Eimer, D. A. (). Measurements and correlations of diffusivities of nitrous oxide and carbon dioxide in monoethanolamine+ water by laminar liquid jet. Industrial & Engineering Chemistry Research 2012, 51(50), 16517-16524.

Zhang, Q., Turton, R., & Bhattacharyya, D. (2016). Development of Model and Model-Predictive Control of an MEA-Based Postcombustion CO2 Capture Process. Industrial and Engineering Chemistry Research, 55(5), 1292–1308. https://doi.org/10.1021/acs.iecr.5b02243

Zhang, Y., & Chen, C. C. Modeling CO2 absorption and desorption by aqueous monoethanolamine solution with Aspen rate-based model. Energy Procedia 2013, 37, 1584-1596.

Zhang, Y., Chen, H., Chen, C. C., Plaza, J. M., Dugas, R., & Rochelle, G. T. Rate-based process modeling study of CO2 capture with aqueous monoethanolamine solution. Industrial & engineering chemistry research, 48(20),

9233-9246, 2009.

Appendix A: FORTRAN codes for Aspen plus® User Models

A.1 Pressure drop FORTRAN code

```
c Revision 1.1  1996/05/20  17:34:17  apbuild
c New Template, Salinas
c
C ========================cvs revision history=======================
      SUBROUTINE USRPCK (MODE,      J,     PJ,   FLMJ,   FVMJ,
     1                   FLVJ,   FVVJ,  RMWLJ,  RMWVJ,  RHOLJ,
     2                  RHOVJ,  XMULJ,  XMUVJ, SIGMAJ,    FPJ,
     3                    QRJ,  FFACJ,   FFRJ, SYSFAC, IPTYPE,
     4                 IPSIZE,  IPMAT, PACKFC,   VOID,  SURFA,
     5                  STICH,  HETPJ,     FA,   DIAM,   NINT,
     6                    INT,  NREAL,   REAL, DPSTGJ, HTSTGJ )
C
C ******************************************************************
C     USER SUBROUTINE TEMPLATE FOR PACKING SIZING AND RATING
C     FOR RADFRAC, MULTIFRAC AND PETROFRAC
C ******************************************************************
C
C      MODE          INTEGER       – Calculation mode: 1 = Sizing, 2 = Rating
C      N                 INTEGER   – Stage number
C      P                 REAL*8    – Stage pressure (N/m2)
C      FLMJ          REAL*8        – Mass liquid flow from the stage (kg/s)
C      FVMJ          REAL*8        – Mass vapor flow to the stage (kg/s)
C      FLVJ          REAL*8        – Volumetric liquid flow from the stage (m3/s)
C      FVVJ          REAL*8        – Volumetric vapor flow to the stage (m3/s)
C      XMWL          REAL*8            – Average molecular weight of liquid from the stage
C      XMWVJ      REAL*8    – Average molecular weight of vapor to the stage
C      RHOLJ         REAL*8            – Mass density of liquid from the stage (kg/m3)
C      RHOVJ      REAL*8        – Mass density of vapor to the stage (kg/m3)
C      XMULJ         REAL*8        – Viscosity of liquid from the stage (N-s/m2)
C      XMUVJ      REAL*8        – Viscosity of vapor to the stage (N-s/m2)
C      SIGMAJ        REAL*8        – Surface tension of liquid from the stage (N/m)
C      FP                REAL*8    – Flow parameter
C      QR                REAL*8        – Reduced vapor throughput (m3s)
C      FFACJ         REAL*8        – F factor (for rating only) (m/s (kg/m3) ½)
C      FFRJ       REAL*8        – Reduced F factor (m/s (kg/m3) ½)
C      SYSFAC        REAL*8            – System foaming factor
C      IPTYPE        INTEGER       – Packing type
C      IPSIZE        INTEGER       – Packing size
C      IPMAT         INTEGER       – Packing material
C      PACKFC        REAL*8            – Packing factor (1/m)
C      VOID          REAL*8            – Packing void fraction
C      SURFA         REAL*8            – Packing surface area (m2/m3)
C      STICH         REAL*8 3      – Stichlmair constants
C      HETPJ         REAL*8            – Height equivalent to a theoretical plate (m)
C      FA                REAL*8        – Fractional approach to flooding Input for sizing,
Output for rating
C      DIAM          REAL*8            – Column diameter (m) Input for sizing, Output for
rating
C      NINT          INTEGER       – Number of integer parameters (see Integer and Real
Parameters)
```

```
C      INT              INTEGER NINT     – Vector of integer parameters (see Integer and
Real Parameters)
C      NREAL         REAL*8            – Number of real parameters (see Integer and Real
Parameters)
C      REAL          REAL*8 NREAL  – Vector of real parameters (see Integer and    Real
Parameters)
C      DPTSG         REAL*8            – Pressure drop per stage (N/m2)
C      HTSTG         REAL*8            – Fractional liquid holdup

      IMPLICIT NONE
C
C     DECLARE VARIABLES USED IN DIMENSIONING
C
      INTEGER NINT
C
C *** ARRAY DIMENSIONS ***
C
C
#include "ppexec_user.cmn"
      EQUIVALENCE (RMISS, USER_RUMISS)
      EQUIVALENCE (IMISS, USER_IUMISS)
C
C *** EXIT SUBROUTINE
C
C     DECLARE ARGUMENTS
C
      INTEGER INT(NINT)
     +        ,    MODE,  J,     IPTYPE, IPSIZE,IPMAT, NREAL
      REAL*8 STICH(3),     PJ,    FLMJ,  FVMJ,  FLVJ,
     +       FVVJ,  RMWLJ, RMWVJ, RHOLJ, RHOVJ,
     +       XMULJ, XMUVJ, SIGMAJ,FPJ,   QRJ,
     +       FFACJ, FFRJ,  SYSFAC,PACKFC,VOID,
     +       SURFA, HETPJ, FA,    DIAM,  DPSTGJ
      REAL*8 HTSTGJ
C
C     DECLARE LOCAL VARIABLES
C
      INTEGER IMISS
      REAL*8 REAL(NREAL),  RMISS
      REAL*8 FRL, REV, UV, UL, HL, fo, FV
      REAL*8 P1, C, ho, DP

C     Code by Anderson Soares Chinen (Summer 2014)
C     Pressure drop correlation for NCCC case, using Stichlmair correlation


C     PRESSURE DROP GENERAL VARIABLES

      UV=FVVJ/(3.1415/4*DIAM**2)
      UL=FLVJ/(3.1415/4*DIAM**2)

      DP=6*(1-VOID)/SURFA

C fo = 1/K in Billet a
      fo=1+2/3*DP/DIAM/(1-VOID)

      REV=UV*DP*RHOVJ/XMUVJ/fo
```

```
      FRL=(UL**2)*SURFA/9.81

      FV=UV*RHOVJ**0.5

C Stichlmair Correlation, currently not being used.

C     fo
C      fo=STICH(1)/REV+STICH(2)/(REV**0.5)+STICH(3)

C     C
C      C=(-STICH(1)/REV-STICH(2)/2/(REV**0.5))/fo

C     Solving using custom holdup instead of the multual dependent function from
Stichlmair/Billet and Schultes
C     STICH(2) and STICH(3) represents the parameters for UQ

      ho=STICH(2)*(3.185966*(XMULJ/RHOLJ)**0.3333*UL)**STICH(3)
C      ho=11.45038*(3.185966*(XMULJ/RHOLJ)**(1/3)*UL)**0.647111

C      P1=0.75*(1-VOID)/VOID**4.65*fo*RHOVJ*UV**2/DP*((1-VOID*(1-ho/VOID)
C     +)/(1-VOID))**((2+C)/3)*(1-ho/VOID)

C Billet and Schultes Pressure drop

C Stich(1) is substituting here the value of Cpo, as it cannot be set
C C = PSIL

C HLS CALC
      HL=(12/9.81*XMULJ/RHOLJ*UL*SURFA**2)**0.3333

      C=STICH(1)*(64/REV+1.8/(REV**0.08))*((VOID-ho)/VOID)**1.5*
     +EXP(13300/(250**1.5)*FRL**0.5)*(ho/HL)**0.3


      P1=C*SURFA/((VOID-ho)**3)*FV**2/2*fo


      HTSTGJ=ho
      DPSTGJ=P1*0.67456
C 0.67456 = packing height for 1 section

      RETURN
      END
```

A.2 Holdup FORTRAN code

```
C $Log: rs_uholdup.f,v $
C
C ========================cvs revision history=======================
      SUBROUTINE USRHLDUP(KSTG,   FRATEL, FRATEV, AVMWLI, AVMWVA,
     1                    VISCML, DENMXL, SIGMAL, VISCMV, DENMXV,
     2                    LHLDUP, VHLDUP, VSPACE, COLTYP, USRCOR,
     3                    TWRARA, COLDIA, HTPACK, PACSIZ, SPAREA,
     4                    CSIGMA, PFACT,  PKPRMS, VOIDFR, PLHOLD,
     5                    PVHOLD, IPAKAR, IPTYPE, IVENDR, IPMAT,
     6                    IPSIZE, WEIRHT, DCAREA, ARAACT, FLOPTH,
```

```
     7                  NPASS,  WEIRL,  IFMETH, SYSFAC, HOLEAR,
     8                  ITTYPE, TRASPC, PITCH,  NINT,   INT,
     9                  NREAL,  REAL)
C
      IMPLICIT NONE
      INTEGER KSTG, COLTYP, USRCOR, IPAKAR, IPTYPE, IVENDR, IPMAT,
     1        IPSIZE, NPASS, IFMETH, ITTYPE, NINT, INT(NINT), NREAL
      REAL*8  FRATEL, FRATEV, AVMWLI, AVMWVA, VISCML, DENMXL,
     1        SIGMAL, VISCMV, DENMXV, LHLDUP, VHLDUP, VSPACE, TWRARA,
     2        COLDIA, HTPACK, PACSIZ, SPAREA, CSIGMA, PFACT,
     3        PKPRMS(20), VOIDFR, PLHOLD, PVHOLD, WEIRHT, DCAREA,
     4        ARAACT, FLOPTH, WEIRL, SYSFAC, HOLEAR, TRASPC, PITCH,
     5        REAL(NREAL)
C***********************************************************************
C  LICENSED MATERIAL.  PROPERTY OF ASPEN TECHNOLOGY, INC.  TO BE       *
C  TREATED AS ASPEN TECH PROPRIETARY INFORMATION UNDER THE TERMS       *
C  OF THE ASPEN PLUS SUBSCRIPTION AGREEMENT.                           *
C***********************************************************************
C-----------------------------------------------------------------------
C         COPYRIGHT (C) 2004
C          ASPEN TECHNOLOGY, INC.
C          CAMBRIDGE, MA
C-----------------------------------------------------------------------
C
C     DESCRIPTION: User provided RateSep routine to calculate the
C                  liquid holdup and vapor holdup
C
C     WRITTEN BY:  Jianjun Peng            DATE WRITTEN: July 02, 2004
C
C     VARIABLES IN ARGUMENT LIST
C
C     VARIABLE I/O  TYPE   DIMENSION   DESCRIPTION AND RANGE
C     -------- ---  ----   ---------   -------------------------------
C     KSTG      I    I         -       SEGMENT NUMBER
C     FRATEL    I    R         -       FLOW OF LIQUID (KMOL/SEC)
C     FRATEV    I    R         -       FLOW OF VAPOR (KMOL/SEC)
C     AVMWLI    I    R         -       AVERAGE MOLECULAR WEIGHT
C                                      OF LIQUID MIXTURE
C                                      (KG/KMOL)
C     AVMWVA    I    R         -       AVERAGE MOLECULAR WEIGHT
C                                      OF VAPOR MIXTURE (KG/KMOL)
C     VISCML    I    R         -       VISCOSITY OF LIQUID
C                                      (N-SEC/SQ.M)
C     DENMXL    I    R         -       DENSITY OF LIQUID MIXTURE
C                                      (KMOL/CU.M)
C     SIGMAL    I    R         -       SURFACE TENSION OF LIQUID
C                                      (N/M)
C     VISCMV    I    R         -       VISCOSITY OF VAPOR MIXTURE
C                                      (N-SEC/SQ.M)
C     DENMXV    I    R         -       DENSITY OF VAPOR MIXTURE
C                                      (KMOL/CU.M)
C     LHLDUP    O    R         -       LIQUID STAGE HOLDUP (CU.M)
C     VHLDUP    O    R         -       VAPOR STAGE HOLDUP (CU.M)
C     VSPACE    O    R         -       VAPOR SPACE HOLDUP (CU.M)
C     COLTYP    I    I         -       TYPE OF COLUMN
C                                        1 = PACKED
C                                        2 = TRAY
C     USRCOR    I    I         -       CALCULATION METHOD (I.E.
```

```
C                                       CHOICE OF USER CORRELATION)
C                                         1 = USER1
C                                         2 = USER2
C                                         3 = USER3
C                                         4 = USER4
C     TWRARA    I    R          -       CROSS-SECTIONAL AREA OF
C                                       TOWER (SQ.M)
C     COLDIA    I    R          -       COLUMN DIAMETER (M)
C     HTPACK    I    R          -       HEIGHT OF PACKING IN THE
C                                       SEGMENT (M)
C     PACSIZ    I    R          -       SIZE OF PACKING (M)
C     SPAREA    I    R          -       SPECIFIC SURFACE AREA OF
C                                       PACKING (SQ.M/CU.M)
C     CSIGMA    I    R          -       CRITICAL SURFACE TENSION
C                                       OF PACKING MATERIAL (N/M)
C     PFACT     I    R          -       PACKING FACTOR (1/M)
C     PKPRMS    I    R         20       PACKING PARAMETERS
C                                       PKPRMS(1) = STICHLMAIR CONSTANT C1
C                                       PKPRMS(2) = STICHLMAIR CONSTANT C2
C                                       PKPRMS(3) = STICHLMAIR CONSTANT C3
C                                       PKPRMS(4) = CL IN BILLET 93
C                                       PKPRMS(5) = CV IN BILLET 93
C                                       PKPRMS(6) = B IN BRF 85
C                                       PKPRMS(7) = S IN BRF 85
C                                       PKPRMS(8) = H IN BRF 85
C                                       PKPRMS(9) = Fse IN BRF 92
C                                       PKPRMS(10) = CE IN BRF 92
C                                       PKPRMS(11) = THETA IN BRF 92
C     VOIDFR    I    R          -       VOID FRACTION OF PACKING
C     PLHOLD    I    R          -       User specified % free volume
C                                       for liquid holdup
C     PVHOLD    I    R          -       User specified % free volume
C                                       for vapor holdup
C     IPAKAR    I    I          -       PACKING ARRANGEMENT
C                                         1 = RANDOM
C                                         2 = STRUCTURED
C     IPTYPE    I    I          -       PACKING TYPE
C                                       See IPTYPE in packsr.f
C     IVENDR    I    I          -       PACKING VENDOR CODE
C     IPMAT     I    I          -       PACKING MATERIAL CODE
C     IPSIZE    I    I          -       PACKING SIZE CODE
C     WEIRHT    I    R          -       AVERAGE WEIR HEIGHT (M)
C     DCAREA    I    R          -       TOTAL AREA OF DOWNCOMER
C                                       ON TRAY (SQ.M)
C     ARAACT    I    R          -       TOTAL ACTIVE AREA AVAILABLE
C                                       ON TRAY (SQ.M)
C     FLOPTH    I    R          -       AVERAGE FLOWPATH LENGTH (M)
C     NPASS     I    I          -       NUMBER OF TRAY PASSES
C     WEIRL     I    R          -       AVERAGE WEIRH LENGTH (M)
C     IFMETH    I    I          -       FLOODING CALCULATION
C                                       METHOD; REQUIRED FOR SIEVE
C                                       TRAY
C     SYSFAC    I    R          -       SYSTEM FACTOR; REQUIRED FOR
C                                       SIEVE TRAY
C     HOLEAR    I    R          -       HOLE AREA/ACTIVE AREA; REQUIRED
C                                       FOR SIEVE TRAY
C     ITTYPE    I    I          -       TRAY TYPE
C                                         1 = BUBBLE-CAP
```

```
C                                        2 = VALVE
C                                        3 = SIEVE
C                                        4 = USER
C     TRASPC    I    R          -       TRAY SPACING (M)
C     PITCH     I    R          -       SIEVE TRAY HOLE PITCH (M)
C     NINT      I    I          -       Size of INT
C     INT      I/O   I          *       BLOCK INT ARRAY
C     NREAL     I    I          -       Size of REAL
C     REAL     I/O   R          *       BLOCK REAL ARRAY
C***********************************************************************
C
C     Define local variables
C
      INTEGER ITER, KHTERR, KDPERR
C     Variables used in the Stichlmair 89 correlation
      REAL*8  DEQ, UL, UV, REV, C1, C2, C3,
     +        DP, DPDRY, DPWET, FRL, HT, HT0, AUX, F, D,
     +        C_S, GRAV, FF, HTETA
C
C     Variables used in the Bennett 83 correlation
      REAL*8  RS_BennettA, RS_BennettC, RS_BennettHL
      REAL*8  FREVOL, US, RHOV, RHOL, ALPHAE, C_B, QL, HL, HF,
     +        VOID, PLH, PVH
      DATA GRAV /9.806599D0/
C
      IF (COLTYP .EQ. 1) THEN
C
C     PACKED COLUMN
C
         VSPACE = 0.0D0
         IF (USRCOR .EQ. 1) THEN
C           user subroutine example for packed column: Stichlmair 89
C
C           Stichlmair, J., Bravo, J.L. and Fair, J.R., "General Model
C             for Prediction of Pressure Drop and Capacity of
C             Countercurrent Gas/Liquid Packed Columns", Gas Sep.
C             Purif., 3, (1989), P19
C
            DEQ = 6D0*(1D0 - VOIDFR)/SPAREA
            RHOL = AVMWLI*DENMXL
            RHOV = AVMWVA*DENMXV
C
C ***       CALCULATE FRICTION FACTOR ***
C
            UV = FRATEV/DENMXV/TWRARA
            REV = DEQ*UV*RHOV/VISCMV
            C1 = PKPRMS(1)
            C2 = PKPRMS(2)
            C3 = PKPRMS(3)
            FF = C1/REV + C2/DSQRT(REV) + C3
            IF (FF .EQ. 0D0) FF = 10D0
            C_S  = (-C1/REV - C2/2D0/DSQRT(REV))/FF
C
C ***       CALCULATE DRY PRESSURE DROP ***
C
            DPDRY = 0.75D0*FF*(1D0 - VOIDFR)/VOIDFR**4.65D0
     1            *RHOV*UV*UV/DEQ/RHOL/GRAV
C
```

```
C ***       CALCULATE LIQUID HOLDUP BELOW THE LOADING POINT ***
C
            UL  = FRATEL/DENMXL/TWRARA
            FRL = UL*UL*SPAREA/GRAV/VOIDFR**4.65D0
            HT0 = .555D0*FRL**(0.33333333D0)
C
C ***       SET INITIAL ESTIMATE OF WET PRESSURE DROP ***
C
            DP  = DPDRY
            ITER = 0
C
C ***       CALCULATE WET PRESSURE DROP USING NEWTON'S METHOD ***
C
  101       KHTERR = 0
            HT = HT0*(1D0 + 20D0*DP*DP)
            HTETA  = HT/VOIDFR
            IF (HTETA .GE. 1D0) THEN
               KHTERR = 1
            ELSE
               AUX = ((1D0 -VOIDFR*(1D0 -HTETA))/(1D0 -VOIDFR))
     1             **((2D0 +C_S)/3D0)
               F = DP/DPDRY -AUX/(1D0 -HTETA)**4.65D0
               D = 1D0/DPDRY -40D0*HT0*DP*AUX/(1D0 -HTETA)**4.65D0*
     1           (4.65/(VOIDFR -HT) +(2D0+C_S)/3D0/(1D0 -VOIDFR +HT))
            END IF
C           END OF IF (HTETA...
C
C ***       CHECK IF LIQUID OCCUPIES THE WHOLE PACKING VOIDAGE ***
C
            IF (KHTERR .EQ. 1) THEN
               HT = DMAX1(VOIDFR, HT0)
               DPWET = DSQRT((HT/HT0 - 1D0)/20D0)
               GOTO 301
            END IF
C           END OF IF (KHTERR...
C
C ***       GET NEW ESTIMATE ***
C
            DPWET = DP - F/D
C
C ***       CHECK FOR CONVERGENCE ***
C
            IF (DABS(DPWET - DP)/DP .GT. 1D-12) THEN
               IF (DPWET .GT. 0.3D0) DPWET = 0.3D0
               IF (DPWET .LT. 0.0D0) DPWET = 0.01D0
               ITER = ITER + 1
               IF (ITER .GT. 30) THEN
                  KDPERR = 5
                  GOTO 201
               END IF
               DP = DPWET
               GOTO 101
            END IF
C           END OF IF (DABS...
C
C ***       CALCULATE TOTAL LIQUID HOLDUP ***
C
  201       HT = HT0 * (1D0 + 20D0*DPWET*DPWET)
```

```
  301       LHLDUP = HT * TWRARA * HTPACK
            VHLDUP = (1D0 - HT - VOIDFR) * TWRARA * HTPACK

C NEW CODE - USRCOR = 2
C BASED ON SPIEGEL AND MEIER, REGRESSED FOR MP252Y FOLLOWING TSAI(2010) INITIAL WORK
C THIS CASE IS FOR THE OPERATIONAL REGION UNDER THE LOADING POINT

C option two for specific case of Mellapak Plus 252Y by Anderson Soares Chinen 2018
         ELSE IF (USRCOR .EQ. 2) THEN
              RHOL = AVMWLI*DENMXL
              UL = FRATEL/DENMXL/TWRARA

              HT=REAL(1)*(3.185966*(VISCML/RHOL)**0.3333*(UL))
     +**REAL(2)
C Total holdup calculation
              LHLDUP = HT * TWRARA * HTPACK
              VHLDUP = (1D0 - HT - VOIDFR) * TWRARA * HTPACK
         END IF
C        END OF IF (USRCOR...
C
      ELSE IF (COLTYP .EQ. 2) THEN
C
C     TRAY COLUMN
C
         IF (USRCOR .EQ. 1) THEN
C           user subroutine example for tray column: Bennett 83
C
C           Bennett, D.L., Agrawal, R. and Cook, P.J., "New Pressure
C             Drop Correlation for Sieve Tray Distillation Columns",
C             AIChE J., 29, (1983) p 434
C
            US = FRATEV/DENMXV/ARAACT
            RHOV = DENMXV * AVMWVA
            RHOL = DENMXL * AVMWLI
            ALPHAE = RS_BennettA(US, RHOL, RHOV)
            C_B = RS_BennettC(WEIRHT)
            QL = FRATEL/DENMXL
            HL =RS_BennettHL (ALPHAE, WEIRHT, C_B, QL, WEIRL)
            HF = HL/ALPHAE
            LHLDUP = HL*ARAACT
            VHLDUP = (HF-HL)*ARAACT
            VSPACE = TRASPC*(ARAACT+DCAREA)
     +             - (LHLDUP+VHLDUP)*(ARAACT+DCAREA)/ARAACT
C
         END IF
C        END OF IF (USRCOR...
C
      END IF
C     END OF IF (COLTYP...

      RETURN
      END
```

A.3 Mass transfer coefficients FORTRAN code

```
      SUBROUTINE USRMTRF3(KSTG,   NCOMPS, IDX,    NBOPST, KPDIAG,
```

```
     1                   XCOMPB, FRATEL, YCOMPB, FRATEV, PRESS,
     2                   TLIQ,   TVAP,   AVMWLI, AVMWVA, VISCML,
     3                   DENMXL, SIGMAL, VISCMV, DENMXV, AREAIF,
     4                   PREK,   EXPKD,  COLTYP, USRCOR, TWRARA,
     5                   COLDIA, HTPACK, PACSIZ, SPAREA, CSIGMA,
     6                   PFACT,  PKPRMS, VOIDFR, IPAKAR, IPTYPE,
     7                   IVENDR, IPMAT,  IPSIZE, WEIRHT, DCAREA,
     8                   ARAACT, FLOPTH, NPASS,  WEIRL,  IFMETH,
     9                   SYSFAC, HOLEAR, ITTYPE, TRASPC, PITCH,
     A                   IPHASE, NINT,   INT,    NREAL,  REAL)
      IMPLICIT NONE
      INTEGER KSTG, NCOMPS, IDX(NCOMPS), NBOPST(6), KPDIAG,
     +        COLTYP, USRCOR, IPAKAR, IPTYPE, IVENDR, IPMAT,  IPSIZE,
     +        NPASS, IFMETH, ITTYPE, NINT, INT(NINT), IPHASE, NREAL
      REAL*8  XCOMPB(NCOMPS), FRATEL, YCOMPB(NCOMPS), FRATEV,
     +        PRESS, TLIQ, TVAP, AVMWLI, AVMWVA, VISCML, DENMXL,
     +        SIGMAL, VISCMV, DENMXV, AREAIF, PREK, EXPKD,
     +        TWRARA, COLDIA, HTPACK, PACSIZ, SPAREA, CSIGMA,
     +        PFACT,  PKPRMS(20), VOIDFR, WEIRHT, DCAREA, ARAACT,
     +        FLOPTH, WEIRL, SYSFAC, HOLEAR, TRASPC, PITCH,
     +        REAL(NREAL)
C***********************************************************************
C  LICENSED MATERIAL.  PROPERTY OF ASPEN TECHNOLOGY, INC.  TO BE       *
C  TREATED AS ASPEN TECH PROPRIETARY INFORMATION UNDER THE TERMS       *
C  OF THE ASPEN PLUS SUBSCRIPTION AGREEMENT.                           *
C***********************************************************************
C-----------------------------------------------------------------------
C         COPYRIGHT (C) 2004
C          ASPEN TECHNOLOGY, INC.
C          CAMBRIDGE, MA
C-----------------------------------------------------------------------
C
C     DESCRIPTION: User provided RateSep routine to calculate the
C                  liquid (IPHASE=0) and vapor (IPHASE=1) binary mass
C                  transfer coefficient parameters (PREK, EXPKD).
C
C     VARIABLES IN ARGUMENT LIST
C
C     VARIABLE I/O  TYPE   DIMENSION   DESCRIPTION AND RANGE
C     -------- ---  ----   ---------   --------------------------------
C     KSTG      I    I         -       SEGMENT NUMBER
C     NCOMPS    I    I         -       NUMBER OF COMPONENTS
C     IDX       I    I       NCOMPS    COMPONENT INDEX VECTOR
C     NBOPST    I    I         6       PHYSICAL PROPERTY OPTION
C                                      SET BEAD POINTER
C     KPDIAG    I    I         -       PHYSICAL PROPERTY
C                                      DIAGOSTIC CODE
C     XCOMPB    I    R       NCOMPS    BULK LIQUID MOLE FRACTION
C     FRATEL    I    R         -       FLOW OF LIQUID (KMOL/SEC)
C     YCOMPB    I    R       NCOMPS    BULK VAPOR MOLE FRACTION
C     FRATEV    I    R         -       FLOW OF VAPOR (KMOL/SEC)
C     PRESS     I    R         -       PRESSURE (N/SQ.M)
C     TLIQ      I    R         -       LIQUID TEMPERATURE (K)
C     TVAP      I    R         -       VAPOR TEMPERATURE (K)
C     AVMWLI    I    R         -       AVERAGE MOLECULAR WEIGHT
C                                      OF LIQUID MIXTURE
C                                      (KG/KMOL)
C     AVMWVA    I    R         -       AVERAGE MOLECULAR WEIGHT
```

```
C                                          OF VAPOR MIXTURE (KG/KMOL)
C     VISCML    I    R          -          VISCOSITY OF LIQUID
C                                          (N-SEC/SQ.M)
C     DENMXL    I    R          -          DENSITY OF LIQUID MIXTURE
C                                          (KMOL/CU.M)
C     SIGMAL    I    R          -          SURFACE TENSION OF LIQUID
C                                          (N/M)
C     VISCMV    I    R          -          VISCOSITY OF VAPOR MIXTURE
C                                          (N-SEC/SQ.M)
C     DENMXV    I    R          -          DENSITY OF VAPOR MIXTURE
C                                          (KMOL/CU.M)
C     AREAIF    I    R          -          INTERFACIAL AREA
C                                          (SEE NOTE-1 BELOW)
C     PREK      O    R          -          BINARY MASS TRANSFER =
C     EXPRKD    O    R          -             PREK*DIFFUSIVITY**EXPKD
C                                          (SEE NOTE-2 BELOW)
C     COLTYP    I    I          -          TYPE OF COLUMN
C                                          1 = PACKED
C                                          2 = TRAY
C     USRCOR    I    I          -          CALCULATION METHOD (I.E.
C                                          CHOICE OF USER CORRELATION)
C                                            1  = USER1
C                                            2  = USER2
C                                            3  = USER3
C                                            4  = USER4
C     TWRARA    I    R          -          CROSS-SECTIONAL AREA OF
C                                          TOWER (SQ.M)
C     COLDIA    I    R          -          COLUMN DIAMETER (M)
C     HTPACK    I    R          -          HEIGHT OF PACKING IN THE
C                                          SEGMENT (M)
C     PACSIZ    I    R          -          SIZE OF PACKING (M)
C     SPAREA    I    R          -          SPECIFIC SURFACE AREA OF
C                                          PACKING (SQ.M/CU.M)
C     CSIGMA    I    R          -          CRITICAL SURFACE TENSION
C                                          OF PACKING MATERIAL (N/M)
C     PFACT     I    R          -          PACKING FACTOR (1/M)
C     PKPRMS    I    R         20          PACKING PARAMETERS
C                                          PKPRMS(1) = STICHLMAIR CONSTANT C1
C                                          PKPRMS(2) = STICHLMAIR CONSTANT C2
C                                          PKPRMS(3) = STICHLMAIR CONSTANT C3
C                                          PKPRMS(4) = CL IN BILLET 93
C                                          PKPRMS(5) = CV IN BILLET 93
C                                          PKPRMS(6) = B IN BRF 85
C                                          PKPRMS(7) = S IN BRF 85
C                                          PKPRMS(8) = H IN BRF 85
C                                          PKPRMS(9) = Fse IN BRF 92
C                                          PKPRMS(10) = CE IN BRF 92
C                                          PKPRMS(11) = THETA IN BRF 92
C     VOIDFR    I    R          -          VOID FRACTION OF PACKING
C     IPAKAR    I    I          -          PACKING ARRANGEMENT
C                                            1 = RANDOM
C                                            2 = STRUCTURED
C     IPTYPE    I    I          -          PACKING TYPE
C                                          See IPTYPE in packsr.f
C     IVENDR    I    I          -          PACKING VENDOR CODE
C     IPMAT     I    I          -          PACKING MATERIAL CODE
C     IPSIZE    I    I          -          PACKING SIZE CODE
C     WEIRHT    I    R          -          AVERAGE WEIR HEIGHT (M)
```

```
C     DCAREA    I    R          -       TOTAL AREA OF DOWNCOMER
C                                       ON TRAY (SQ.M)
C     ARAACT    I    R          -       TOTAL ACTIVE AREA AVAILABLE
C                                       ON TRAY (SQ.M)
C     FLOPTH    I    R          -       AVERAGE FLOWPATH LENGTH (M)
C     NPASS     I    I          -       NUMBER OF TRAY PASSES
C     WEIRL     I    R          -       AVERAGE WEIRH LENGTH (M)
C     IFMETH    I    I          -       FLOODING CALCULATION
C                                       METHOD; REQUIRED FOR SIEVE
C                                       TRAY
C     SYSFAC    I    R          -       SYSTEM FACTOR; REQUIRED FOR
C                                       SIEVE TRAY
C     HOLEAR    I    R          -       HOLE AREA/ACTIVE AREA; REQUIRED
C                                       FOR SIEVE TRAY
C     ITTYPE    I    I          -       TRAY TYPE
C                                         1 - BUBBLE CAPS
C                                         2 - SIEVE
C                                         3 - GLITSCH BALLAST
C                                         4 - KOCH FLEXITRAY
C                                         5 - NUTTER FLOAT VALVE
C     TRASPC    I    R          -       TRAY SPACING (M)
C     PITCH     I    R          -       SIEVE TRAY HOLE PITCH (M)
C     IPHASE    I    I          -       PHASE QUALIFIER
C                                         0 = LIQUID
C                                         1 = VAPOR
C     NINT      I    I          -       Size of INT
C     INT      I/O   I       NINT      User correlation INT array
C     NREAL     I    I          -       Size of REAL
C     REAL     I/O   I       NREAL     User correlation REAL array
C
C    NOTE-1:
C         SPECIFIC INTERFACIAL AREA "AREAIF" HAS THE FOLLOWING UNITS.
C           FOR PACKED COLUMNS, THE UNITS IS "SQ.M/CU.M OF PACKING"
C           FOR TRAY COLUMNS, THE UNITS IS "SQ.M/SQ.M ACTIVE TRAY AREA"
C
C    NOTE-2:
C         BINMTP = PREK * DIFFUSIVITY**EXPKD
C         BINARY MASS TRANSFER COEFFCIENTS "BINMTP" HAVE UNITS (KMOL/SEC)
C         DIFFUSIVITY HAVE UNITS (SQ.M/SEC)
C         BINMTP HAS MOLAR DENSITY AND INTERFACIAL AREA INCLUDED
C
C*********************************************************************
C     Declare local variables used in the user correlations
C
      REAL*8 RS_BennettHL
      REAL*8 RS_BennettA
      REAL*8 RS_BennettC
      REAL*8 ScLB,   ScVB,   rhoLms, rhoVms, ReLPrm, P, GM,
     +       uL,     uV,     Fs,     QL, tL, THETA, dEQ, C,
     +       uSV,   alphae, hL,     ShLB,   ReV, uSL, S, B, H, CE,
     +       dTemp, Gz, Ka, Fth, uLE, uVE, DELTA, hld, G1, G2,
     +        vel, hydia, qsoln, w, dtempa
C
C     Instead of computing BINMTP from diffusivity as in RATEFRAC
C     compute PREK and EXPKD for RateSep
C
      IF (COLTYP .EQ. 1) THEN
C
```

```
C**** PACKED COLUMN
C
         IF (USRCOR .EQ. 1) THEN
C           user subroutine example for packed column: Onda 68
C
C           Onda, K., Takeuchi, H. and Okumoto, Y., "Mass Transfer
C             Coefficients between Gas and Liquid Phases in Packed
C             Columns", J. Chem. Eng. Jap., 1, (1968) P56
C
            IF (IPHASE.EQ.0) THEN
C
C              Liquid phase
C
               rhoLms = DENMXL * AVMWLI
               uL = FRATEL / TWRARA / DENMXL
               ReLPrm = rhoLms * uL / VISCML / AREAIF
               dTemp = (rhoLms/9.81D0/VISCML)**(0.33333333D0)
               dTemp = 0.0051D0 * (ReLPrm**(0.66666667D0))
     +                *((SPAREA*PACSIZ)**(0.4D0)) / dTemp
C
C              CONVERT K FROM M/S TO KMOL/S
               dTemp = dTemp * TWRARA * HTPACK * AREAIF * DENMXL
C
C              COMPOSITION INDEPENDENT PART OF SCHMIDT NUMBER
               ScLB = VISCML / rhoLms
C
               PREK  = dTemp / DSQRT(ScLB)
               EXPKD = 0.5D0
C
            ELSE
C
C              Vapor phase
C
                rhoVms = DENMXV * AVMWVA
                uV = FRATEV / TWRARA / DENMXV
                ReV = rhoVms * uV / VISCMV / SPAREA
                dTemp = SPAREA*PACSIZ
                dTemp = dTemp * dTemp
                   IF (PACSIZ .GE. 0.015D0) THEN
                       dTemp = 5.23D0 / dTemp
                   ELSE
                       dTemp = 2.0D0 / dTemp
                   END IF
                dTemp = dTemp * (ReV**(0.7D0)) * SPAREA
C
C               CONVERT K FROM M/S TO KMOL/S
                dTemp = dTemp * TWRARA * HTPACK * AREAIF * DENMXV
C
C               COMPOSITION INDEPENDENT PART OF SCHMIDT NUMBER
                ScVB = VISCMV / rhoVms
C
                PREK = dTemp * ScVB ** 0.33333333D0
                EXPKD = 0.66666667D0
             END IF
C            END OF IF (IPHASE)
C
         ELSE IF (USRCOR .EQ. 2) THEN
C        This code is for mass transfer coefficients using Wang Chao 2013.
```

```
C        The gas coefficient uses a modified version BRF-96
C        Modifying factor kL = REAL(1) kG = REAL(2)
C        HOLDUP = REAL(3)
C        THETA = REAL(4)
C        S = REAL(5)
C
         dTemp = REAL(1)
         CE = REAL(2)
         hld = REAL(3)
         THETA = REAL(4)
         S = REAL(5)
         G1 = REAL(6)
         G2 = REAL(7)



            IF (IPHASE.EQ.0) THEN
C
C           Liquid phase
C
C           Access to user variable array     (Except for PREK, this is no longer needed)
                uL = FRATEL / (TWRARA * DENMXL)

                PREK = hld*(uL)**THETA
C
C           Conversion of K from m/s to kmol/s
                PREK = dTemp * PREK * DENMXL *AREAIF * HTPACK * TWRARA
                EXPKD = 0
            ELSE
C
C           Vapor phase
C
                     uV = FRATEV / TWRARA / DENMXV
                     PREK = G1*(uV)**G2
C
C           Conversion of K from m/s to kmol/s
                PREK = CE * PREK * DENMXV *AREAIF * HTPACK * TWRARA
                EXPKD = 0
            END IF
C           END OF IF (PHASE)

CCCCCCCCCCCCCCCCCCCCCCCC
         ELSE IF (USRCOR .EQ. 3) THEN
C        This code is for mass transfer coefficients using ROCHA 1996.
             rhoVms=DENMXV*AVMWVA
             rhoLms=DENMXL*AVMWLI
             uL=FRATEL/(TWRARA*DENMXL)
             uV=FRATEV/TWRARA/DENMXV
             hld=11.45*(3.185966*(VISCML/rhoLms)**0.3333*(uL))**0.6471
             uV=uV/VOIDFR/(1-hld)/0.7071
             uL=uL/VOIDFR/hld/0.7071

            IF (IPHASE.EQ.0) THEN
C
C           Liquid phase
C
C           Access to user variable array     (Except for PREK, this is no longer needed)
```

```
                PREK=2*(0.9*uL/3.14/0.017)**0.5
C
C           Conversion of K from m/s to kmol/s
                PREK = PREK * DENMXL *AREAIF * HTPACK * TWRARA
                EXPKD = 0.5
            ELSE
C
C           Vapor phase
C

                      PREK = 0.054/0.017*((uV+uL)*rhoVms*0.017/VISCMV)**0.8
     +*(VISCMV/rhoVms)**0.33
C
C           Conversion of K from m/s to kmol/s
                PREK = REAL(5)*PREK*DENMXV*AREAIF*HTPACK*TWRARA
                EXPKD = 0.67
            END IF
C           END OF IF (PHASE)
CCCCCCCCCCCCCCCCCCCCCCCC


C     FOR WWC
      ELSE IF (USRCOR .EQ. 9) THEN
C
      IF (IPHASE.EQ.0) THEN
C
C Liquid phase
C
CC      qsoln =FRATEL/DENMXL / 100
C The factor of 100 is needed since the simulation has 10x diamter (100x flow).
C
CCC      w = 0.03958407
C w is the circumfrence of the column in meters. Diamter of WWC is 0.0126m
C
CCC      dTemp = 3**0.3333*2**0.5/3.1416**0.5
CCC      dTemp = dTemp*qsoln**0.3333*0.091**0.5*w**0.6667/0.003852
CCC      dTemp = dTemp*(9.81*DENMXL/VISCML*AVMWLI)**0.1667
C     The proceeding equation is a simplification of the equaitons in Cullinane's thesis,
pages 57-60. The simplification for theta is used to allow the form Aspen requires.
C      The constants 0.091, 0.003852, and 9.81 refer to the height of the WWC, the area
of the
C     WWC and acceleration due to gravity.

C CONVERT K FROM M/S TO KMOL/S
CCC      dTemp = dTemp*TWRARA*HTPACK*AREAIF*DENMXL
C This is the conversion used in the Onda mass transfer routine
CCC      PREK = dtemp*1.0
CCC      EXPKD = 0.5D0
      dTemp = 0.042064*(DENMXL/FRATEL*0.0004)**1.3333
      dTemp = dTemp*(DENMXL*AVMWLI*9.81/VISCML)**0.3333
      PREK = dTemp**0.3333*FRATEL/DENMXL/AREAIF/1.46592
      PREK = PREK*TWRARA*HTPACK*DENMXL*AREAIF
      EXPKD = 0.3333
C
      ELSE
C
C Vapor phase
C
```

```
C From Pacheco's correlation: R*T*kg*d/DCO2=1.075(Re*Sc*d/h)^0.85
C Simplified, this gives RTkg=1.075*DCO2^.15*d^.7*(v/h)^.85
C
CCC      vel = FRATEV/TWRARA/DENMXV
CCC      hydia = 0.0044D0
C This corresponds to the estimated hydraulic diameter of the WWC, 0.44cm.
c
CCC      dTemp = 1.075D0*hydia**0.7D0
CCC      dTemp = dTemp*(vel/(0.091D0))**0.85D0
C The constant, 0.091, corresponds to the height of the WWC. Aspen has a argument for the
C height of a stage but nothing for the # of stages. Therefore the total height was
hardwired.
C
CCC      dTemp = dTemp*DENMXV*AREAIF*TWRARA*HTPACK
C This time the number of stages is not need bc this mass tranfer coeffient is the moles
reacted by stage
C Note: this correlation results in a MT value (in mol/s) 100 times greater than the
calculated excel value due to 10x diameter.
C
CCC      PREK = dtemp
CCC      EXPKD = 0.15D0
C
      dTemp = 0.002897*(FRATEV/TWRARA/DENMXV/0.091)**0.85
      PREK = dTemp*TWRARA*HTPACK*DENMXL*AREAIF
      EXPKD = 0.15

      END IF
C END OF IF (IPHASE)
C

      END IF
C END OF IF (USRCOR)
c
C This is the end of the Dugas Modification


      ELSE IF (COLTYP .EQ. 2) THEN
C
C**** TRAY COLUMN
C
         IF (USRCOR .EQ. 1) THEN
C           user subroutine example for tray column: AIChE 58
C
C           AIChE, Bubble Tray Design Manual: Prediction of Fractionation
C             Efficiency, New York, 1958
C
C           For bubble cap, valve, and sieve trays
C
            IF (IPHASE.EQ.0) THEN
C
C              Liquid phase
C
               rhoVms = DENMXV * AVMWVA
               rhoLms = DENMXL * AVMWLI
               uV = FRATEV /DENMXV /ARAACT
               Fs = uV * DSQRT(rhoVms)
               C = 0.5D0 + 0.438D0 * DEXP(-137.8 * WEIRHT)
               QL = FRATEL/DENMXL
```

```
               ALPHAE = DEXP(-12.55D0*(uV*DSQRT(RHOVMS/DABS(RHOLMS-
     1                   RHOVMS)))**0.91D0)
               hL =ALPHAE*(WEIRHT + C*(QL/WEIRL/ALPHAE)**0.67D0)
               dTemp = 19700.0D0 *(0.4D0*Fs+0.17D0) * hL
     +                 * ARAACT * DENMXL
C
               PREK = dTemp
               EXPKD = 0.5D0
C
            ELSE
C
C              Vapor phase
C
               rhoVms = DENMXV * AVMWVA
               uV = FRATEV /DENMXV /ARAACT
               Fs = uV * DSQRT(rhoVms)
               QL = FRATEL/DENMXL
               dTemp = 0.776 + 4.57*WEIRHT - 0.238*Fs
     +                + 104.8*QL/WEIRL
               dTemp = dTemp * uV * ARAACT * DENMXV
C
C              COMPOSITION INDEPENDENT PART OF SCHMIDT NUMBER
               ScVB = VISCMV / rhoVms
C
               PREK = dTemp /DSQRT(ScVB)
               EXPKD = 0.5D0
             END IF
C            END OF IF (IPHASE)
C
          END IF
C         END OF IF (USRCOR)
C
        END IF
C      END OF IF (COLTYP)
C
       RETURN
       END
```

A.4 Interfacial area FORTRAN code

```
       SUBROUTINE awang(KSTG,   NCOMPS, IDX,    NBOPST, KPDIAG,
      1                 XCOMPB, FRATEL, YCOMPB, FRATEV, PRESS,
      2                 TLIQ,   TVAP,   AVMWLI, AVMWVA, VISCML,
      3                 DENMXL, SIGMAL, VISCMV, DENMXV, AREAIF,
      4                 COLTYP, USRCOR, TWRARA, COLDIA, HTPACK,
      5                 PACSIZ, SPAREA, CSIGMA, PFACT,  PKPRMS,
      6                 VOIDFR, IPAKAR, IPTYPE, IVENDR, IPMAT,
      7                 IPSIZE, WEIRHT, DCAREA, ARAACT, FLOPTH,
      8                 NPASS,  WEIRL,  IFMETH, SYSFAC, HOLEAR,
      9                 ITTYPE, TRASPC, PITCH,  NINT,   INT,
      A                 NREAL,  REAL)
       IMPLICIT NONE
       INTEGER KSTG, NCOMPS, IDX(NCOMPS), NBOPST(6), KPDIAG,
      +        COLTYP, USRCOR, IPAKAR, IPTYPE, IVENDR, IPMAT,  IPSIZE,
      +        NPASS, IFMETH, ITTYPE, NINT, INT(NINT), NREAL
       REAL*8  XCOMPB(NCOMPS), FRATEL, YCOMPB(NCOMPS), FRATEV,
```

```
     +         PRESS, TLIQ, TVAP, AVMWLI, AVMWVA, VISCML, DENMXL,
     +         SIGMAL, VISCMV, DENMXV, AREAIF, TWRARA, COLDIA,
     +         HTPACK, PACSIZ, SPAREA, CSIGMA, PFACT, PKPRMS(20),
     +         VOIDFR, WEIRHT, DCAREA, ARAACT, FLOPTH, WEIRL,
     +         SYSFAC, HOLEAR, TRASPC, PITCH, REAL(NREAL)
C***********************************************************************
C  LICENSED MATERIAL.  PROPERTY OF ASPEN TECHNOLOGY, INC.  TO BE       *
C  TREATED AS ASPEN TECH PROPRIETARY INFORMATION UNDER THE TERMS       *
C  OF THE ASPEN PLUS SUBSCRIPTION AGREEMENT.                           *
C***********************************************************************
C-----------------------------------------------------------------------
C         COPYRIGHT (C) 2004
C          ASPEN TECHNOLOGY, INC.
C          CAMBRIDGE, MA
C-----------------------------------------------------------------------
C
C     DESCRIPTION: User provided RateSep routine to calculate the
C                  specific interface area AREAIF (see NOTE-1).
C
C     VARIABLES IN ARGUMENT LIST
C
C     VARIABLE I/O  TYPE   DIMENSION   DESCRIPTION AND RANGE
C     -------- ---  ----   ---------   --------------------------------
C     KSTG      I    I         -       SEGMENT NUMBER
C     NCOMPS    I    I         -       NUMBER OF COMPONENTS
C     IDX       I    I       NCOMPS    COMPONENT INDEX VECTOR
C     NBOPST    I    I         6       PHYSICAL PROPERTY OPTION
C                                      SET BEAD POINTER
C     KPDIAG    I    I         -       PHYSICAL PROPERTY
C                                      DIAGOSTIC CODE
C     XCOMPB    I    R       NCOMPS    BULK LIQUID MOLE FRACTION
C     FRATEL    I    R         -       FLOW OF LIQUID (KMOL/SEC)
C     YCOMPB    I    R       NCOMPS    BULK VAPOR MOLE FRACTION
C     FRATEV    I    R         -       FLOW OF VAPOR (KMOL/SEC)
C     PRESS     I    R         -       PRESSURE (N/SQ.M)
C     TLIQ      I    R         -       LIQUID TEMPERATURE (K)
C     TVAP      I    R         -       VAPOR TEMPERATURE (K)
C     AVMWLI    I    R         -       AVERAGE MOLECULAR WEIGHT
C                                      OF LIQUID MIXTURE
C                                      (KG/KMOL)
C     AVMWVA    I    R         -       AVERAGE MOLECULAR WEIGHT
C                                      OF VAPOR MIXTURE (KG/KMOL)
C     VISCML    I    R         -       VISCOSITY OF LIQUID
C                                      (N-SEC/SQ.M)
C     DENMXL    I    R         -       DENSITY OF LIQUID MIXTURE
C                                      (KMOL/CU.M)
C     SIGMAL    I    R         -       SURFACE TENSION OF LIQUID
C                                      (N/M)
C     VISCMV    I    R         -       VISCOSITY OF VAPOR MIXTURE
C                                      (N-SEC/SQ.M)
C     DENMXV    I    R         -       DENSITY OF VAPOR MIXTURE
C                                      (KMOL/CU.M)
C     AREAIF    O    R         -       INTERFACIAL AREA
C                                      (SEE NOTE-1 BELOW)
C     COLTYP    I    I         -       TYPE OF COLUMN
C                                      1 = PACKED
C                                      2 = TRAY
C     USRCOR    I    I         -       CALCULATION METHOD (I.E.
```

```
C                                       CHOICE OF USER CORRELATION)
C                                         1 = USER1
C                                         2 = USER2
C                                         3 = USER3
C                                         4 = USER4
C     TWRARA    I    R          -       CROSS-SECTIONAL AREA OF
C                                       TOWER (SQ.M)
C     COLDIA    I    R          -       COLUMN DIAMETER (M)
C     HTPACK    I    R          -       HEIGHT OF PACKING IN THE
C                                       SEGMENT (M)
C     PACSIZ    I    R          -       SIZE OF PACKING (M)
C     SPAREA    I    R          -       SPECIFIC SURFACE AREA OF
C                                       PACKING (SQ.M/CU.M)
C     CSIGMA    I    R          -       CRITICAL SURFACE TENSION
C                                       OF PACKING MATERIAL (N/M)
C     PFACT     I    R          -       PACKING FACTOR (1/M)
C     PKPRMS    I    R         20       PACKING PARAMETERS
C                                       PKPRMS(1) = STICHLMAIR CONSTANT C1
C                                       PKPRMS(2) = STICHLMAIR CONSTANT C2
C                                       PKPRMS(3) = STICHLMAIR CONSTANT C3
C                                       PKPRMS(4) = CL IN BILLET 93
C                                       PKPRMS(5) = CV IN BILLET 93
C                                       PKPRMS(6) = B IN BRF 85
C                                       PKPRMS(7) = S IN BRF 85
C                                       PKPRMS(8) = H IN BRF 85
C                                       PKPRMS(9) = Fse IN BRF 92
C                                       PKPRMS(10) = CE IN BRF 92
C                                       PKPRMS(11) = THETA IN BRF 92
C     VOIDFR    I    R          -       VOID FRACTION OF PACKING
C     IPAKAR    I    I          -       PACKING ARRANGEMENT
C                                         1 = RANDOM
C                                         2 = STRUCTURED
C     IPTYPE    I    I          -       PACKING TYPE
C                                       See IPTYPE in packsr.f
C     IVENDR    I    I          -       PACKING VENDOR CODE
C     IPMAT     I    I          -       PACKING MATERIAL CODE
C     IPSIZE    I    I          -       PACKING SIZE CODE
C     WEIRHT    I    R          -       AVERAGE WEIR HEIGHT (M)
C     DCAREA    I    R          -       TOTAL AREA OF DOWNCOMER
C                                       ON TRAY (SQ.M)
C     ARAACT    I    R          -       TOTAL ACTIVE AREA AVAILABLE
C                                       ON TRAY (SQ.M)
C     FLOPTH    I    R          -       AVERAGE FLOWPATH LENGTH (M)
C     NPASS     I    I          -       NUMBER OF TRAY PASSES
C     WEIRL     I    R          -       AVERAGE WEIRH LENGTH (M)
C     IFMETH    I    I          -       FLOODING CALCULATION
C                                       METHOD; REQUIRED FOR SIEVE
C                                       TRAY
C     SYSFAC    I    R          -       SYSTEM FACTOR; REQUIRED FOR
C                                       SIEVE TRAY
C     HOLEAR    I    R          -       HOLE AREA/ACTIVE AREA; REQUIRED
C                                       FOR SIEVE TRAY
C     ITTYPE    I    I          -       TRAY TYPE
C                                         1 - BUBBLE CAPS
C                                         2 - SIEVE
C                                         3 - GLITSCH BALLAST
C                                         4 - KOCH FLEXITRAY
C                                         5 - NUTTER FLOAT VALVE
```

```
C     TRASPC    I    R         -       TRAY SPACING (M)
C     PITCH     I    R         -       SIEVE TRAY HOLE PITCH (M)
C     NINT      I    I         -       Size of INT
C     INT      I/O   I       NINT      User correlation INT array
C     NREAL     I    I         -       Size of REAL
C     REAL     I/O   I       NREAL     User correlation REAL array
C
C     NOTE-1:
C          SPECIFIC INTERFACIAL AREA "AREAIF" HAS THE FOLLOWING UNITS.
C           FOR PACKED COLUMNS, THE UNITS IS "SQ.M/CU.M OF PACKING"
C           FOR TRAY COLUMNS, THE UNITS IS "SQ.M/SQ.M ACTIVE TRAY AREA"
C
C***********************************************************************
C     Declare local variables used in the user correlations
C
      REAL*8 WeL,   dTemp,  uV,    rhoVms,
     +       uL,    rhoLms, ReL,   FrL,    uL2,
     +       ReV,    d,     Wprime, LP, Ca, Aa, Bb

C
C     Compute specific interface area as described above
C     Check COLTYP/USRCOR if providing multiple area correlations
C
      IF (COLTYP .EQ. 1) THEN
C
C**** PACKED COLUMN
C
         IF (USRCOR .EQ. 1) THEN
C           user subroutine example for packed column: Onda 68
C
C           Onda, K., Takeuchi, H. and Okumoto, Y., "Mass Transfer
C             Coefficients between Gas and Liquid Phases in Packed
C             Columns", J. Chem. Eng. Jap., 1, (1968) p. 56
C
            rhoLms = DENMXL * AVMWLI
            uL = FRATEL / TWRARA / DENMXL
            uL2 = uL * uL
            ReL = rhoLms * uL / VISCML / SPAREA
            FrL = SPAREA * uL2 / 9.81D0
C           WHERE 9.81D0 IS GRAVITY CONSTANT IN M/S^2
            WeL    = rhoLms * uL2 / SIGMAL / SPAREA
            dTemp = -1.45D0*((CSIGMA/SIGMAL)**0.75D0)
     +                    *(ReL**0.1D0)*(FrL**(-0.05D0))
     +                    *(WeL**0.2D0)
            dTemp = 1.D0 - DEXP(dTemp)

            AREAIF = SPAREA*dTemp
C
          ELSE IF (USRCOR .EQ. 2) THEN
C**** *  Correlation for Packing based on Tsai
C         ae/ap = 1.34*(WeL*FrL**(-1/3))**0.116
C
            rhoLms = DENMXL * AVMWLI
            uL = FRATEL / TWRARA / DENMXL
            uL2 = uL * uL
            ReL = rhoLms * uL / VISCML / SPAREA
            FrL = SPAREA * uL2 / 9.81D0
            WeL    = rhoLms * uL2 / SIGMAL / SPAREA
```

```
            rhoLms = AVMWLI * DENMXL
            uL = FRATEL / TWRARA / DENMXL
            Aa=Real(2)
            Bb=Real(3)

            dTemp = Aa*((WeL*FrL**(-1/3))**Bb)

            AREAIF = (SPAREA*dTemp)

          ELSE IF (USRCOR .EQ. 3) THEN
C**** *  Correlation for Packing based on Tsai
C         ae/ap = 1.34*(WeL*FrL**(-1/3))**0.116
C
            rhoLms = DENMXL * AVMWLI
            uL = FRATEL / TWRARA / DENMXL
            uL2 = uL * uL
            dTemp=1.5*(4*VOIDFR)**(-0.5)
            dTemp=dTemp*(uL*rhoLms*4*VOIDFR/SPAREA/VISCML)**(-0.2)
            dTemp=dTemp*(uL*rhoLms*4*VOIDFR/SPAREA/SIGMAL)**(0.75)
            dTemp=dTemp*(uL2*SPAREA/9.81/4/VOIDFR)**(-0.45)

            AREAIF = (SPAREA*dTemp)

C     Here we start for WWC

          ELSE IF (USRCOR .EQ. 4) THEN
C**** *  Correlation for Packing based on Bravo (1985)
C         ae/ap = 1
C
            AREAIF = (SPAREA)

          Else if (USRCOR .EQ. 9) THEN
          AREAIF = 325.444D0

c Actual wetted are of the WWC is 38.52cm2.
c Column diamter is listed as 0.128655m (a factor of 10 bigger than the area which
matches gas flow area) and height as 9.1cm.
c This gives a surface area of 325.444m2/m3 for the Aspen Simulations.
       END IF
C END OF IF (USRCOR)


      ELSE IF (COLTYP .EQ. 2) THEN
C
C**** TRAY COLUMN
C
         IF (USRCOR .EQ. 1) THEN
C           user subroutine example for tray column: Scheffe-Weiland 87
C
C           Scheffe, R.D. and Weiland, R.H., "Mass Transfer
C           Characteristics of Valve Trays." Ind. Eng. Chem. Res.
C           26, (1987) p. 228
C
C           The original paper only mentioned valve tray.
C           It is also used for bubble-cap tray and sieve tray.
C
C           CHARACTERISTIC LENGTH IS ALWAYS 1 METER.
            d = 1.0D0
```

```
            rhoLms = DENMXL * AVMWLI
            rhoVms = DENMXV * AVMWVA
            uL = FRATEL / TWRARA / DENMXL
            uV = FRATEV / TWRARA / DENMXV
            ReL = rhoLms * uL * d / VISCML
            ReV = rhoVms * uV * d / VISCMV
            Wprime = WEIRHT / d
            AREAIF = 0.27D0 * ReV**0.375D0 * ReL**0.247D0
            AREAIF = AREAIF * Wprime**0.515
         END IF
C        END OF IF (USRCOR)
C
       END IF
C     END OF IF (COLTYP)
C
      RETURN
      END
```

A.5 Diffusivity FORTRAN code

```
C Log keyword added
C
C$ #1 BY: SUPHAT WATANASIRI 09-SET-2007 USER ROUTINE FOR LIQUID BINARY
C                                       DIFFUSION COEFFICIENTS
C
C ==========================cvs revision history=======================
      SUBROUTINE DL0U ( T, P, X, N, IDX, IRW, IIW, KCALC, KOP,
     *                  NDS, KDIAG, QBIN, KER )
C***********************************************************************
C     Template for DL0U routine for binary liquid diffusion coefficients
C     STUB ROUTINE
C
C     T = temperature
C     P = pressure (system)
C     X(N) = mole fraction
C     N = number of components present in X
C     IDX(N) = index of component present
C     IRW = real work area index
C     IIW = integer work area index
C     KCALC = calculation code (0=do not calculate, 1 = calculate)
C     KOP(10) = model option code
C     NDS = data set number
C     KDIAG = diagnostic message level
C     QBIN(N,N) = results. Binary diffusion coeffcients.
C     QBIN(i,j) is binary diffusion coefficient of component i in component j
C     KER = error return code (0 = no error)
C     All input and output in this user routine are in SI Units
C     with Gas constant = 8314.33
C***********************************************************************
C
      IMPLICIT NONE
C
C     DECLARE VARIABLES USED IN DIMENSIONING
C
      INTEGER N
```

```
#include "dms_global.cmn"
#include "dms_errout.cmn"
#include "ppexec_user.cmn"
#include "dms_maxwrt.cmn"
#include "dms_plex.cmn"
C
C     DECLARE ARGUMENTS
C
      INTEGER IDX(N), IRW, IIW, KCALC, NDS, KDIAG, KER, KOP
       INTEGER IWATER, IMEACOO, ICO2, IHCO3
       INTEGER IMEAH, IMEA, ICO3, IN2, IO2
       INTEGER DMS_KCCIDC, DMS_IFCMNC
      REAL*8 X(N), QBIN(N,N), T, P
       REAL*8 WATER, MEACOO, CO2, HCO3, MEAH, MEA
       REAL*8 CO3, VBMEA, MUWO
       REAL*8 LDG, XCO2T, XMEAT, EFACT1
       REAL*8 MWMEA, MWCO2, MWH2O, XH2O, MWT, XWMEA
       REAL*8 XWAMINE, B(1), DFACTCO2, DFACTMEA
       REAL*8 IOND, CO2D, MEAD, XMOLT, CO2DW
       REAL*8 MA, MB, MC, MD, ME, MUMX, MUMX1
       REAL*8 A, E, BB, THET, C, MU0, MUW, R, HG
       Real*8 VISC, LVISC, B1, C1, DZERO, MU0MEA, T0
       EQUIVALENCE (B(1), IB(1))
       Integer DFACT1, EFACT
       integer nbopst(6), name(2)
       CHARACTER*256 BUFFER(1)
C
C     DECLARE LOCAL VARIABLES
C
      INTEGER IPROG(2), I, J, K
C
C      DATA STATEMENTS
C
      DATA IPROG /4HDL0U, 4H    /
C
C     BEGIN EXECUTABLE CODE
C      DIFFUSIVITIES CALCULATED BY (...) METHOD
C      VALUES OBTAINED FROM THE DIFFUSIVITY REGRESSION
       KER = 0
       IF (KCALC .EQ. 0) RETURN
c
C      INDEX VALUES FOR COMPONENTS IN SIMULATION
C
      IWATER = DMS_KCCIDC('H2O')
      IMEACOO = DMS_KCCIDC('MEACOO-')
      ICO2 = DMS_KCCIDC('CO2')
       IHCO3  = DMS_KCCIDC('HCO3-')
      IMEAH = DMS_KCCIDC('MEAH+')
      IMEA = DMS_KCCIDC('MEA')
       ICO3 = DMS_KCCIDC('CO3--')
       IN2 = DMS_KCCIDC('N2')
       IO2 = DMS_KCCIDC('O2')
C
C
C      ASSIGNMENT OF INDEX NUMBERS FOR SPECIES PRESENT
C
       DO 50 I = 1, N
       IF (IDX(I). EQ. IWATER) IWATER = I
```

```
      IF (IDX(I). EQ. IMEACOO) IMEACOO = I
      IF (IDX(I). EQ. ICO2) ICO2 = I
      IF (IDX(I). EQ. IHCO3) IHCO3 = I
      IF (IDX(I). EQ. IMEAH) IMEAH = I
      IF (IDX(I). EQ. IMEA) IMEA = I
      IF (IDX(I). EQ. ICO3) ICO3 = I
      IF (IDX(I). EQ. IN2) IN2 = I
      IF (IDX(I). EQ. IO2) IO2 = I
   50 CONTINUE
C
C     LOADING CALCULATION
      XCO2T = X(IMEACOO)+X(ICO2)+X(IHCO3)
      XMEAT = X(IMEACOO)+X(IMEAH)+X(IMEA)
      LDG = XCO2T/(XMEAT)
C
C
C     AMINE MASS FRACTION CALCULATION
C
      MWMEA = 61.8D0
      MWCO2 = 44.01D0
      MWH2O = 18D0
      XH2O = X(IWATER)
      MWT = XCO2T*MWCO2 + XMEAT*MWMEA + XH2O*MWH2O

c     Viscosity of solution from Aspen
      call PPUTL_GOPSET ( NBOPST , NAME )
c
      CALL PPMON_VISCL (T, P, X, N, IDX, NBOPST, KDIAG, VISC, KER)
      LVISC = VISC
      MUMX = LVISC
C
C     Viscosity of water according to Likhachev E.R. Technical Physics, Vol. 48 N0.4 2003
pp. 514-515
C     Viscosity in Pa-s
      E = 4.753D0
      MU0 = 0.000024055D0
      THET = 139.7D0
       A = 0.000442D0
       BB = 0.0009565D0
       C = 0.0124D0
       R = 0.008314D0
       P = P / 100000D0
       HG = A * P +((E - BB * P)/(R * (T - THET - C * P)))
       MUW = (MU0 * EXP(HG))
C
C     DFACT1, EFACT STORE THE POSITION OF REGRESSED PARAMETERS FOR DIFF. CORRELATION
C      THEY REFER TO THE VALUES SPECIFIED IN PROPERTY-PARAMETER-USRDEF

      DFACT1 = DMS_IFCMNC('DFACT1')
      EFACT = DMS_IFCMNC('EFACT')
C      DFACT2 = DMS_IFCMNC('DFACT2')
C     ASSIGNS THE DFACT1 POSITION TO CO2 AND DFACT2 POSITION TO MEA
       DFACTCO2 = B(DFACT1+IDX(ICO2))
      DFACTMEA = B(DFACT1+IDX(IMEA))
      EFACT1 = B(EFACT+IDX(ICO2))
C
C     DIFFUSIVITY OF CO2 IN WATER
      CO2DW = 0.00000235D0 * EXP(-2119D0 / T)
```

```
C
C     DIFFUSIVITY OF CO2 IN SOLUTION BASED ON VERSTEEG, 1988
      CO2D = CO2DW * (MUW / MUMX)**(0.8D0)*((T/313.15)**(EFACT1))
      CO2D = CO2D * DFACTCO2

      CO2D = ((DFACTCO2)**2)/DFACTMEA * (MUW/MUMX)**0.8
      CO2D = CO2D*(T/313.15)**(EFACT1)
C

C     Diffusivity of Amine in water Hayduk and Laudie, 1974. AIChe Journal Vol.20 No. 3
C     DZERO in cm^2/s
C


C
C     Diffusivity of amine in solution - Aboudheir
C
      MEAD = (1/((MUMX/MUW)**0.8D0))*((T/313.15)**(EFACT1))
      MEAD = MEAD * DFACTMEA
C
C
C
C     ASSIGNING VALUES IN THE DIFFUSIVITY MATRIX
C
C
      DO 200 I = 1, N
        DO 100 J = 1, N
          IF (I.EQ.J) THEN
            QBIN(I,J) = 0D0

          ELSE
            QBIN(I,J) = MEAD

            IF (I.EQ.ICO2)QBIN(I,J) = CO2D
            IF (J.EQ.ICO2)QBIN(I,J) = CO2D
            IF (I.EQ.IN2)QBIN(I,J) = CO2D
            IF (J.EQ.IN2)QBIN(I,J) = CO2D
          END IF
  100   CONTINUE
  200 CONTINUE

c
C      WRITE VARIABLES TO HISTORY FILE
C
C       THE WRITE TO UNIT USER_NHSTRY WRITES TO THE HISTORY FILE
       WRITE (BUFFER, *) 'Executed fortran subroutine'
       CALL DMS_WRTALN(USER_NHSTRY, BUFFER(1))
       WRITE (BUFFER, *) 'Pressure ', P
       CALL DMS_WRTALN(USER_NHSTRY, BUFFER(1))
       WRITE (BUFFER, *) 'Temperature ', T
       CALL DMS_WRTALN(USER_NHSTRY, BUFFER(1))
       WRITE (BUFFER, *) 'LVISC ', LVISC
       CALL DMS_WRTALN(USER_NHSTRY, BUFFER(1))
       WRITE (BUFFER, *) ' '
       CALL DMS_WRTALN(USER_NHSTRY, BUFFER(1))



C 999      RETURN
```

```
      END
```

A.6 Reaction Kinetics FORTRAN code

```
C Edited on 9/1/2015 to create a version in which forward reaction rate constants are
adjustable
C $Log: usrknt.f,v $
C Revision 1.1  1997/04/14 15:52:38  kishore
C commit converted files
C
C Revision 1.3  1996/05/21  19:25:07  apbuild
C ANAVI 9.3 upgrade
C
C Revision 1.2  1996/04/26  19:15:09  apbuild
C Introduce 3phase modifications, Venkat
C
C ========================cvs revision history=======================
C$ #3 BY: SIVA DATE: 15-NOV-1994 ADD DOCUMENTATION
C$ #2 BY: SIVA DATE: 21-JUL-1994 ADD X TO ARGUMENT LIST
C$ #1 BY: ANAVI DATE:  1-JUL-1994 NEW FOR USER MODELS
C
C     User Kinetics Subroutine for RADFRAC, BATCHFRAC, RATEFRAC
C     (REAC-DIST type Reactions)
C
C     EXAMPLE FOR AN ACTIVITY-BASED POWER-LAW KINETIC MODEL
C     WRITTEN BY C. MOELLMANN, ASPENTECH EUROPE, 25 MAY 2001
C
C       REACTION 1: HOAC  + ETOH --> ETOAC + H2O
C       REACTION 2: ETOAC + H2O  --> ETOH  + HOAC
C
C       Kinetics uses FRMULA
C
C       REAL(1)  is pre-exponential factor [SI] for reaction 1
C       REAL(2)  is activation energy      [SI] for reaction 1
C       REAL(3)  is pre-exponential factor [SI] for reaction 2
C       REAL(4)  is activation energy      [SI] for reaction 2
C
C     THE MODEL ASSUMES A LIQUID HOLDUP SPECIFICATION IN KMOL
C
C
      SUBROUTINE ACTKIN2 (N,      NCOMP,   NR,     NRL,     NRV,
     2                    T,      TLIQ,    TVAP,   P,       PHFRAC,
     3                    F,      X,       Y,      IDX,     NBOPST,
     4                    KDIAG,  STOIC,   IHLBAS, HLDLIQ,  TIMLIQ,
     5                    IHVBAS, HLDVAP,  TIMVAP, NINT,    INT,
     6                    NREAL,  REAL,    RATES,  RATEL,   RATEV,
     7                    NINTB,  INTB,    NREALB, REALB,   NIWORK,
     8                    IWORK,  NWORK,   WORK)
C
C***********************************************************************
C  LICENSED MATERIAL.  PROPERTY OF ASPEN TECHNOLOGY, INC.  TO BE       *
C  TREATED AS ASPEN TECH PROPRIETARY INFORMATION UNDER THE TERMS       *
C  OF THE ASPEN PLUS SUBSCRIPTION AGREEMENT.                           *
C***********************************************************************
C-----------------------------------------------------------------------
```

```
C         COPYRIGHT (C) 1994
C          ASPEN TECHNOLOGY, INC.
C          CAMBRIDGE, MA
C-----------------------------------------------------------------------
C
C     DESCRIPTION: TO CALCULATE REACTION RATES FOR KINETIC REACTIONS
C                  USING USER SUPPLIED SUBROUTINE
C
C      VARIABLES IN ARGUMENT LIST
C
C       VARIABLE  I/O  TYPE     DIMENSION     DESCRIPTION AND RANGE
C       N          I    I          -          STAGE NUMBER
C       NCOMP      I    I          -          NUMBER OF COMPONENTS
C       NR         I    I          -          TOTAL NUMBER OF KINETIC
C                                             REACTIONS
C       NRL        I    I          3          NUMBER OF LIQUID PHASE
C                                             KINETIC REACTIONS.
C                                             NRL(1): NUMBER OF
C                                                     OVERALL LIQUID
C                                                     REACTIONS.
C                                             NRL(2): NUMBER OF
C                                                     LIQUID1 REACTIONS.
C                                             NRL(3): NUMBER OF
C                                                     LIQUID2 REACTIONS.
C       NRV        I    I          -          NUMBER OF VAPOR PHASE
C                                             KINETIC REACTIONS
C       T          I    R          -          STAGE TEMPERATURE (K)
C       TLIQ       I    R          -          LIQUID TEMPERATURE (K)
C                                             * USED ONLY BY RATEFRAC **
C       TVAP       I    R          -          VAPOR TEMPERATURE (K)
C                                             * USED ONLY BY RATEFRAC **
C       P          I    R          -          STAGE PRESSURE (N/SQ.M)
C       PHFRAC     I    R          3          PHASE FRACTION
C                                             PHFRAC(1): VAPOR FRACTION
C                                             PHFRAC(2): LIQUID1 FRACTIO
C                                             PHFRAC(3): LIQUID2 FRACTIO
C       F          I    R          -          TOTAL FLOW ON STAGE
C                                             (VAPOR+LIQUID) (KMOL/SEC)
C       X          I    R        NCOMP,3      LIQUID MOLE FRACTION
C       Y          I    R        NCOMP        VAPOR MOLE FRACTION
C       IDX        I    I        NCOMP        COMPONENT INDEX VECTOR
C       NBOPST     I    I         6           OPTION SET BEAD POINTER
C       KDIAG      I    I         -           LOCAL DIAGNOSTIC LEVEL
C       STOIC      I    R        NCOMP,NR     REACTION STOICHIOMETRY
C       IHLBAS     I    I         -           BASIS FOR LIQUID
C                                             HOLDUP SPECIFICATION
C                                             1:VOLUME,2:MASS,3:MOLE
C       HLDLIQ     I    R         -           LIQUID HOLDUP
C                                             IHLBAS    UNITS
C                                             1         CU.M.
C                                             2         KG
C                                             3         KMOL
C       TIMLIQ     I    R         -           LIQUID RESIDENCE TIME
C                                             (SEC)
C       IHVBAS     I    I         -           BASIS FOR VAPOR
C                                             HOLDUP SPECIFICATION
C                                             1:VOLUME,2:MASS,3:MOLE
C       HLDVAP     I    R         -           VAPOR HOLDUP
```

```
C                                                IHVBAS    UNITS
C                                                1         CU.M.
C                                                2         KG
C                                                3         KMOL
C       TIMVAP     I    R          -           VAPOR RESIDENCE TIME (SEC)
C       NINT       I    I          -           LENGTH OF INTEGER VECTOR
C       INT       I/O   I         NINT         INTEGER VECTOR
C       NREAL      I    I          -           LENGTH OF REAL VECTOR
C       REAL      I/O   R         NREAL        REAL VECTOR
C       RATES      O    R         NCOMP        COMPONENT REACTION RATES
C                                               (KMOL/SEC)
C       RATEL      O    R         NRLT         INDIVIDUAL REACTION RATES
C                                               IN THE LIQUID PHASE
C                                               (KMOL/SEC)
C                                               WHAT IS NRLT?
C                                               NRLT = NRL(1)+NRL(2)+NRL(3
C                                               NRLT IS NOT INCLUDED IN TH
C                                               ARGUMENT LIST.
C                                               * USED ONLY BY RATEFRAC *
C       RATEV      O    R         NRV          INDIVIDUAL REACTION RATES
C                                               IN THE VAPOR PHASE
C                                               (KMOL/SEC)
C                                               * USED ONLY BY RATEFRAC *
C       NINTB      I    I          -           LENGTH OF INTEGER VECTOR
C                                               (FROM UOS BLOCK)
C       INTB      I/O   I         NINTB        INTEGER VECTOR
C                                               (FROM UOS BLOCK)
C       NREALB     I    I          -           LENGTH OF REAL VECTOR
C                                               (FROM UOS BLOCK)
C       REALB     I/O   R         NREALB       REAL VECTOR
C                                               (FROM UOS BLOCK)
C       NIWORK     I    I          -           LENGTH OF INTEGER WORK
C                                               VECTOR
C       IWORK     I/O   I         NIWORK       INTEGER WORK VECTOR
C       NWORK      I    I          -           LENGTH OF REAL WORK VECTOR
C       WORK      I/O   R         NWORK        REAL WORK VECTOR
C
C*****************************************************************************
C
      IMPLICIT NONE
C
C     DECLARE VARIABLES USED IN DIMENSIONING
C
      INTEGER NCOMP, NR, NRV, NINT, NINTB, NREALB, NIWORK, NWORK
C
#include "ppexec_user.cmn"
      EQUIVALENCE (RMISS, USER_RUMISS)
      EQUIVALENCE (IMISS, USER_IUMISS)
C
#include "dms_maxwrt.cmn"
C
#include "pputl_ppglob.cmn"
C
#include "dms_plex.cmn"
      EQUIVALENCE (IB(1), B(1))
C
#include "dms_ipoff3.cmn"
C
```

```
#include "dms_rglob.cmn"
C
#include "dms_lclist.cmn"
C
C**********************************************************************
C
C
C
C     DECLARE ARGUMENTS
C
      INTEGER NRL(3), IDX(NCOMP), NBOPST(6), INT(NINT), INTB(NINTB),
     2        IWORK(NIWORK), N, KDIAG, IHLBAS, IHVBAS, NREAL,FN,
     3        L_GAMMA,L_GAMUS,GAM,US,DMS_ALIPOFF3
C
      REAL*8 PHFRAC(3), X(NCOMP,3), Y(NCOMP), STOIC(NCOMP,NR),
     2       RATES(NCOMP), RATEL(1), RATEV(NRV), REALB(NREALB),
     3       WORK(NWORK), T, TLIQ, TVAP, P, F, HLDLIQ, TIMLIQ,
     4       HLDVAP, TIMVAP,DUM,STOI(100),LNRKO
C
C     DECLARE LOCAL VARIABLES
C
      INTEGER IMISS, LFRMUL, DMS_IFCMNC, DMS_KFORMC,N_MEAH,N_MEAC,N_MEA,
     2 N_CO2,N_H2O,N_HCO3, KPHI, KER, I, J, K, LGAMMA, LGAM,IHELGK
C
      REAL*8 REAL(NREAL), RMISS, B(1), PHI(100), DPHI(100), GAMMA(100),
     2       RXNRATES(100),ACCO2,ACMEA,ACH2O,ACMEAC,ACMEAH,ACHCO3,A1,A2,
     3       A3,A4,B1,B2,B3,B4,R,GAMUS(100),COEFFCO2,COEFFMEA,KEQ1,KEQ2
C
C
C     BEGIN EXECUTABLE CODE
C
C     FORTRAN STATEMENT FUNCTIONS
C
      FN(I)=I+LCLIST_LBLCLIST
      L_GAMMA(I)=FN(GAM)+I
      L_GAMUS(I)=FN(US)+I
      LFRMUL = DMS_IFCMNC('FRMULA')
C
C     COMPONENT INDEX NUMBERS FROM FORMULA
C
      N_H2O   = DMS_KFORMC('H2O')
      N_CO2   = DMS_KFORMC('CO2')
      N_MEA    = DMS_KFORMC('C2H7NO')
      N_MEAH  = DMS_KFORMC('C2H8NO+')
      N_MEAC = DMS_KFORMC('C3H6NO3-')
      N_HCO3 = DMS_KFORMC('HCO3-')

       t=tliq
C
C     CALCULATION OF LIQUID PHASE FUGACITY
C
      KPHI = 1
      CALL PPMON_FUGLY (T,    P,      X,     Y,    NCOMP,
     2                  IDX,  NBOPST, KDIAG, KPHI, PHI,
     3                  DPHI, KER)
C
C     SET OFFSET LGAM TO ACCESS ACTIVITY COEFFICIENTS
C
```

```
      GAM = DMS_ALIPOFF3(24)
C
      DO I=1,NCOMP
         GAMMA(I) = 1.D0
        IF (INT(1) .EQ. 1) GAMMA(I) = DEXP(B(L_GAMMA(I)))
      END DO

      US=DMS_ALIPOFF3(29)

C     DO I=1,NCOMP
C          GAMUS(I)=1.D0
C        IF (INT(1).EQ.1) GAMUS(I)=DEXP(B(L_GAMUS(I)))
C      END DO
      COEFFCO2=DEXP(B(L_GAMUS(N_CO2)))
      COEFFMEA=DEXP(B(L_GAMUS(N_MEA)))


C     ACCO2=GAMMA(N_CO2)*X(N_CO2,1)
C     ACMEA=GAMMA(N_MEA)*X(N_MEA,1)
      ACCO2=COEFFCO2*X(N_CO2,1)
      ACMEA=COEFFMEA*X(N_MEA,1)
      ACH2O=GAMMA(N_H2O)*X(N_H2O,1)
      ACMEAH=GAMMA(N_MEAH)*X(N_MEAH,1)
      ACMEAC=GAMMA(N_MEAC)*X(N_MEAC,1)
      ACHCO3=GAMMA(N_HCO3)*X(N_HCO3,1)

      A1=85616000000
      B1=3963.9
      A2=24800
      B2=59600
      A3=22991.13
      B3=49000
      A4=18.35308
      B4=96230
      R=PPGLOB_RGAS/1000
C      KEQ1=DEXP(-35.849+5612.903/TLIQ+7.517958*LOG(TLIQ)-0.03608*TLIQ)
C      KEQ2=DEXP(-138.48+6440.715/TLIQ+25.61665*LOG(TLIQ)-0.0736*TLIQ)

C     CALL FIRST EQUILIBRIUM CONSTANT

      DO I=1,100
          STOI(I)=0D0
      ENDDO

      DO I=1,NCOMP
          IF (IDX(I).EQ.N_MEA) STOI(I)=-2D0
          IF (IDX(I).EQ.N_CO2) STOI(I)=-1D0
          IF (IDX(I).EQ.N_MEAH) STOI(I)=1D0
          IF (IDX(I).EQ.N_MEAC) STOI(I)=1D0
      ENDDO

      LNRKO=RGLOB_RMISS

      CALL PPELC_ZKEQ(T,1,1,0,STOI,0D0,NCOMP,IDX,0,1,1,NBOPST,KDIAG,
     2 LNRKO,P,IHELGK,DUM)

      KEQ1=DEXP(LNRKO)
```

```
C     CALL SECOND EQUILIBRIUM CONSTANT

      DO I=1,100
          STOI(I)=0D0
      ENDDO

      DO I=1,NCOMP
          IF (IDX(I).EQ.N_MEA) STOI(I)=-1D0
          IF (IDX(I).EQ.N_CO2) STOI(I)=-1D0
          IF (IDX(I).EQ.N_H2O) STOI(I)=-1D0
          IF (IDX(I).EQ.N_MEAH) STOI(I)=1D0
          IF (IDX(I).EQ.N_HCO3) STOI(I)=1D0
      ENDDO

      LNRKO=RGLOB_RMISS

      CALL PPELC_ZKEQ(T,1,1,0,STOI,0D0,NCOMP,IDX,0,1,1,NBOPST,KDIAG,
     2 LNRKO,P,IHELGK,DUM)

      KEQ2=DEXP(LNRKO)

C     KINETIC MODEL (FORWARD/REVERSE REACTION RATES)
C
C      RXNRATES(1)=A1*DEXP(-B1/R*(1/TLIQ-1/298.15))*ACMEA**2*ACCO2
C      RXNRATES(1)=RXNRATES(1)*(1-ACMEAC*ACMEAH/(KEQ1*ACMEA**2*ACCO2))
      RXNRATES(1)=REAL(1)*DEXP(-REAL(3)/R*(1/TLIQ-1/298.15))*
     2 (ACMEA**2*ACCO2-ACMEAC*ACMEAH/KEQ1)
      RXNRATES(2)=REAL(2)*DEXP(-REAL(4)/R*(1/TLIQ-1/298.15))*
     2(ACMEA*ACCO2-ACMEAH*ACHCO3/(KEQ2*ACH2O))
C      RXNRATES(2)=A2*DEXP(-B2/R*(1/TLIQ-1/298.15))*ACMEAH*ACMEAC
c      RXNRATES(2)=A3*DEXP(-B3/R*(1/TLIQ-1/298.15))*ACMEA*ACCO2
c      RXNRATES(2)=RXNRATES(2)*(1-ACMEAH*ACHCO3/(KEQ2*ACMEA*ACCO2*ACH2O))
C      RXNRATES(4)=A4*DEXP(-B4/R*(1/TLIQ-1/298.15))*ACMEAH*ACHCO3/ACH2O


       DO K = 1,NRL(1)
         RXNRATES(K) = RXNRATES(K) * HLDLIQ
         ratel(k)=rxnrates(k)
       END DO
C
C     INITIALIZATION OF COMPONENT REACTION RATES
C
      DO I = 1,NCOMP
         RATES(I) = 0.D0
       END DO
C
C     COMPONENT REACTION RATES in kmol/sec
C
      DO K=1,NRL(1)
        DO I=1,NCOMP
          IF (DABS(STOIC(I,K)) .GE. RGLOB_RMIN) RATES(I) = RATES(I) +
     1    STOIC(I,K) * RXNRATES(K)
        END DO
      END DO
C
      RETURN
      END
```

Appendix B: Novel high-viscosity solvent work

High-Viscosity Solvent

- A novel solvent designed by GE is being investigated by the CCSI team. Some features of this solvent are:
  - High-viscosity and its strong dependence on the CO_2 loading
  - Low vapor-pressure
  - Higher degradation temperature leading to high-pressure operation of the desorber thus reducing the CO_2 compression penalty
- Experimental data including VLE and heat of absorption data were obtained for developing thermodynamic and transport properties model.
- Experiments were also conducted at a bench-scale system as well as on a wetted wall column apparatus. The experimental data were utilized to develop models for the interfacial area, mass transfer coefficients and holdup, that are directly affected by the viscosity.

CCSI Carbon Capture Simulation Initiative · NETL · Lawrence Livermore National Laboratory · Los Alamos · Pacific Northwest · U.S. DEPARTMENT OF ENERGY

1

Viscosity Model

Andrade Model in Aspen Plus

$$\ln(\mu_{mix}) = \sum_i w_i \ln(\mu_i) + \sum_i \sum_j (k_{ij} w_i w_j + m_{ij} w_i^2 w_j^2)$$

$$k_{ij} = a_{ij} + \frac{b_{ij}}{T} \qquad m_{ij} = c_{ij} + \frac{d_{ij}}{T} \qquad \ln(\mu_i) = a_i + \frac{b_i}{T} + c_i \ln(T)$$

Akaike Information Criterion (Parameter Selection)

$$AIC = N \ln\left(\frac{SSE}{N}\right) + 2k$$

k = Number of Parameters
N = Number of Data
SSE = Sum of Square Error

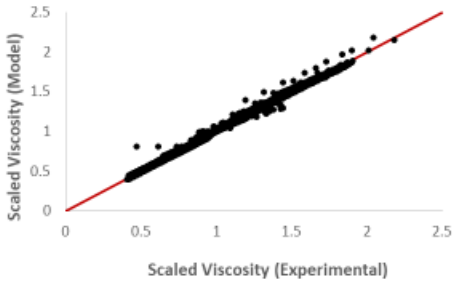

* Data and Model predictions given in terms of $\ln(\mu_{mix})$.

CCSI Carbon Capture Simulation Initiative · NETL · Lawrence Livermore National Laboratory · Los Alamos · Pacific Northwest · U.S. DEPARTMENT OF ENERGY

2

Thermodynamic Framework

Physical Equilibrium $P_{CO_2} = H_{CO_2} x_{CO_2} \gamma_{CO_2}$ **Chemical Equilibrium** $K_{eq} = \frac{[Prod]}{[React][CO_2]}$

Model parameters calibrated to optimize fit to VLE data:

$$H_{CO_2} = \exp\left(H_1 + \frac{H_2}{T}\right) \qquad K_{eq} = \exp\left(K_1 + \frac{K_2}{T}\right)$$

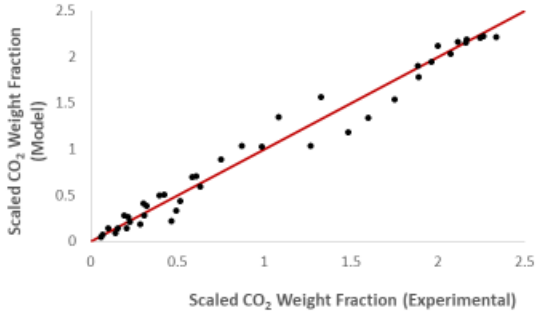

Model Validation Using Bench Scale Data

- Rate-based Aspen Plus™ model
  - Mass transfer coefficients: Modified Billet and Schultes model[1] (1993)
  - Interfacial area: Modified Tsai Model (2010)
  - Holdup: Modified Billet and Schultes model (1999)

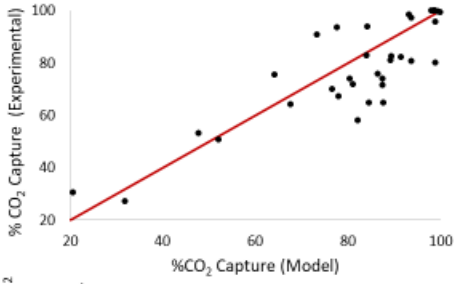

- The pre-exponential factor and activation energy of the forward reaction were regressed

$$r_{CO2} = k_f\left([CO_2][Reac] - \frac{1}{K_{eq}}[Prod]\right)$$

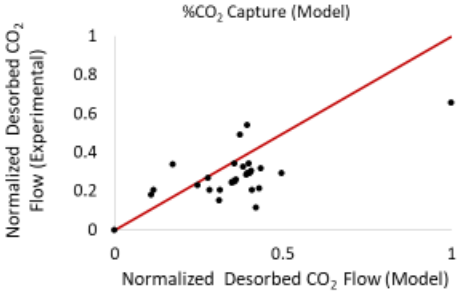

[1]Billet R, Schultes M. *Predicting Mass Transfer in Packed Columns. Chem. Eng. Technol.*1993;16(1):1-9.

[2]Tsai R.E. *Mass Transfer Area of Structured Packing*. Ph.D. Dissertation, UT, Austin, 2010

[3]Billet R, Schultes M. Prediction of Mass Transfer Columns with Dumped and Arranged Packings: Updated Summary of the Calculation Method of Billet and Schultes. Chem. Eng. Res. Des. 1999; 77(A6): 498-504.

Model Validation Using Bench Scale Data

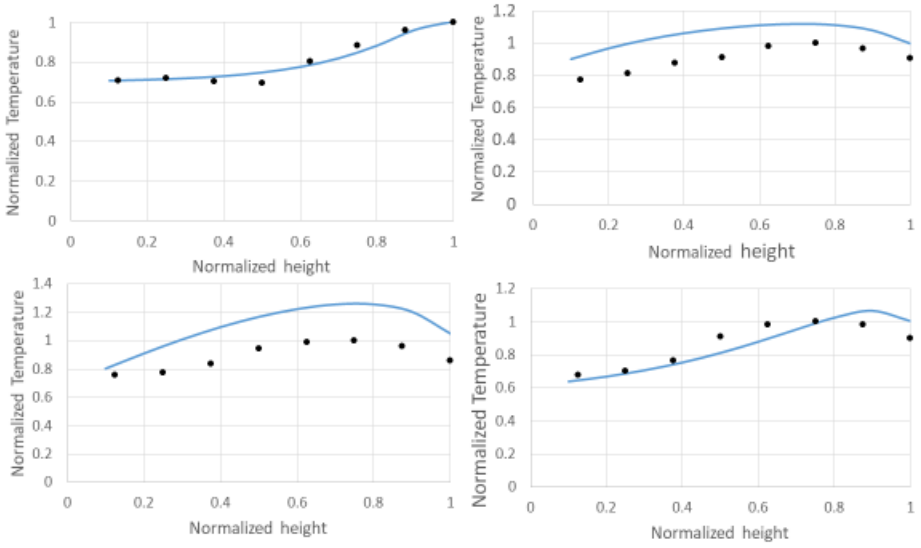

CCSI Carbon Capture Simulation Initiative · NETL · Lawrence Livermore National Laboratory · Los Alamos · Pacific Northwest · U.S. DEPARTMENT OF ENERGY

5

Comparison with the Wetted Wall Column Data

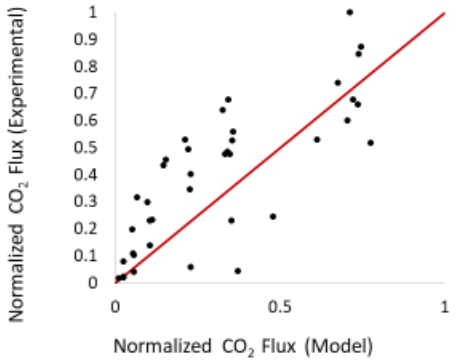

- Experiments were conducted at 40°C, 60°C, and 80°C for normalized CO_2 loadings of 1 and 0.31
- Rigorous Aspen Plus™ model is used to study the WWC. This model is developed by modifying the Aspen Plus™ model of the bench-scale system and the comparison with the data is made without changing the models or parameters.

CCSI Carbon Capture Simulation Initiative · NETL · Lawrence Livermore National Laboratory · Los Alamos · Pacific Northwest · U.S. DEPARTMENT OF ENERGY

6

This page is intentionally left blank